Department of Bioproducts and Biosystems

Electrostatic Self-Assembly of Protein Cage -Based Hybrid Materials

Antti Korpi

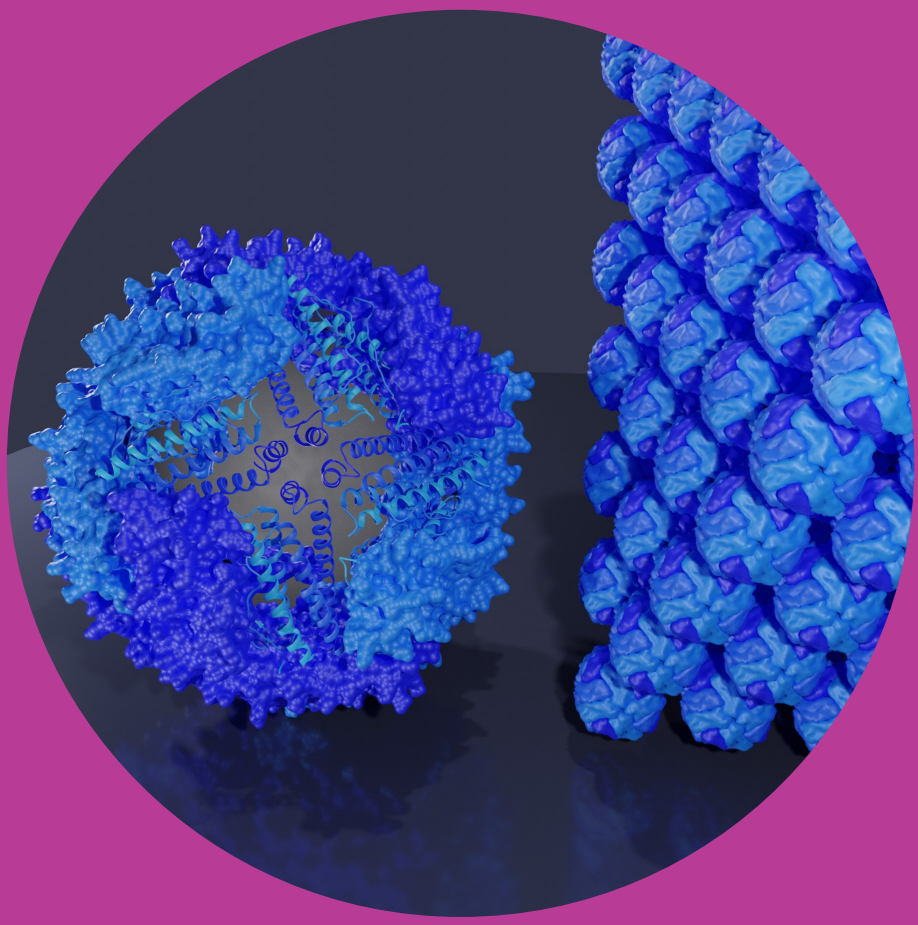

Aalto University

DOCTORAL DISSERTATIONS

Aalto University publication series
DOCTORAL DISSERTATIONS 2/2021

Electrostatic Self-Assembly of Protein Cage -Based Hybrid Materials

Antti Korpi

A doctoral dissertation completed for the degree of Doctor of Science (Technology) to be defended, with the permission of the Aalto University School of Chemical Engineering, remotely at https://us04web.zoom.us/j/76076799993?pwd=NHR2bE82SnFlVnFKN3hSdk5qNi82UT09, on 29th of January 2021 at 12 noon.

Aalto University
School of Chemical Engineering
Department of Bioproducts and Biosystems
Biohybrid Materials

Supervising professors
Professor Mauri Kostiainen
Aalto University, Finland

Thesis advisors
Professor Mauri Kostiainen
Aalto University, Finland

Preliminary examiners
Professor Tobias Beck,
University of Hamburg, Germany

Professor Vesa Hytönen
Tampere University, Finland

Opponents
Professor Jeroen Cornelissen
University of Twente, The Netherlands

Aalto University publication series
DOCTORAL DISSERTATIONS 2/2021

ISBN 978-952-64-0227-7 (printed)
ISBN 978-952-64-0228-4 (pdf)
ISSN 1799-4934 (printed)
ISSN 1799-4942 (pdf)
http://urn.fi/URN:ISBN:978-952-64-0228-4

Unigrafia Oy
Helsinki 2021

Finland

Printed matter
4041-0619

Aalto University

Abstract

Aalto University, P.O. Box 11000, FI-00076 Aalto www.aalto.fi

Author
Antti Korpi

Name of the doctoral dissertation
Electrostatic Self-Assembly of Protein Cage -Based Hybrid Materials

Publisher School of Chemical Engineering

Unit Department of Bioproducts and Biosystems

Series Aalto University publication series DOCTORAL DISSERTATIONS 2/2021

Field of research Chemical Engineering

Manuscript submitted 14 December 2020 **Date of the defence** 29 January 2021

Permission for public defence granted (date) 16 December 2020 **Language** English

☐ **Monograph** ☒ **Article dissertation** ☐ **Essay dissertation**

Abstract

Supramolecular self-assembly is a modern tool for development of materials with well-defined nanostructure. The process is simple and has low energy requirements, making it appealing as a production method. Electrostatic interaction is a versatile driving force for self-assembly due to the quantity of applicable components and environmental sensitivity of the phenomenon. Protein cages are a subclass of proteins characterized by a hollow interior, which can store smaller particles within. The cages have well-defined and symmetric structures, making them optimal particles for self-assembling systems. In this thesis, electrostatic self-assembly of two protein cages, apoferritin (aFT) and cowpea chlorotic mottle virus (CCMV), and synthetic molecules as well as inorganic particles is studied by focusing on both the assembly process itself and the obtained structures.

In publication I, aFT is complexed with synthetic block copolymers with cationic and thermoresponsive segments. The obtained systems are multi-responsive and can be assembled or disassembled by changing temperature or electrolyte concentration.

In publication II, CCMV is used to form aggregates with cationic colloidal lignin particles (c-CLPs). Significance of the charged nature of lignin is quantified and c-CLPs are found effective in removing virus particles from water as aggregates by sedimentation or filtration.

Publication III demonstrates self-assembly of aFT and CCMV structures with green fluorescent protein (GFP) carrying a cationic polypeptide tail. GFP is successfully incorporated in the assemblies and the order of the obtained structures varies with the dimensions of the assembling protein cage.

In publication IV, aFT is complexed with various cationic cyclophanes to initiate self-assembly. With optimisation of cyclophane structure, charge density and solution conditions, highly ordered crystal structures are obtained.

In publication V, properties of aFT with open and close cage morphology are compared. Both selfassemble with cationic gold nanoparticles, but the closed cages are found to reach higher level of order.

Publication VI demonstrates production of mesoporous silica using aFT crystals as templates. The crystals are encased in silica and removed by calcination to yield mesoporous material, where the order of the crystals is retained in orientation of the pores.

The research shows that protein cages are versatile particles for self-assembling systems and electrostatic interactions are an applicable driving force for their construction. Combination of different cages and synthetic co-assembly agents enables design of specific hybrid materials for targeted applications.

Keywords protein cages, self-assembly, electrostatic interaction, hybrid materials

ISBN (printed) 978-952-64-0227-7 **ISBN (pdf)** 978-952-64-0228-4

ISSN (printed) 1799-4934 **ISSN (pdf)** 1799-4942

Location of publisher Helsinki **Location of printing** Helsinki **Year** 2021

Pages 210 **urn** http://urn.fi/URN:ISBN:978-952-64-0228-4

Tekijä
Antti Korpi

Väitöskirjan nimi
Proteiinihäkkeihin Pohjautuvien Hybridimateriaalien Elektrostaattinen Itsejärjestyminen

Julkaisija Kemian tekniikan korkeakoulu

Yksikkö Biotuotteiden ja biotekniikan laitos

Sarja Aalto University publication series DOCTORAL DISSERTATIONS 2/2021

Tutkimusala Kemian tekniikka

Käsikirjoituksen pvm 14.12.2020 **Väitöspäivä** 29.01.2021

Väittelyluvan myöntämispäivä 16.12.2020 **Kieli** Englanti

☐ **Monografia** ☒ **Artikkeliväitöskirja** ☐ **Esseeväitöskirja**

Tiivistelmä

Supramolekulaarinen itsejärjestyminen on nykyaikainen työkalu tarkkaan määritellyn nanorakenteen omaavien materiaalien kehitykseen. Prosessi on yksinkertainen ja vaatii vähän energiaa, mikä tekee siitä houkuttelevan tuotantomenetelmän. Elektrostaattinen vuorovaikutus on monikäyttöinen voima itsejärjestymiselle käytettävissä olevien osasten suuren määrän ja ilmiön ympäristöherkkyyden vuoksi. Proteiinihäkit ovat proteiinien alaluokka, joille on ominaista ontto sisus, jonne pienempiä hiukkasia voidaan säilöä. Häkeillä on hyvin määritellyt ja symmetriset rakenteet, mikä tekee niistä ihanteellisia kappaleita itsejärjestyviin järjestelmiin. Tässä väitöskirjassa tutkitaan kahden proteiinihäkin, apoferritiinin (aFT) ja lehmänpavun kloroosiläikkäviruksen (CCMV), itsejärjestymistä synteettisten molekyylien ja epäorgaanisten hiukkasten kanssa, keskittyen sekä itse itsejärjestymisprosessiin että tuotettuihin rakenteisiin.
Julkaisussa I aFT kompleksoidaan synteettisten lohkopolymeerien kanssa, jotka sisältävät kationisen ja lämpöherkän osion. Järjestelmät ovat herkkiä useille muuttujille, ja ne voidaan järjestää tai purkaa muuttamalla lämpötilaa tai elektrolyyttikonsentraatiota.
Julkaisussa II CCMV:tä käytetään muodostamaan aggregaatteja kationisten kolloidisten ligniini hiukkasten (c-CLP) kanssa. Ligniinin varauksen merkitys järjestelmille määritellään ja c-CLP havaitaan tehokkaaksi virusten poistamiseen vedestä aggregaatteina sedimentaation tai suodatuksen avulla.
Julkaisu III esittelee aFT:n ja CCMV:n itsejärjestymisen vihreän fluoresentin proteiinin (GFP) kanssa, joka kantaa kationista polypeptidi häntää. GFP sisällytetään onnistuneesti rakenteisiin, joiden järjestys vaihtelee käytetyn proteiinihäkin mukaan.
Julkaisussa IV aFT kompleksoidaan useiden kationisten syklofaanien kanssa itsejärjestymisen käynnistämiseksi. Syklofaanirakenteen ja sen varaustiheyden sekä liuosolosuhteet optimoimalla onnistutaan tuottamaan hyvin järjestyneitä kiderakenteita.
Julkaisussa V avoimen ja suljetun rakenteen omaavien aFT häkkien ominaisuuksia vertaillaan. Molemmat itsejärjestyvät kultananoparttikkelien kanssa, mutta suljettulla rakenteella saavutetaan paremmin järjestyneitä rakenteita.
Julkaisu VI esittelee keskihuokoisen silikan valmistusta aFT kidemuottien avulla. Kiteet koteloidaan silikaan ja poistetaan kalsinoimalla, mikä jättää jäljelle keskihuokoisen materiaalin, jossa kiteiden järjestys säilyy huokosten suuntautumisessa.
Tutkimus osoittaa, että proteiinihäkit ovat monikäyttöisiä hiukkasia itsejärjestyviin järjestelmiin, ja elektrostaattinen vuorovaikutus soveltuu niiden tuottamiseen. Eri häkkien ja niiden kanssa järjestyvien hiukkasten yhdisteleminen mahdollistaa erityisiin sovelluksiin suunniteltujen hybridimateriaalien valmistamisen.

Avainsanat proteiinihäkit, itsejärjestyminen, elektrostaattinen vuorovaikutus, hybridimateriaalit

ISBN (painettu) 978-952-64-0227-7 **ISBN (pdf)** 978-952-64-0228-4

ISSN (painettu) 1799-4934 **ISSN (pdf)** 1799-4942

Julkaisupaikka Helsinki **Painopaikka** Helsinki **Vuosi** 2021

Sivumäärä 210 **urn** http://urn.fi/URN:ISBN:978-952-64-0228-4

Preface

The research described in this dissertation was conducted between June 2016 and November 2020 in the Biohybrid Materials Group at Aalto University. I have been lucky to be a part of this group and work alongside with all its brilliant researchers. I would like to thank Aalto CHEM for funding my doctoral student position for 2017-2020 and Finnish Foundation for Technology Promotion for personal financial support.

I am immensely grateful to my supervising professor Mauri Kostiainen for offering me a position in the group and for all your guidance and support. Your leadership has been inspirational, as you let me use my own methods to obtain results and solve issues but offered your knowledge and experience when needed. My time at Aalto would not have been as productive and educational without your supervision.

I am thankful to all the co-authors, whose expertise, ideas and efforts during the projects led to such fine research results and publications. I am especially grateful to Guillaume Rivière, Prof. Ngong Kodiah Beyeh and Dr. Soumyananda Chakraborti for inviting me to collaborate with them. Assisting you in your research was a pleasure and a great learning experience. I also want to acknowledge Piotr Skumial for his contribution to the synthetic and analytical work for publication **I** and thank you for the rich conversations during the more monotonic parts of the work.

I thank Prof. Tobias Beck and Prof. Vesa Hytönen for your thorough pre-examintaion of this dissertation and the valuable comments. I am also very grateful to Prof. Jeroen Cornelissen for accepting to act as the opponent in the upcominc defense.

From the beginning of my doctoral studies, small angle X-ray scattering has been a central part of my research and opened a lot of opportunities for me, even though I knew next to nothing of the topic when I started at Aalto. I would like to thank Dr. Ville Liljeström and Dr. Ulla Vainio for helping me with understanding both the phenomenon and the instrumentation where it is used for materials analysis.

The direct and indirect support from all the people in the Biohybrid Materials Group throughout the years has helped me to strive for better science and to cope with all the related pressure, and I owe you a big thank you for that. The group has increase in size since I joined and the change of members has been extensive, but the group spirit has always been healthy and enthusiastic. I think Mauri can be proud of what he has founded and confident that more excellent

results will be made in the years to come. I want to especially thank Dr. Salla Välimäki, as you were the one who got me to join the group and were an awesome office mate. Big thanks also to my later office buddies Heini Ijäs and Sofia Julin for always keeping up the good mood.

I would also like to thank all the memebers and especially the directors and coordinators of HYBER Centre of Excellence, of which our group has been a part of during my studies. The meetings and high quality events of HYBER have offered possibilities for comparing my results with my peers, getting fresh ideas and making connections, all of which have given me high respect towards the efforts of the researchers and inspired me to try my best.

Outside the laboratories, my friends have kept me going throughout the years when the pressure at work was tough. Big shout out to Toni Tykkä and Iiro Enkenberg for the soothing gaming sessions and innumerable laughs throughout the years. Thanks also to all the other dear friends who have been the safe haven when I needed to take my mind off from the science for a while.

I am grateful to my family for all their love and support. Thank you Maya Korpi, Pekka Korpi and Hanna Happo for being interested in the progress of my studies even if the topic was not in your area of expertise. I also want to thank Elli-Lotta Happo, as you have sparked joy everytime I got to visit you.

And last but definitely not least, words cannot express my gratitude to Milla Viitasuo. You have stood at my side throughout my studies and brought love and wonder into every single day.

Helsinki, 13 December 2020
Antti Korpi

Contents

Preface i
List of Abbreviations v
List of Publications vii
Author's Contribution ix
1. Introduction 1
1.1 Objectives and Outline 2
2. Background 5
2.1 Protein Cages 5
2.1.1 Apoferritin 6
2.1.2 Cowpea Chlorotic Mottle Virus 9
2.2 Self-Assembly 11
2.2.1 Electrostatic Self-Assembly 13
2.2.2 Thermo-Responsive Self-Assembly 15
2.2.3 Self-Assembly of Crystalline Protein Structures 16
2.3 Synthetic Polycations 18
2.4 Cyclophanes 20
2.5 Superporous Silica 21
3. Materials and Methods 23
3.1 Apoferritin and Cowpea Chlorotic Mottle Virus 23
3.2 Synthesis of Block Copolymers 23
3.3 K72 and GFP-K72 Protein Expression 24
3.4 Ferritin Crystallization and Silica Hybridization 25
3.5 Dynamic Light Scattering 25
3.6 Agarose Gel Electrophoresis Mobility Shift Assay 26
3.7 Electron Microscopy 26
3.7.1 Transmission Electron Microscopy 26
3.7.2 Scanning Electron Microscopy 26
3.8 Small Angle X-Ray Scattering 26
4. Results and Discussion 29

4.1 Self-Assembly with Organic Synthetic Materials.....29
4.1.1 Thermo-Responsive Self-Assembly of Ferritin.....29
4.1.2 Aggregation of CCMV with Cationic Lignin.....32
4.2 Crystalline Hybrid Self-Assembly.....34
4.3 Self-Assembly of Enzyme Loaded Ferritin 40
4.4 Mesoporous Silica from Ferritin Scaffolds 43
5. Conclusions and Outlook.....47
References 51
Publications.....67

List of Abbreviations

2D	two-dimensional
3D	three-dimensional
AfFtn	ferritin from *Archaeoglobus fulgidus*
AFM	atomic force microscopy
aFT	apoferritin
ATRP	atom transfer radical polymerization
AuNP	gold nanoparticle
CCMV	cowpea chlorotic mottle virus
c-CLP	cationic colloidal lignin particle
CLP	colloidal lignin particle
cryo-TEM	cryogenic transmission electron microscopy
DH	Debye-Hückel theory
DLS	dynamic light scattering
E. coli	*Escherichia coli*
ECPA	ethyl α-chlorophenylacetate
EDTA	ethylenediaminetetraacetic acid
EMSA	electrophoresis mobility shift assay
fcc	face centered cubic
FH	Flory-Huggins theory
GFP	green fluorescent protein
GFP-K72	recombinant fusion protein composed of GFP and K72
GPC	gel permeation chromatography
HDVD	hanging drop vapor diffusion
K72	specific polypeptide chain containing 72 lysine repeating units

LCST	lower critical solution temperature
NaAc	sodium acetate
NMR	nuclear magnetic resonance
OP	optical microscopy
PDEGMA	poly[di(ethylene glycol)methyl ether methacrylate]
PDMAEMA	poly[2-(dimehtylamino)ethyl methacrylate]
PfFtn	ferritin from *Pyrococcus furiosus*
SAXS	small angle X-ray scattering
SEM	scanning electron microscopy
SUP	supercharged polypeptide
T	triangulation number
TEM	transmission electron microscopy
TEOS	tetraethoxysilane
TMAPS	N-[3-(trimethoxysilyl)propyl]-N,N,N-trimethylammonium chloride (TMAPS)
TmFtn	ferritin from *Thermotoga maritima*
TMV	tobacco mosaic virus
VLP	virus-like particle
VO	Voorn-Overbeek theory

List of Publications

This doctoral dissertation consists of a summary and of the following publications which are referred to in the text by their numerals

I. Antti Korpi, Piotr Skumial, Mauri A. Kostiainen, *Thermally Induced Reversible Self-Assembly of Apoferritin–Block Copolymer Complexes*, Macromolecular Rapid Communications, **2019**, 40, 18, 1900308, DOI: 10.1002/marc.201900308.

II. Guillaume N. Rivière, **Antti Korpi**, Mika Henrikki Sipponen, Tao Zou, Mauri A. Kostiainen, Monika Österberg, *Agglomeration of Viruses by Cationic Lignin Particles for Facilitated Water Purification*, ACS Sustainable Chemistry & Engineering, **2020**, 8, 10, 4167-4177, DOI: 10.1021/acssuschemeng.9b06915.

III. Antti Korpi, Chao Ma, Kai Liu, Nonappa, Andreas Herrmann, Olli Ikkala, Mauri A. Kostiainen, *Self-Assembly of Electrostatic Cocrystals from Supercharged Fusion Peptides and Protein Cages*, ACS Macro Letters, **2018**, 7, 3, 318-323, DOI: 10.1021/acsmacrolett.8b00023.

IV. Ngong Kodiah Beyeh, Nonappa, Ville Liljeström, Joona Mikkilä, **Antti Korpi**, Davide Bochicchio, Giovanni M. Pavan, Olli Ikkala, Robin H. A. Ras, Mauri A. Kostiainen, *Crystalline Cyclophane–Protein Cage Frameworks*, ACS Nano, **2018**, 12, 8, 8029-8036, DOI: 10.1021/acsnano.8b02856.

V. Soumyananda Chakraborti, **Antti Korpi**, Mantu Kumar, Piotr Stępień, Mauri A. Kostiainen, Jonathan G. Heddle. *Three-Dimensional Protein Cage Array Capable of Active Enzyme Capture and Artificial Chaperone Activity*, Nano Letters, **2019**, 19, 6, 3918-3924, DOI: 10.1021/acs.nanolett.9b1148.

VI. Antti Korpi; Mauri A. Kostiainen, *Sol-Gel Synthesis of Mesoporous Silica Using a Protein Crystal Template*, Angewandte Chemie International Edition, submitted.

Author's Contribution

Publication I: Thermally Induced Reversible Self-Assembly of Apoferritin–Block Copolymer Complexes

AK conducted all the synthetic work and analysis with assistance from PS in optimisation of synthesis methods and some of the DLS measurements. AK wrote the manuscript and made corrections according to the suggestions by co-authors and reviewers.

Publication II: Agglomeration of Viruses by Cationic Lignin Particles for Facilitated Water Purification

GNR synthesized the c-CLPs and did most of the related analysis. AK did all the gel EMSA experiments and assisted GNR in data interpretation. MHS carried out the TEM imaging. TZ synthesized the initial CLPs. GNR wrote the manuscript and made corrections according to the suggestions by co-authors and reviewers.

Publication III: Self-Assembly of Electrostatic Cocrystals from Supercharged Fusion Peptides and Protein Cages

AK conducted all the self-assembly experiments and data analysis apart from the cryo-TEM imaging which was done by N. CM and KL synthesized and characterized the fusion proteins. AK wrote the manuscript and made corrections according to the suggestions by co-authors and reviewers.

Publication IV: Crystalline Cyclophane–Protein Cage Frameworks

NKB synthesized all the host molecules and performed the binding studies. N performed the cryo-TEM imaging. VL and AK participated in the SAXS measurements and data analysis. JM carried out the OM imaging. DB and GMP conducted the molecular simulations. NKB wrote the manuscript and made corrections according to the suggestions by co-authors and reviewers.

Publication V: Three-Dimensional Protein Cage Array Capable of Active Enzyme Capture and Artificial Chaperone Activity

SC conducted all the synthetic work and most of the analysis. AK performed the SAXS experiments and most related data analysis, as well as the binding efficiency experiments and analysis. MK assisted SC in the ferritin disassembly

experiments. PS assisted SC in gel filtration of the cargo encapsulation experiments. SC wrote the manuscript and made corrections according to the suggestions by co-authors and reviewers.

Publication VI: Sol-gel synthesis of mesoporous silica using a protein crystal template

AK carried out all the assembly experiments, synthesis and materials characterization. AK wrote the manuscript and made corrections according to the suggestions by MAK.

1. Introduction

Self-assembly is a versatile concept used to describe autonomous arrangement of numerous nanometer-scale building blocks, for example molecules, into more ordered systems. However, the concept is not restricted only to small particles, as self-assembly is present in all scales up to heavenly bodies and galaxies. These processes often strive for equilibrium, which is why no external energy is required to drive the assembly, suggested by the prefix "self".[1] Alternatively, in non-equilibrium self-assembly, fuel is consumed to reach an assembled state, but the order is still determined by the assembling units and no guidance is required. The order often persist after addition of fuel is stopped.[2] This makes the processes significant for practical applications, as the order within the systems originates from the assembling components themselves and no guiding procedures are needed. Therefore, the complexity of the systems and the required energy input to obtain larger structures are decreased. On molecular level, both synthetic and natural self-assembling particles are known and used in research and practical applications.[3–6] Synthetic block copolymers are among the most widely used such molecules, as the pool of applicable monomers is vast and by adjusting their ratios and configuration of the blocks, the number of obtainable molecules is practically limitless.[7] However, natural self-assembling molecules reach precision and complexity that cannot be matched by synthetic methods, which is why they are constantly being studied. Over the last few decades, research of molecules isolated from flora and fauna has increased as the molecules are understood better and new ones are studied. They are especially interesting candidates for medical applications, as they are often biocompatible and remain active in the conditions within a human body.[8]

The degree of order in self-assembling structures may vary greatly. Both amorphous aggregates without regular orientation between molecules that are not in immediate contact, and crystal lattices with the same interparticle distance and orientation in every region of the material, can be considered assembled structures. Both types of structures can be advantageous depending on the application, as ordered structures give rise to specific properties, like optic response, but disordered materials are often tougher and easier to produce.[9] Self-assembly is typically characterized by noncovalent interactions, which provide the structures with beneficial properties such as self-healing[10] and environmental responsiveness.[11] Noncovalent interactions also tend to be reversible and the system can therefore be regarded to be composed of small particles instead of being one large continuous molecule. In many cases, the assembled structures

can be disassembled back to their molecular components, making the material similar to a structure built using toy blocks.[12] This is the case for most complex biomolecules, which has inspired efforts to better understand the principles behind noncovalent interactions.[13] Electrostatic interactions between oppositely charged particles is a notable driving force for self-assembly, as it is inherent to numerous natural and synthetic molecules and is highly tunable by adjusting the density of charges on the assembling molecules, either by choice of materials or by modification. As electrostatic interactions occur between specific functional groups in molecules, they can even provide systems with a high degree of spatial orientation if the systems are designed correctly.[14]

Unique structures and properties can be achieved by assembling large, complex particles instead of low molecular weight molecules.[15] Among the most sophisticated structures available for research are proteins, which are self-assembled units on their own. Peptide chains fold onto themselves to place functional sites at specific spatial distance from one another, providing proteins with both selectivity and synergistic effectivity.[16] A special class among proteins are protein cages, which are characterized by a hollow interior. For example, iron storage protein ferritin[17] and various viruses, which carry their infectious genome inside a peptide shell,[18,19] fall under this category. They are capable of encapsulating smaller molecules within themselves and selectively interacting with their surroundings via recognition reactions on the cage surfaces, making them ideal units for self-assembling systems.[20,21] However, these studies mostly focus on properties of individual protein cages, but newer research has also considered the possibility of combining them into larger systems.[22]

Supramolecular self-assembly by noncovalent interactions is an effective method for producing materials with controllable repating structure in nanometer-scale, as the dimensions can be controlled by selection of the used particles. Protein cages are optimal building blocks for this process as they possess superb size and shape distribution, which enables formation of well-defined assemblies.[23] The functionalities on surfaces of protein cages are also distributed symmetrically, permitting order over relatively long distances in the assembled materials.[24,25] Electrostatic interactions are particularly appealing for the production of such systems, as most native protein cages have charged surfaces in neutral solutions,[26,27] and the strength of the interactions can be controlled by tuning the solution conditions, for example electrolyte concentration,[28] pH[29] or temperature.[30] This enables environmentally sensitive (dis)assembly of the cages, and in specific cases can be used to alter the structure of the assembled systems.[31]

1.1 Objectives and Outline

This thesis describes development of functional hybrid materials produced by electrostatic self-assembly of two protein cage molecules: apoferritin (aFT) and cowpea chlorotic mottle virus (CCMV). These are among the most studied protein cages, making them ideal for research of general behaviour of similar molecules and production of novel proof-of-concept systems. Both cages carry an

overall negative charge on their outer surface in aqueous solutions at neutral pH, enabling electrostatic self-assembly in the presence of suitable positively charged co-assembly particles. Synthetic cationic molecules and simple ions are used in this research. Protein cages are well-studied materials, but their applications are still limited as their complexity restricts their usage. They have been studied extensively as individual functional molecules, but their usage as self-assembling building blocks has been limited. However, the robust structure and symmetric nature of protein cages make them ideal for this purpose. Additionally, as hollow nanocontainers, they are suitable for the production of multifunctional organic materials. The research presented in the publications aims to show protein cages as components capable of self-assembly with various co-assembly agents that carry their own functionalities, enabling design of sophisticated hybrid materials. The presented systems also demonstrate that with further research, protein cage self-assemblies can potentially find uses in real life applications.

The theoretical background of electrostatically self-assembling protein cages and justification for interest in them is presented in chapter 2. The properties of the synthetic materials used in the research are described in the same chapter. Chapter 3 contains description of the used synthesis methods as well as the characterization techniques used to study the assembly processes and the obtained structures. The results of each publication are discussed in chapter 4, with focus as stated in the previous paragraph. Finally, conclusions and future aspects of the research are presented in chapter 5.

In publication **I**, aFT is subjected to temperature triggered self-assembly by complexing them with synthetic block copolymers composed out of thermo-responsive and cationic segments. Behaviour of the systems depends on the overall polymer and electrolyte concentrations in the solution, and under optimal conditions they undergo reversible environmentally sensitive self-assembly.

Publication **II** demonstrates the possibility of removing viruses from water by inducing electrostatic self-assembly and separating the aggregates by centrifugation or filtration. Cationic colloidal lignin particles (c-CLPs) are selected as co-assembly agents and their effectiness in virus removal is quantified by using them to aggregate and separate CCMV.

In publication **III**, green fluorescent protein (GFP) is genetically modified to carry a cationic polypeptide tail and electrostatically self-assembled with both aFT and CCMV. The research is a proof-of-concept demonstration that additional proteins can be incorporated into protein cage assemblies using electrostatic interactions, resulting in multifunctional systems.

Publication **IV** describes a similar process of self-assembling smaller functional molecules with protein cages. Cyclophanes resorcin[4]arene and pillar[5]arene are modified with side chains carrying varying number of cationic charges and self-assembled with aFT. Cyclophanes are known to promote host-guest interactions, and combination with aFT capable of encapsulating various heavy metals produces a material potentially capable of retaining both organic and inorganic molecules.

In publication **V**, properties of aFT from *Thermotoga maritima* (TmFtn) are studied in terms of thermal stability, enzyme encapsulation and electrostatic self-assembly with cationic gold nanoparticles (AuNPs). TmFtn has common octahedral symmetry but is specifically applicable for encapsulation process as the cage can be broken down and reassembled exceptionally easily. The properties of TmFtn are compared with aFT from *Archaeoglobus fulgidus* (AfFtn), which has rare tetrahedral symmetry and also enables easy encapsulation process but is less efficient in isolating the cargo from surrounding media.

Publication **VI** presents the concept of using aFT as a three-dimensional (3D) template material for production of mesoporous silica materials. aFT crystals are formed by electrostatic self-assembly, encased in silica and removed by calcination, leaving behind the porous silica. The crystalline structure of assembled aFT provides the final material with high spatial orientation of the pores.

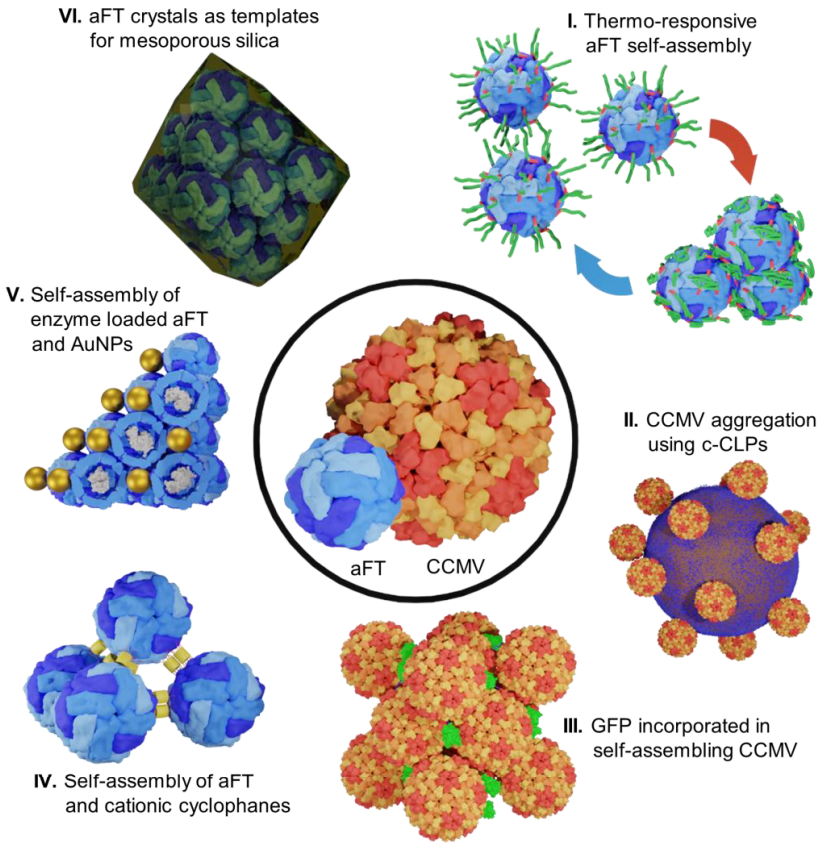

Figure 1. Schematic representations of the electrostatically self-assembling systems studied in the publications. Middle: aFT and CCMV protein cages, the key building blocks used in the publications. **I**. Thermo-responsive self-assembly of aFT with synthetic block copolymers. **II**. Aggregation of CCMV with c-CLPs. **III**. Co-crystals of CCMV and GFP with cationic polypeptide tail. **IV**. Co-crystals of aFT and cationic cyclophanes. **V**. Co-crystals of aFT loaded with lysozyme enzymes and AuNPs. **VI**. aFT crystals encased in silica for production of mesoporous material. The images were produced using UCSF Chimera based on X-ray diffraction resolved crystal structure for PfFTn (PDB ID: 2JD6), CCMV (PDB ID: 1CWP) and GFP (PDB ID: 3ADF).

2. Background

2.1 Protein Cages

Proteins are highly specialized biological molecules with functionalities relying on their 3D structures.[32] Protein cages are a special group defined by a hollow interior that is surrounded by a peptide shell of varying shape. They are composed of multiple subunits that self-assemble in a symmetric manner to form the complete cage.[33,34] Well-known protein cages include ferritins and virus-like particles (VLPs). Ferritins are spherical particles that store iron in their inner cavity and are native to most known living organisms.[35] Empty ferritin cage is referred to as apoferritin (aFT). VLPs are viruses without the infectious genome. They can be considered protein cages as the viral capsid is composed of peptides and contains an empty cavity within it, which normally houses the genome.[36] Both aFT and VLPs are potential molecular carrier units, as the vacant space left by the iron or viral genome can be occupied by other molecules. Various particles can be encapsulated in the cages through simple disassembly and reassembly. The reassembly happens in the presence of the cargo, which gets trapped. However, appropriately charged particles often show higher loading efficiency in aFT and VLPs, as iron ions and viral genome are charged particles and the cavity is receptive to similar molecules.[37,38] These interactions are not as specific as other interactions with proteins that require multiple oriented interactions because they are based solely on electrostatic attraction. Therefore, compatibility of non-charged cargo molecules can be improved by tagging them with charged molecules, making the encapsulation more effective for a greater pool of cargo molecules.[39] Encapsulation often provides the cargo with increased resistance to environmental harm by isolating it from the surrounding conditions. This is valuable when working with effective but sensitive molecules, for example enzymes.[40] Both aFT and VLPs have well defined sizes, shapes and functional sites that have evolved in nature. Proteins exist as a part of cellular design and viruses have evolved to enter living organisms and target specific cell types. Therefore, both are considered important in medical applications and materials chemistry.[41–44]

aFT from different sources is fairly uniform in shape and size and CCMV is one specific virus, but the dimensions of other protein cages may vary. For example, small heat shock protein is spherical with an outer diameter of 12 nm[45] and tobacco mosaic virus (TMV) tubular with a cross section diameter of 18 nm and length of 300 nm.[46] The dimensions of the cages are obviously important in encapsulation processes, as they determine the maximum amount and size of

the possible cargo molecules. With appropriate porosity of the cages, the encapsulated molecules can remain active and react with their surroundings,[47] with the drawback of compromising the aforementioned protection of the cargo. By selection of protein cages of appropriate size, it is possible to construct more intricate systems like cages inside larger cages, which can act as specialized delivery vehicles and reaction chambers.[48]

Protein cages are versatile molecules with large number of active functionalities at different sections of the cage. The hollow interior is an obvious active location and has applications in, for example, drug delivery[49–51] and confined catalysis.[52] However, the interfaces between the subunits are also functional sites, which can be modified to tune the properties of the cage. The most obvious factor that can be controlled in this manner is the self-assembly of subunits into cage formation.[53,54] Finally, the outer surfaces of the cages also hold various functionalities, as the exposed peptide moieties can react with the surroundings. These interactions can be modified by using chemical or genetic methods to change the chemical composition of the surface groups. Due to the symmetrical nature of protein cages arising from the subunit structure, these moieties are repeated across the surface at a specific distance from each other. In combination with the monodispersity of the molecules, this makes protein cages ideal building blocks for spatially ordered nanometer-scale structures like crystals.[42] The functional sites of a protein cage are demonstrated in Figure 2.

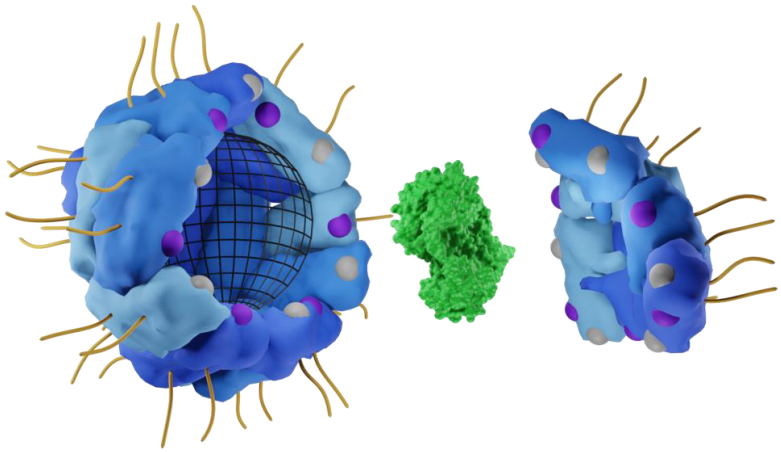

Figure 2. Schematic representation of the functional sites of a spherical protein cage. The interior of the cage is represented by a wired sphere and houses a smaller protein inside (the green particle). The yellow strands on the surface of the cage are additional functionalities that can interact with the surroundings. The purple and grey half spheres are functionalities at the interfaces between the subunits that direct their self-assembly process. The image was produced using UCSF Chimera based on X-ray diffraction resolved crystal structure for PfFTn (PDB ID: 2JD6) and GFP (PDB ID: 3ADF).

2.1.1 Apoferritin

Among native protein cages, aFT remains one of the most studied due to its biocompatibility,[55] chemical and thermal stability,[56,57] encapsulation capabili

ties[58,59] and genetic modifiability.[60] It is a hollow spherical protein with an overall negative charge on the outer surface which typically composes of 24 subunits.[61] Each subunit has a molecular weight of roughly 20 kDa, but the exact molecular weight differs between aFT from different sources.[62] Each subunit is built of four parallel helical peptide chains, providing them and, by extension, the entire cage with considerable rigidity.[63] A smaller variety of aFT composed of 12 subunits also exists, but it is only found in archaea and bacteria.[64,65] The subunits are classified into H and L type, which stand either for heavy and light chain or for heart and liver type. Both names are accurate, as the H type subunit has higher molecular weight than the L type, and H type is highly expressed in heart and L type in liver.[66,67] A third middle M type chain has also been identified, but it is not found in mammals.[65] An assembled 24 subunit aFT has an outer diameter of 12 nm and contains an inner cavity of 7-8 nm (Figure 3).[68,69] The cavity also has an overall negative charge, enabling aFT to encapsulate iron as Fe(III) oxide-hydroxide phosphate, and a single cage can house up to 4500 iron ions.[70] Due to the charged interior, the cage is effective in encapsulating all types of positively charged molecules that are sufficiently small.

aFT has been widely studied as a template material for production of inorganic nanomaterials, as the inner cavity is optimal for encapsulation of various metal materials, which besides iron oxide include metal particles like platinum and gold nanoparticles. Encapsulation in ferritin improves hydrophilicity and biocompatibility of the inorganic cargo, making such systems potentially useful in biomedical applications.[71]

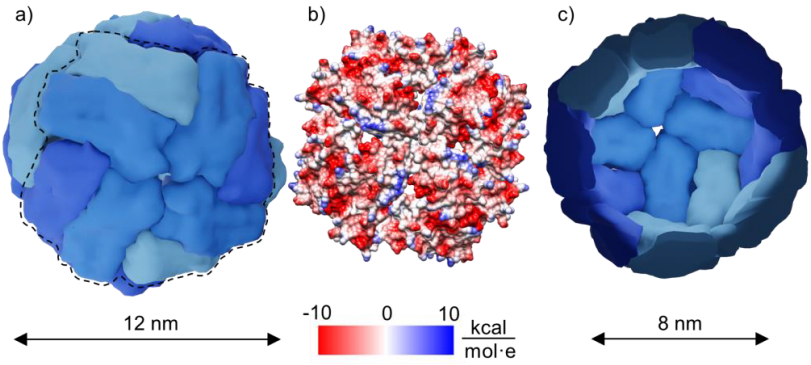

Figure 3. Schematic representation of aFT cage. a) Full aFT coloured by the repeating subunits. Four connected subunits share the same colour that repeats on the opposite side of the molecule. b) The section of aFT surface containing eight subunits outlined in a) coloured by Coulombic surface potential. c) aFT similar to a) but cut in half to show the inner cavity. The images and charge calculations were produced using UCSF Chimera based on X-ray diffraction resolved crystal structure for PfFTn (PDB ID: 2JD6).

Even though aFT from different sources all share the same functionality and the overall structure of a hollow sphere roughly 12 nm in diameter,[72] there are specific differences. The most common aFT structure has octahedral symmetry. Such protein cages have a mostly closed surface, and the inner cavity is connected to the outside via 3–4 Å diameter channels, through which iron ions move in an out of the cage.[73] Twelve channels are located along the 2-fold axes,

eight along the 3-fold and six along the 4-fold (Figure 4.a).[74] These channels are spread symmetrically across the cage surface in all octahedral aFT, making them optimal sites for directional interactions, which are important in formation of oriented assemblies. Therefore, the channels are considered vital points for supramolecular self-assembly of native aFT and sites of interest for chemical or biological modification to enhance such assembly.[75] The octahedral structure is not shared by all aFT, as these proteins differ in various lifeforms, for example in mammals and insects.[76] Human aFT is obviously ideal for medical applications, as it is native to our body and therefore should pose minimal immunologic response and toxicity. By using recombinant proteins, the risk of viral infections can also be minimized.[77] However, the in vitro properties are not the best available, especially for the purpose of encapsulating smaller molecules within the cage, as human aFT is not easily disassembled and reassembled. Chemical conditions in different parts of the human body differ and human aFT needs to remain functional in most of them.[78] To find more appropriate candidates for practical applications, aFT from simpler organisms, mainly archaea and bacteria, have drawn a lot of interest, as many of them have evolved to very specific environmental conditions.[79–81] aFT from three different sources have been used in the research work of this thesis and are now introduced in more detail.

aFT from a hyperthermophilic archaeon Pyrococcus furiosus (PfFtn) has the advantage that it can survive temperatures of over 100 °C for over 30 minutes without denaturation.[82] Due to this property, it is a promising candidate to be used as a biological nanoreactor, as reactions that require elevated temperatures can also be carried out. The cage adopts octahedral symmetry[83] and can be disassembled at pH below 2.0 or above 13.0 and reassembled at neutral conditions, enabling encapsulation of molecules too large to fit into the cage through the pores. However, this method is not an effective way to carry out the encapsulation as only a fraction of the PfFtn is recovered as reassembled cage and the harsh conditions also limit the pool of potential cargo molecules as many biomaterials would not survive the steep change in pH.[84] In comparison, AfFtn, which is also obtained from an archaeon, is the only characterized 24 subunit aFT with tetrahedral symmetry, a structure that is more common in the 12 subunit cages.[85] AfFtn has four relatively large 4,5 nm channels along the 3-fold axes, permitting movement of much larger species than in octahedral cages (Figure 4.b).[86] The disadvantage is that small cargo molecules may diffuse out of the cage at a higher rate and are also poorly protected from surrounding conditions. Notably, AfFtn can undergo reversible (dis)assembly between separated subunits and spherical cage in neutral pH in response to overall electrolyte concentration in the solution. This property has been exploited to load the cage with particles that are too large to fit through even the larger channels in the tetrahedral symmetry.[87] Finally, combining the beneficial properties of aFT from both these sources, TmFtn is intriguing among the ferritins from simple organisms. It has octahedral symmetry but can still undergo electrolyte induced (dis)assembly. This allows facile encapsulation of relatively large molecules into a cage with closed surface that isolates the cargo more effectively from the surroundings.[81] TmFtn originates from a hyperthermophilic bacterium and the

cage is also highly thermostable, similarly to PfFtn, broadening its possible applications.

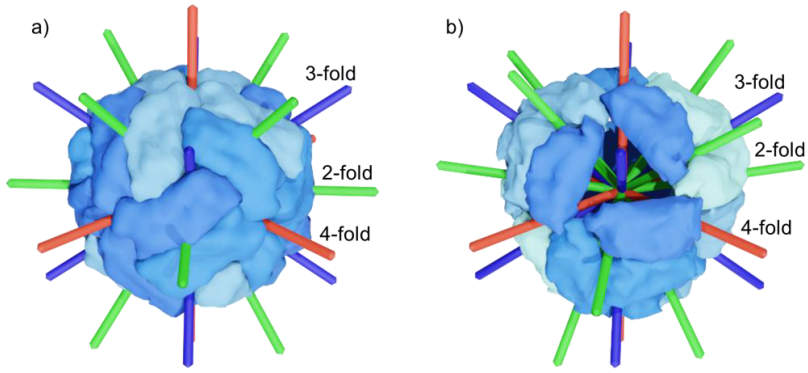

Figure 4. Comparison between a) octahedral PfFtn and b) tetrahedral AfFtn structures. The 8 channels along the 3-fold axes (blue rods) are the widest channels of both cages, but four of them are significantly larger in tetrahedral structure. The images were produced using UCSF Chimera based on X-ray diffraction resolved crystal structure for PfFTn (PDB ID: 2JD6), and AfFtn (PDB ID: 1SQ3).

2.1.2 Cowpea Chlorotic Mottle Virus

CCMV is a type of bromovirus commonly used for encapsulation and transport studies. It resembles aFT as it is a hollow sphere and carries negative surface chrge,[88] but it is considerably larger and has an outer diameter of 28 nm (Figure 5.a) and an inner cavity of 18 nm (Figure 5.c).[89] The negative charge of CCMV is highly localized, as can be seen in the potential map in Figure 5.b. Therefore, electrostatic interactions with CCMV have a tendency for high spatial orientation, making the cage an effective particle for electrostatic self-assembly.[90] Unlike aFT, the inner cavity of CCMV has a positive overall charge, enabling encapsulation of different types of molecules by electrostatic interactions.[91] The protein cage has icosahedral symmetry with triangulation number $T = 3$[92] and is composed out of 180 identical subunits with a molecular weight of roughly 20 kDa each.[58,93] CCMV is an exceptionally versatile protein cage, as it can undergo reversible disassembly and reassembly, like many other protein cages, but depending on the solution conditions, namely pH and electrolyte concentration, the reassembled cage may have different morphology than the original. Cages with $T = 1$ structures can be obtained in this manner.[94] In a typical process, CCMV disassembles into 90 dimer units which can then be reassembled in a controlled manner.[95]

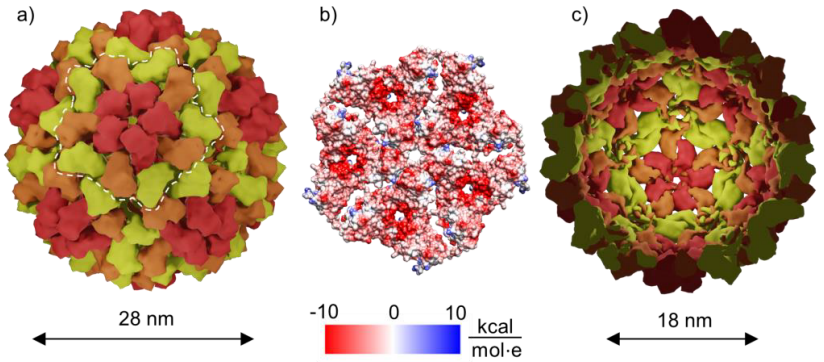

Figure 5. Schematic representation of CCMV cage. a) Full CCMV coloured by the repeating subunits. Each trimer subunit is coloured identically with three different colours for each monomer subunit to highlight its orientation. b) The section of CCMV surface containing five trimer subunits outlined in a) coloured by Coulombic surface potential c) CCMV cage similar to a) but cut in half to show the inner cavity. The images and charge calculations were produced using UCSF Chimera based on crystal structure for CCMV (PDB ID: 1CWP).

CCMV also goes through another morphological change besides dissambly in response to a change in pH. Native CCMV undergoes 10 % swelling in size at low ionic strength solutions when the pH of the solution is raised from 5.0 to 7.0 or above (Figure 6).[96] However, it has been suggested that this behaviour is not necessary for the release of RNA from the virus, as mutated viruses incapable of the swelling are also infectious. Another structural opening route exists via channel formation in the pentameric vertex, which is likely how the genome is released from these mutated cages.[97] The swelling process relates to the removal of divalent calcium or magnesium ions from the structure, which hold the monomer units together by noncovalent interactions. Therefore, similar swelling can be induced near neutral pH by removing the ions using chelating agents, making the swelling behaviour of CCMV multi-responsive. Below pH 6.5, sidechains are in their protonated state and the capsid remains in its closed state even without the divalent ions.[98] The cage can be reversed back to the closed morphology by lowering the pH below 5.0 or by increasing concentration of divalent ions.[99]

Although the swelling of CCMV is not the only route for particles to move to and from the inner cavity, gated pores on the capsid do open during the process. Therefore, pH can be used for controlled encapsulation and release of nanometer-scale cargo.[100] Furthermore, if pH is increased to 7.5 at ionic strength above 0.4, CCMV disassembles into dimeric subunits. As the cage can be reassembled by altering the surrounding conditions, encapsulation of particles too large to fit through the pores is also possible similarly to ferritin.[101] Due to the repeating structure of the cage, modification of the dimers can be used to enhance encapsulation efficiency of specific molecules. Such a method is especially efficient for CCMV as the cage is composed of almost one hundred dimers and the modified functionality will be repeated equally many times in the assembled structure.[102] As CCMV is a relatively large particle, encapsulation of multiple enzymes in a single cage has been reported, which may be efficient in catalysis of cascade reactions.[103] It is also worth noting that the conditions required for pH activated (dis)assembly of CCMV are milder that those for aFT.

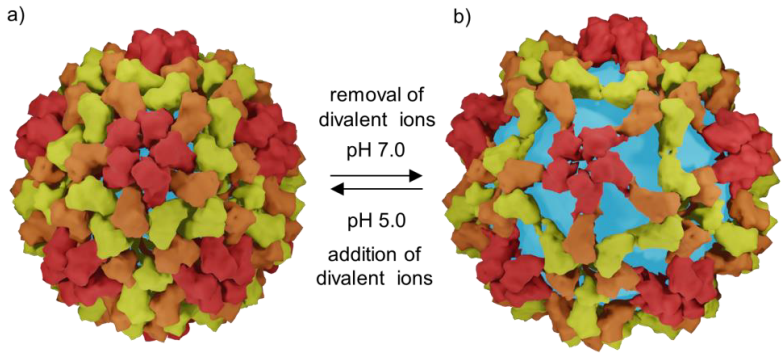

Figure 6. Comparison between CCMV in its a) compact and b) swollen state. The cage can be reversibly switched between the two states by controlling pH or divalent ion concentration. The swollen state is 10 % larger and has wide channels throughout the surface, enabling larger molecules to pass through the cage. Both models contain a light blue sphere to better display the channels. The images were produced using UCSF Chimera based on X-ray diffraction resolved crystal structure for CCMV (PDB ID: 1CWP).

2.2 Self-Assembly

Assembly processes rely on individual units associating with each other to form larger and more complex structures, quite like using toy blocks to build structures. Therefore, they are also referred to as "bottom-up" processes, as the design is built up from individual particles that are the basis of the structures. This is in contrast to "top-down" processes, where structures are produced by stripping apart larger systems, similar to carving a sculpture out of a block of wood.[9] Both methods have their advantages and disadvantages, but bottom-up method is superior when it comes to the resolution at which the fine-structure of the produced materials can be controlled.[104] It is noteworthy that numerous advanced structures critical to living beings are produced in nature by self-assembly.[105] For example, cell walls are formed from lipids by self-assembly into bilayers, suggesting that it is the most favourable method for such structures found by nature through millions of years of evolution. Self-assembly can be driven by covalent interactions,[106,107] but it is commonly carried out by noncovalent interactions, including electrostatic, hydrophilic and van der Waals interactions as well as hydrogen and metal-to-ligand bonding. For example, the afore-mentioned lipid bilayers are formed by hydrophilic and hydrophobic interactions between the amphiphilic lipids and water. Despite being held together by weak interactions, lipids can assemble into large sheets that can in turn assemble into multilayers (Figure 7.a).[108]

Basically any kind of particles can undergo self-assembly, but recently especially functional biomacromolecules, mainly proteins and DNA, have drawn a lot of attention.[109] In special cases self-assembly can also enhance properties of individual molecules by synergistic effects. For example, nanostructures formed by peptide self-assembly are stabilized by multiple noncovalent interactions, which give the structures greater stability than the strength of the individual forces would lead to assume.[110] Such systems are highly complex and have not

been broadly explored, but are becoming increasingly interesting for biomolecules[111] and inorganic nanoparticles.[112]

Due to self-assembly being mostly relying on relatively weak interactions, which have strength comparable to thermal energies at ambient conditions, equilibrium between forming and breaking of bonds can often be reached without harsh conditions. Such dynamic movement between the assembling particles is striving for minimum energy state of the system and provides robustness to the assemblies, as unfavourable interactions can be corrected after they have taken effect.[113] More powerful covalent interactions can also result in well-defined systems, as the strength of the interactions can largely prevent structural imperfections. Through innovative design, such interactions may also be reversible. For example, aFT mutated to carry additional cysteine groups has been reported to self-assemble during oxidation by forming disulfide bonds with neighbouring cages (Figure 7.b).[114] Relatively free molecular movement is required for all these interactions to be effective, which is why self-assembly is most commonly carried out in solutions.[115]

Due to the low energy requirements and self-driving nature of self-assembling systems, they can be easily upscaled, making them suitable for advanced industrial applications. Recently, usage of self-assembling systems has been studied in, for example, light harvesting materials[116,117] and lithium ion batteries.[118] Additionally, the reforming of the bonds can in many cases give rise to long-reaching spatial order in the produced materials.[119] Such order can be further enhanced by using particles with definite shape and spread of functional groups, which is why proteins have been widely studied for formation of specific assemblies like nanorods[120] and vesicles.[121]

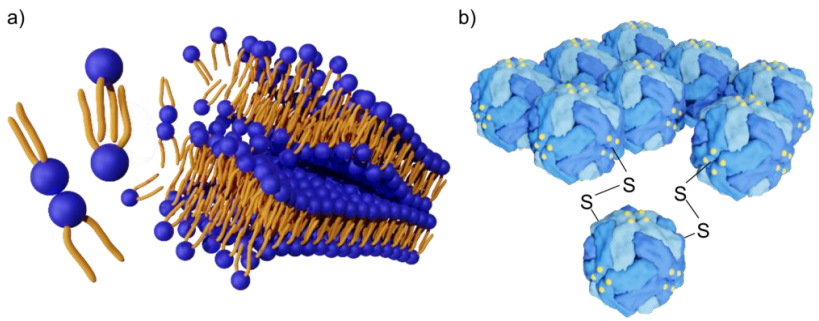

Figure 7. Schematic representations of natural and synthetic self-assembly. a) Multi-layered lipid membranes are formed from lipids with hydrophilic heads (blue spheres) and hydrophobic tails (yellow tendrils) by minimizing the repulsion between different ends of the molecules and maximizing attraction of similar ones. b) 2D sheets formed by single point mutation of aFT at 4-fold axes to introduce cysteine groups (yellow spots) that form disulfide bonds to covalently self-assemble aFT.[114] The images in were produced using Blender and UCSF Chimera based on X-ray diffraction resolved crystal structure for PfFTn (PDB ID: 2JD6).

2.2.1 Electrostatic Self-Assembly

Among the driving forces of self-assembly, electrostatic interactions are noteworthy due to their effectiveness and versatility.[122–124] In the simplest case, these interactions are attraction between oppositely charged particles and repulsion between similarly charged ones. This can be observed in inorganic salt formation from single ions, like NaCl, which typically produce highly ordered structures, as all the particles feel both the attractive and repulsive forces from their neighbouring charges, guiding them to assemble in a systematic manner.[125] However, the systems become much more complex when other charged particles than simple ions are assembling. Electrostatically self-assembling polymers,[126] nanoparticles,[127] biological macromolecules[128] or mixtures of these[46,129] are examples of such more advanced systems. Due to their complexity, a lot of the models explaining their behaviour are based on experimental data and are lacking in theoretical processing. Many of these models rely on the Debye-Hückel theory (DH),[130] which is still a good estimation of electrostatic interactions, although corrections have been presented during the almost 100 years since it was introduced. The theory states that charged particles are surrounded by a cloud of oppositely charged particles in close proximity and predicts how behaviour of these particles deviates from an ideal system with increasing electrolyte concentration. The theory includes many assumptions, for example ignoring close range interactions between particles and considering solvent as continuous media regardless of solvent composition. It is also limited to simple charged particles such as simple ions.[131] Describing more complex systems, for example charged polymers, requires combination of the DH with others. Flory-Huggins theory (FH) describes thermodynamic behaviour of molten polymer mixtures, where different polymers typically have a tendency to phase separate from each other on a microscopic level.[132] The theory has been combined with the DH to describe also systems containing charged polymers, which was first presented by Voorn and Overbeek (VO).[133] However, this theory is also limited due to the simplifying approximations, most notably the random phase approximation. Unlike neutral ones, oppositely charged polymers are typically mixable without phase separation by polymers, but separation occurs into concentrated and dilute polymer phases.[134] Therefore, the assumption of VO that mixtures are a continuous and randomly distributed mixture does not apply for most real systems.[135]

The effect of a charge of a particle on its neighboring charged particles depends on the overall electrolyte concentration in the solution. The distance to which the interparticle interactions are effective is expressed using the Debye screening length (κ^{-1}). This length is determined according to equation (1)

$$\kappa^{-1} = \sqrt{\frac{\varepsilon_0 \varepsilon_r k_B T}{e^2 \Sigma_i c_i z_i^2}} \tag{1}$$

where ε_0 is vacuum permittivity, ε_r dielectric constant of the solvent, k_B Boltzmann constant, T absolute temperature, e elementary charge, c_i number densities of the electrolyte ions and z_i valences of the electrolyte ions.[136] It can be seen

from the equation that increasing the overall electrolyte concentration or using more dense or higher valency ions decreases κ^{-1}. This is called screening and it can be used to control the strength of electrostatic interactions.[137] The phenomenon is mostly significant in solutions with electrolyte concentration below 1 M. With decreasing κ^{-1}, significance of short-range interactions increase and they become dominant.[138] Despite the limitations in the theories of electrostatic interactions, screening is an important phenomenon especially when structures with a high level of order are desired, as too strong electrostatic interactions lead to immediate and permanent bonding without long-distance orientation between the assembling units (Figure 8). Interactions weakened by screening enable the particles to move about each other and adopt thermodynamically most favourable orientation.[127,139] Excessively high electrolyte concentration can be used to disassemble the formed structures, as κ^{-1} can be decreased until the interactions can no longer hold even the closest particles together.[140]

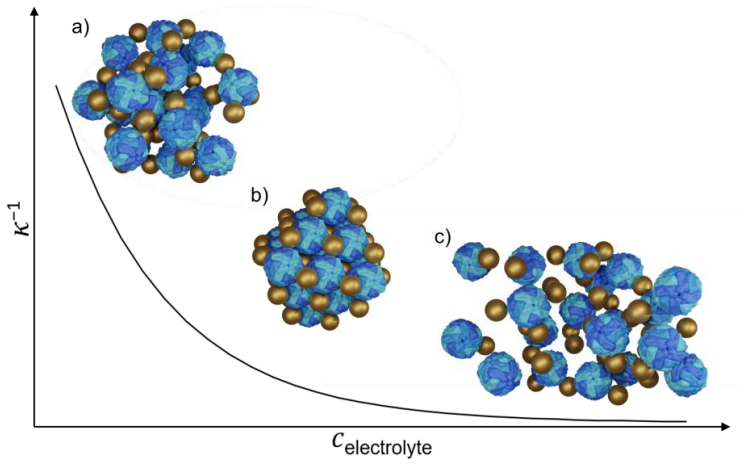

Figure 8. Schematic representation of effect of concentration of low molecular weight electrolytes on κ^{-1} and electrostatic self-assembly. a) At low electrolyte concentration κ^{-1} is large and electrostatic interactions strong. Oppositely charged particles form irregular aggregates as binding is instantaneous. b) Moderate electrolyte concentration decreases κ^{-1}, partially screening interactions between charged particles. Charged particles attach to and detach from each other in a dynamic manner, enabling forming of well-ordered assemblies. c) Excessive electrolyte concentration greatly decreases κ^{-1}, causing electrostatic interactions to become screened and electrostatic interactions become insufficient for self-assembly. The images were produced using Blender and UCSF Chimera based on X-ray diffraction resolved crystal structure for PfFTn (PDB ID: 2JD6).

Properties of electrostatically self-assembling systems can be altered by switching one of the assembling units. For example, 3D orientation of protein cage assemblies change when either rigid inorganic particles or soft organic molecules are used as co-assembly agents.[141] The high number of available building blocks has led to usage of electrostatic self-assembly in specific applications such as composite materials,[142] carbon based hydrogen production[143] and quantum dot assemblies in supercapacitors[144] and disease treatment.[145]

2.2.2 Thermo-Responsive Self-Assembly

It was stated in section 1 that no external energy input is required for self-assembly to occur. However, external change in conditions surrounding the assembling particles can in some cases be used to trigger the spontaneous assembly. Such systems are called stimuli-responsive, as the stimulus causes a distinct change in the behaviour of the particles.[146] For example, many polymers are thermo-responsive, and heating a solution containing them above a certain threshold temperature will cause the soluble polymers to precipitate out or insoluble precipitate to dissolve.[147] Temperature is the most studied trigger in stimuli-responsive polymers[148] and perhaps the most effective method to control molecule solubility. It affects molecular vibration and thus the strain on chemical and physical bonds inside the dissolved molecules as well as between them and solvent molecules, determining whether bonds are formed or broken.[149] Other typical stimuli for polymers include change in pH[150] or solvent[151] and light irradiation.[152] Multi-responsive systems are sensitive to more than one stimuli[153,154] ore even simultaneous combination of multiple factors.[155–157] In resent research, self-assembly has even been triggered by chemical reactions such as polymerization,[158,159] or with delay by using clocked reactions.[160]

Lower critical solution temperature (LCST) behaviour is the most typical temperature-based form of stimuli-responsiveness. LCST systems are soluble at low temperatures, but precipication is triggered by rising temperature above a critical temperature, which is unique for each system (Figure 9). In aqueous solvents, change in solubility often occurs near room temperature, enabling LCST activity in biological solvents and conditions.[161] In most systems, the division between soluble and insoluble phase is not definite as the transition occurs in domains. The reversibility of the change may also show some hysteresis, but for most practical applications these phenomena are not relevant.[162] Favourable conditions for dissolving are presented by the change in Gibbs free energy of mixing, ΔG_{mix}, which is expressed according to equation (2)

$$\Delta G_{\mathrm{mix}} = \Delta H_{\mathrm{mix}} - T\Delta S_{\mathrm{mix}} \tag{2}$$

where ΔH_{mix} is enthalpy change of mixing, T temperature and ΔS_{mix} entropy change of mixing. Hydrogen bonds become unstable when ΔG_{mix} becomes positive, and phase separation occurs.[163] In case of molecules with LCST behaviour, hydrogen bond formation has negative ΔH_{mix} due to hydrophilic nature of the molecules, which enables solubility at low temperatures. However, ΔS_{mix} is negative, as a system where the thermo-responsive molecules have formed hydrogen bonds with the solvent molecules has less microstates available than one where the molecules have not formed bonds.[164] Two things that can be observed from equation (2) are that an increase in temperature will enhance the effect of ΔS_{mix}, and if ΔS_{mix} is negative it will push ΔG_{mix} towards positive values. These factors promote phase separation at high temperature. LCST is the point where the sign of ΔG_{mix} changes due to a change in temperature.[165]

The effect of concentration of the thermo-responsive species to the LCST relates to the ratio between the functional sites and solvent molecules. To a certain

point, more thermo-responsive functionalities lower the amount of thermal energy needed for phase separation as more hydrophobic groups become available for bonding. However, excessive amount of polymer chains diminishes the interactions between the themo-responsive groups and solvent molecules, which again dampens the responsive effect.[166]

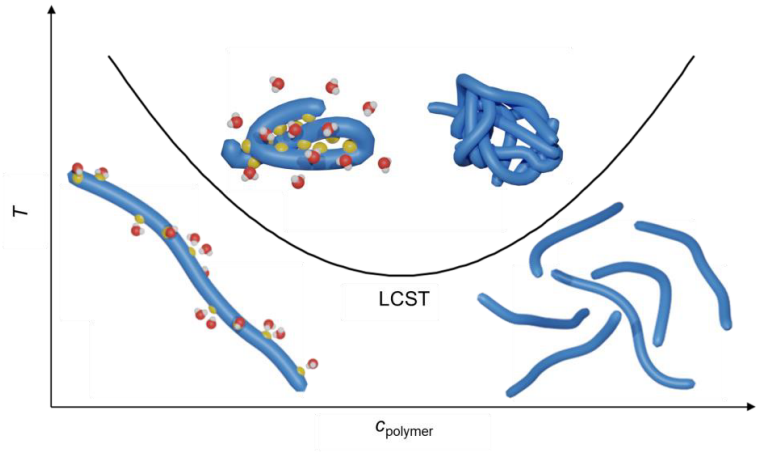

Figure 9. Schematic representation of typical LCST behaviour of linear polymer chains in water as a function of temperature and polymer concentration. The curve opening upwards represents the LCST at each given polymer concentration. Below the curve polymer chains are hydrophilic and have adopted open chain conformation. Above the curve they are hydrophobic and collapse on themselves and each other to minimize interactions with solvent molecules. The images on the left side of the figure represent interactions between lone polymer chains and water molecules and the ones on the right interactions of several polymer chains with each other. The images were produced using Blender.

2.2.3 Self-Assembly of Crystalline Protein Structures

Inorganic materials arranged into regular nanometer-scale arrays or crystals are studied because of their useful properties provided by the specific repeating structure. Such properties include optical, conductive, sensory and memory properties.[167] Light propagates through anisotropic crystals differently depending on the angle of the structures, which is useful in, for example, polarization splitters[168] and dispersion engineering.[169] Similarly, electric conductivity of crystals can be anisotropic[170] and control over the structure enhances performance of the materials.[171] However, production of such materials remains challenging as robust production methods that can be scaled up to practically useful extent are elusive.[172,173] Hybrid materials of organic and inorganic materials can provide a solution to this problem, as they offer different synthesis methods to obtain the ordered structures.[174] Biomimetic self-assembly and crystal template based methods are examples of such synthesis methods.[175] Furthermore, the methods enable production of well-defined structures as the resolution of the arrangements is limited by the size and shape of the template, and in nature various suitable molecules exist with dimensions ranging from only a few to hundreds of nanometers.[176] Self-assembly of these molecules can even be used

to incorporate additional inorganic particles in the structures with high accuracy, for example by encapsulation.[46] Production is facilitated by keeping the systems as simple as possible, as complex systems are less robust.[177] Advanced template systems are constantly developed and understood better, for example colloidal crystals[178] and chiral helical nanofibers.[179] Templates based on self-assembly of molecules found in nature are interesting for research, as they offer usable functional units capable of forming highly complex supramolecular structures via noncovalent interactions.[180] Protein crystals are especially intriguing due to their encapsulation properties[181] and spatial order.[182]

Rigid molecular structure is often favourable for formation of crystal lattices, as the assembling particles do not bend into different conformation, and order over long distances is possible. Inorganic salts are typically crystalline when dried, as they are composed of either small or single atomic ions that have no alternative conformations. In order to crystallize, larger molecules require additional rigidity from self-supporting structures, like nanorods or cyclic shapes.[183] This is why large organic molecules are difficult or impossible to crystallize, as they become less rigid with increasing molecular weight and often adopt amorphous state instead of completely crystalline.[184] However, molecules with a folded structure like rings,[185] tubes[186] and spheres,[187] are more rigid because the structures loop onto each other, offering additional support to the system and enabling assembly into ordered structures.[188] Protein cages possess such rigid structures, but selection of both the assembling cage and the co-assembly agent is crucial for obtaining crystalline structures.[189] Compatible orientation of both components can yield complex 3D assemblies, like rotating nanorod bundles (Figure 10.a)[46] and conductive nanowires.[190] In specific cases, obtained crystalline symmetry may be so delicate that it can be altered by changing solution conditions while maintaining the assembling particles in constant concentrations.[31]

Especially spherical protein cages have a tendency to form close-packed crystalline lattices, as such structures are most favourable in terms of space.[191] If the co-assembly agent is small compared to the protein cage,[192] or even another protein cage,[128] dense crystals can be obtained as free space between the cages is minimized (Figure 10.b). Close proximity can be beneficial for the cargo inside the cages, for example metal nanoparticles may obtain increased electrical conductivity.[193]

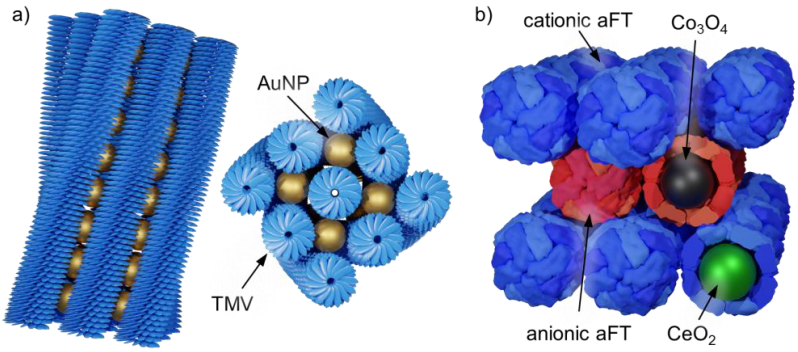

Figure 10. Schematic representation of electrostatically self-assembled cocrystal systems composing of protein cages and metal nanoparticles. a) TMV (blue tubes) directing gold nanoparticles (yellow spheres) into ordered arrays with a right handed twist viewed from across and along the wires.[46] b) Ferritin modified to carry high overall negative (red) or positive (blue) charge assembled into altering layers. Negative cages are carrying Co_3O_4 and cationic cages CeO_2 nanoparticles in their cavities.[128] The images were produced using Blender and UCSF Chimera based on X-ray diffraction resolved crystal structure for PfFTn (PDB ID: 2JD6).

Without designed dense structure, proteins have intrinsic tendency to form highly porous structures when crystallized. This is relevant for chemical activity, as in addition to having high spatial order all the molecules remain relatively accessible. This enables the proteins even at the center of the crystals to interact with molecules small enough to penetrate the structures, which is important in, for example, catalysis. This is also true for protein cages, allowing encapsulated cargo to remain active even at the centre of a 3D crystal.[194] Incorporating cargo molecules into crystal structures may enhance the properties of individual particles, for example catalytic activity.[195] The amount of naturally available protein cages and their modifiability make them a versatile material for use as self-assembling crystal scaffolds.[22] However, the porosity of the structures often makes them labile and they may not withstand significant changes to the chemical and physical conditions under which they were formed. This can be mended by cross-linking of the crystal surfaces, with the obvious drawback of losing reversibility of the self-assembly.[196] Recent research suggests that more robust structures can be obtained by integrating protein crystals with polymer hydrogels, which provides chemical stability but enables the proteins to retain their mobility, leading to nontypical properties in crystals like swelling and self-healing.[197]

2.3 Synthetic Polycations

Polymers are one of the most common synthetic materials and used in myriad applications, also in the biomedical field.[198–200] Polyelectrolytes are polymers composed of monomers with ionizable groups. Positive and negative charge carrying polymers are referred to as polycations and polyanions, respectively, and polymers with both types of charges as zwitterionic polymers.[201] Unlike chargeless polymer chains, which typically have a strong tendency to intertwine with themselves and each other, polyelectrolytes typically adopt relatively straightened conformations due to intramolecular electrostatic repulsion. This effect is

further enhanced in aqueous solutions, as the conformation also enables maximum interaction between the hydrophilic groups and solvent molecules.[202] The rigidity of the chains depends on the charge density along the chain, but it can be altered using electrostatic screening by controlling the electrolyte concentration of the solution.[203] The straightened conformation of polyelectrolytes facilitates bonding of multiple charged sections of each chain with oppositely charged surfaces, compensating for the weakness of individual interactions. Combined with the instantaneous nature of electrostatic bonding, polyelectrolytes are mainly used in analysis and filtration of flowing media.[204,205] However, as mentioned in section 2.2.1, electrostatic interactions of polyelectrolytes are complicated and research is still being conducted to develop more accurate models for such systems. Several theories based on VO have been developed that account for the phase separation between polyelectrolytes. However, forming a quantitative theory is challenging due to the numerous relevant variables in systems, including polymer chain length, charge density and electrolyte concentration.[134] Therefore, much of the current knowledge of polyelectrolyte systems is based on experimental data and is often confirmed only for specific polyelectrolytes.[206–208]

The quaternized ammonium group is the most commonly used cationic functionality in polycations and multiple synthesis routes are available for production of these polymers. The monomer can be used for polymerization either in the charged quaternary form or in the neutral tertiary form and quaternized once the polymerization has been completed.[209] Configuration of polycations can also be altered, for example between linear and branched chains, which significantly affects the properties of the molecules as it changes the charge density.[210] Additionally, polymerization of cationic chains can be initiated from surfaces or macromolecules to produce cationic coatings.[211]

Recently, research of polycations has focused on copolymers and most common applications are in biomedicine as delivery agents, for example in drug[212] and DNA delivery[213,214] and gene therapy.[215] More advanced polycations include polypeptides, which can be produced with great precision over the structure,[216] and biohybrid materials, where synthetic polycations are attached to biological molecules.[217] The control over the polypeptide synthesis even enables the produced molecules to fold into α-helixes and β-sheets, incorporating spatial control into the molecules.[218] Cationic polypeptides are typically incapable of adopting α-helical folding due to electrostatic repulsion, but this can be overcome by having enough neutral peptides between the repeating cationic ones, which makes the chains more flexible.[219] Therefore, linear polypeptides can carry higher overall charge density along the polymer chain, while folded ones can form presice 3D assemblies due to the rigidity provided by the folded conformation.[220] Structures beyond the scale of polypeptides have also been achieved by using supercharged variants of proteins. They are produced by recombinant methods, enabling precise control over the number and positioning of the charged residues on the molecules.[221] They possess high charge density while maintaining their 3D structure, providing them with increased affinity towards

oppositely charged molecules compared to their native state.[222] The rigidity provided by the folded structure of the proteins has led to their use in self-assembling systems, for example 3D oriented structures of supercharged GFP[223] and catalysis systems based on ferritin containing metal oxide nanoparticles.[224]

2.4 Cyclophanes

Cyclophanes are defined as compounds including one or more aromatic rings with at least two atoms connected into another ring system than the initial aromatic ring.[225] The close proximity of the rings causes steric compression and provides the molecules with unique molecular dynamic properties.[226] They are a special group of molecules due to their rigidity arising from the aromatic rings, and their cavities, which are large compared to the molecular weight. The structure gives rise to optical and electric properties,[227] making cyclophanes applicable in host-guest chemistry[228] and catalysis.[229] Cyclophanes are also a versatile group of compounds, as the structure and size of the rings may vary and the molecules can be chemically modified, summing up to practically unlimited amount of structures.[230] However, challenges in cyclophane chemistry include designing molecules that interact with complex biomolecules, like proteins, and are soluble in aqueous solvents, as the numerous aromatic rings in the structures tend to make the molecules highly hydrophobic.[231] The latter issue can be solved by using cyclophanes with charged groups on each ring, especially if they are located on both sides of the ring structures.[232] Charges enable use of cyclophanes also in biomedicine, for example as bioreceptors[233] and in cell imaging.[234]

Multiple subclasses of cyclophanes exist, and among them macrocycles composed of interconnected phenyl rings are well-studied structures due to their high concentration of π-bonds and accessibility to guest molecules.[235] Calixarenes are one such subclass formed by phenyl rings reacting with an aldehyde connected at the meta-position. This gives the molecules a specific vase-like symmetry, which led to the name of the compounds (Greek calix means chalice). The shape causes the accessibility of the inner cavity of the cyclophanes to be different from opposing sides due to steric hindrance.[236] Specific calixarenes that all share the same overall structure are obtained from specific phenyl compounds, for example resorcinarenes are produced by reacting resorcinol with an aldehyde (Figure 11.a).[237] Similar macrocyclic cyclophanes include pillararenes, which differ from calixarenes because the rings are connected at the para-position. This gives the structures symmetrical cylindrical shape, making the molecules both conformationally stable and equally accessible from both sides (Figure 11.b).[238] This makes pillararenes especially potent as host-guest binders.[239]

Cyclophanes have multiple advanced applications, mainly related to host-guest chemistry. Delivery agents and sensors are the most obvious such applications.[240] Cyclophanes have also been studied as potential co-assembly agents in self-assembling 3D structures to provide additional functionalities into the assembled systems.[241]

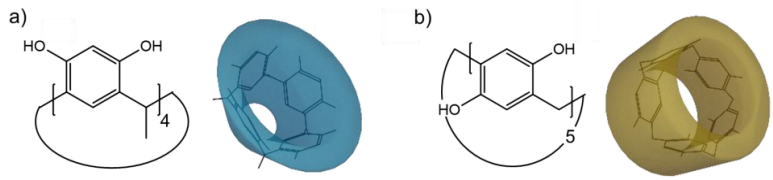

Figure 11. Molecular structures and shape representations of a) vase-like resorcin[4]arene and b) cylindrical pillar[5]arene.

2.5 Superporous Silica

Silicon dioxide, also known as silica, is an amorphous inorganic network material.[242] It is a versatile substance for production of functional materials, as it is resistant to chemical corrosion and high temperatures and is biocompatible. Therefore, it is applicable to both biomedicine and outside of body usage.[243] Due to its robustness and modifiability, silica has been a material of choice for production of porous materials, as they have numerous uses in various fields,[244] mainly as adsorbents.[245,246] Zeolites are a commonly used alternative, but they have pore sizes of only a few nanometers or even less.[247,248] With silica, specific porous materials with hierarchical pore structure can be produced with relative ease. The pore size of such structures can reach hundreds of nanometers or even few micrometers.[249] However, pore size in the mesoporous region, between 2 and 50 nm, provides porous materials with interesting properties, as it can be penetrated by atoms and low molecular weight molecules, but it retains more complex particles, for example most biomolecules.[250] The most common application of mesoporous silica, and porous silica in general, is as adsorbent in separation applications,[251] but they are also actively studied as potential delivery units in biomedicine.[252–254] In these applications control over the morphology of the material, both pores and the complete network, is beneficial as it can be used to control selectivity and efficiency of adsorption.[255] Mesoporous materials can also be used in specific recognition of large organic compounds due to the size of the pores and their spatial orientation, which is not possible for traditionally produced nanoporous zeolites.[256] Therefore, mesoporous materials have practical applications as catalysts, particle separation matrices and delivery agents.[257] Synthesis methods for such materials heve been reported already decades ago,[258,259] but alternative production methods are still sparse mostly due to demanding synthesis conditions.[260]

Inorganic porous structures are used as matrix for protein encapsulation, as this offers mechanical support and both thermal and chemical stability to the proteins while keeping them accessible for small molecules.[261] Mesoporous structures are especially effective for this as they have similar pore size to some proteins.[262] Inorganic matrices are also used to improve stability of crystalline materials that are brittle and soluble in certain solvents in their natural state.[263] Additionally, encapsulation of organic materials enables usage of the incorpo-

rated structures to produce porous materials. The organic species can be removed by calcination, which leaves the inorganic material, for example silica, intact and with empty spaces where the removed organic materials were.[264] Mesoporous silica materials have been produced in this way using protein cages as templates.[265] Cage structures can also carry additional particles into inorganic matrix inside their cavities, and if the cargo is inorganic, it is incorporated into the porous material once organic material is removed (Figure 12).[266] Large template molecules like proteins that produce one pore per molecule enable more control over the pore size than, for example, using surfactants during synthesis. Traditional surfactant methods are limited to pore sizes of a few nanometers, and increasing this size typically leads to loss in order of the structures. Compromises have been found in recent studies, but finding balance between the pore size and structural orientation remains an issue.[267] Template methods are effective when control over both aspects are required, and can be carried out using simple molecules.[255,268] However, protein templates would incorporate the systems with additional functionalities, and protein cages would enable encapsulation of other particles within the silica with controlled spatial order.[269] This is still largely unexplored research area, although some promising systems have been reported.[270,271]

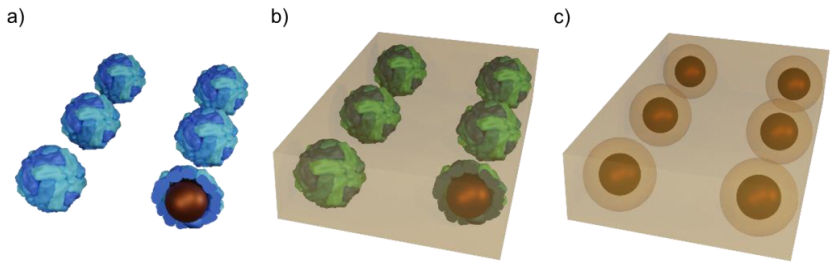

Figure 12. Schematic representation of encapsulating metal nanoparticles in mesoporous silica using ferritin template. a) Iron containing ferritin is b) encased in silica and removed by calcination, yielding c) iron nanoparticles contained inside pores in silica matrix. The images were produced using Blender and UCSF Chimera based on X-ray diffraction resolved crystal structure for PfFTn (PDB ID: 2JD6).

3. Materials and Methods

Detailed descriptions of the used materials and methods are provided in publications **I**-**VI** and only brief summary is provided here.

3.1 Apoferritin and Cowpea Chlorotic Mottle Virus

aFT used in publications **I**, **III**, **IV** and **VI** was PfFtn provided by MoLiRom in double distilled water and used without further purification. The integrity of PfFtn was confirmed using dynamic light scattering (DLS). In publication **V**, gene encoding TmFtn was purchased from Genscript and expressed in Escherichia coli (E. coli) bacteria. The cells were ruptured by sonication in lysis buffer and TmFtn separated from cell debris by centrifugation. TmFtn was further purified by preliminary membrane filtration and finally by passing it through a Superdex 200 Increase high performance size exclusion column (GE Healthcare) connected to an ÄKTA purifier. AfFtn in the same publication was ordered from MoLiRom in double distilled water and used without further purification.

CCMW used in publications **II** and **III** was obtained by infecting live cowpea with wild-type CCMV. The infected plant was blended in pH 4.7 acetate buffer-with ascorbic acid and the homogenate expressed through cheesecloth. CCMV was separated by centrifugation and precipitated using polyethylene glycol 6000.[272]

3.2 Synthesis of Block Copolymers

The block copolymers used in publication **I** were composed of two blocks: poly[2-(dimethylamino)ethyl methacrylate] (PDMAEMA), which carries an amine group in the repeating sidechain that can be quaternized to yield a cationic charge,[273] and poly[di(ethylene glycol)methyl ether methacrylate] (PDEGMA), which undergoes LCST behaviour typically close to body temperature.[274] The polymerizations were carried out using atom transfer radical polymerization (ATRP) method with ethyl α-chlorophenylacetate (ECPA) as initiator because it carries a phenyl group that can be distinguished in nuclear magnetic resonance (NMR) spectrum from the signals arising from the repeating polymer chain to facilitate determination of chain length. The PDMAEMA block was synthesized first and the polymer was purified by passing it through a neutral aluminium oxide column to remove copper used as a catalyst in the

polymerization and by precipitation from *n*-hexane to remove any unreacted monomer. The obtained polymer was then used as an initiator for the PDEGMA block, which was synthesised and purified using the same procedure. In case of the triblock copolymer, the PDMAEMA-PDEGMA diblock copolymer was used as an initiator for the final PDMAEMA block, which was synthesized and purified using the same method. The quaternization of the PDMAEMA block(s) was achieved by reacting the purified polymers with iodomethane in tetrahydrofuran. The polymer structures are presented in Figure 13. The quaternization was always carried out for the completed block copolymer, not for the intermediary synthesis products. The polymers were characterized by NMR spectroscopy using Bruker Avance 400 MHz instrument and gel permeation chromatography (GPC) analysis using a system containing 510 HPLC solvent pump, four linear PL gel columns in series and 2414 differential refractometer, all produced by Waters.

Previous studies show that binding between cationic polymers and virus cages relatively similar to aFT becomes more effective with increasing number of cationic charges per chain.[275] NMR analysis of the PDMAEMA blocks synthesized in the publication revealed them to contain approximately 50 repeating units each carrying a single charge. To ensure pronounced thermo-responsive effect, the mass ratio of quaternized PDMAEMA to PDEGMA was aimed to be 1:4. Based on NMR, in the diblock copolymer the mass ratios were 1:3.86 and in the triblock 1:3.86:0.95 (PDMAEMA:PDEGMA:PDMAEMA).

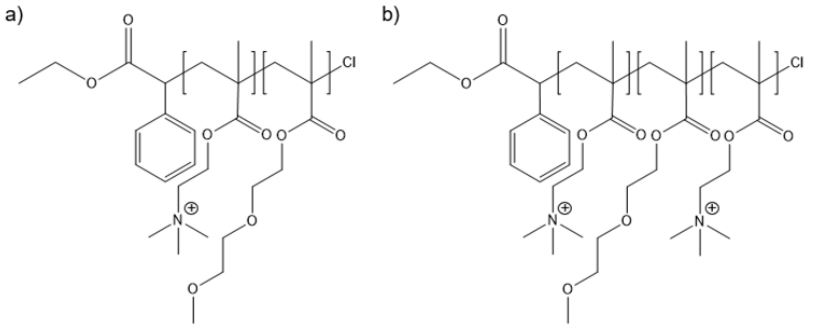

Figure 13. Molecular structures of the a) diblock PDMAEMA-PDEGMA and b) triblock PDMAEMA-PDEGMA-PDMAEMA block copolymers.

3.3 K72 and GFP-K72 Protein Expression

The cationic supercharged polypeptide genes were synthesized using recursive directional ligation. The gene fragments were subcloned into the expression vector pET25b(+). Expression was carried out in E. coli BLR (DE3) competent cells. The cells were collected using centrifugation, resuspended in lysis buffer and disrupted with a constant cell disrupter (Constant Systems Ltd.). The products were separated from cell debris by centrifugation and purified using Ni-sepharose chromatography, dialysis against ultrapure water and anion exchange chromatography using a Q HP column. After additional dialysis, the products were obtained by lyophilization.

3.4 Ferritin Crystallization and Silica Hybridization

aFT crystals were produced using hanging drop vapor diffusion (HDVD) method. $CdSO_4$ was mixed in 1 % agarose solution which was left to form a gel, and a mixture of aFT and $(NH_4)_2SO_4$, which was added to help in the precipitation of aFT from the solution, in pH 7.5 buffer solution was placed on top of it. The solution drop was hung upside down over a reservoir solution containing all the same reactants as the drop, except for aFT and agarose, but in higher concentration. The cell containing the hung drop and the reservoir solution was sealed airtightly, which caused the system to move towards equilibrium by evaporation of water from the drop into the reservoir to dilute the more concentrated solution. This triggered the crystallization of aFT, as its concentration in the drop increased. Additionally, the sharp concentration gradient of $CdSO_4$ between the agarose gel and the drop offered a nucleation point for the crystallization. The crystallization was then continued for 24–48 hours.

The produced crystals were integrated with silica gel by suspending them in a solution of prehydrolysed cationic silica precursor clusters. The solution was produced by mixing tetraethoxysilane (TEOS) and N-[3-(trimethoxysilyl)propyl]-N,N,N-trimethylammonium chloride (TMAPS) in an aqueous solution with pH 7.5. The resulting cationic clusters were attracted to the negatively charged aFT crystals due to electrostatic interactions. The crystals were first treated with glutaraldehyde to crosslink the crystal surfaces permanently into solid assemblies to prevent disassembly when they are brought to contact with the cationic clusters. Then, the silica solution was moved into a similar container where the hanging drop crystallization was carried out and the crystals were suspended in contact with the silica solution on top of a glass plate. The sol-gel condensation was continued for 7 days, after which excess silica was washed away with water.

The mesoporous silica was obtained by calcinating the sample in air at 500 °C for 4 hours.

3.5 Dynamic Light Scattering

DLS measurements were used to monitor the self-assembly processes in publications **I**-**V**. The measurements in publications **I**-**IV** were carried out using Nano ZS ZEN3600 tabletop DLS device and in publication **V** Zetasizer Nano ZSP, both manufactured by Malvern Instruments. The samples were inserted into the instrument in semi-micro UV-cuvettes made of poly(methyl methacrylate). The samples were either loaded into the cuvettes in their final solution composition and measured, or an initial solution of protein cages was prepared and the co-assembly agents were titrated into this solution during the measurements to observe the assembly-process stepwise. In publications **III** and **IV** the disassembly of the formed structures was also studied using DLS by titrating NaCl into the samples once the assembled structures had formed to reduce the supramolecular structures back to individual particles. In publications **I** and **V** the measurements were conducted also at elevated temperatures to observe

changes in the complexes and individual protein cages, respectively. The samples were heated in the cuvettes within the instruments.

3.6 Agarose Gel Electrophoresis Mobility Shift Assay

Agarose gel electrophoresis mobility shift assay (EMSA) was used in publications **II** and **III** to study the required ratio of co-assembly agent to completely assemble a set amount of CCMV. 1 % strength agarose gel stained with ethidium bromide was used. Free CCMV was used as a control sample and sample wells in the gel were loaded with CCMV complexed with an increasing amount of co-assembly agent to determine the minimum concentration at which migration of CCMV is completely halted. In publication **II** 10 mM sodium acetate (NaAc) with 1 mM ethylenediaminetetraacetic acid (EDTA) and pH 4.7 was used as a running buffer and the gel was run at 100 V for 35 min. In publication **III** 10 mM NaAc with pH 4.8 was used as a running buffer and the gel was run at 145 V for 35 min. The images were obtained using Bio-Rad Gel DocTM EZ imaging system.

3.7 Electron Microscopy

3.7.1 Transmission Electron Microscopy

Transmission electron microscopy (TEM) images in publications **I** and **II** were obtained using FEI Tecnai 12 Bio-Twin instrument with 120 kV accelerating voltage in bright field mode. The samples were imaged on square mesh copper grids. The samples in publication **I** were stainednegatively with uranyl formate and in publication **II** with uranyl acetate.

Cryogenic transmission electron microscopy (cryo-TEM) images in publications **III**-**V** were obtained using JEOL JEM 3200FSC field emission microscope operated at 300 kV in bright field mode. The samples were placed on plasma cleaned square mesh copper grids, which were frozen by plunge freezing in 1:1 volume ratio liquid propane-ethane mixture with 3 seconds blotting time. During the imaging, the samples were kept at -187 °C.

3.7.2 Scanning Electron Microscopy

Scanning electron microscopy (SEM) images in publication **VI** were obtained using Zeiss Sigma VP SEM with 8.0 kV accelerating voltage and an InLens detector. The samples were attached to aluminium sample stubs using a double-sided graphene tape and prior to imaging the samples were sputtered with 1 nm iridium coating to improve conductivity.

3.8 Small Angle X-Ray Scattering

Small angle X-ray scattering (SAXS) scattering patterns of publications **III**-**V** were recorded using a homemade device consisting of a Bruker Microstar mi-

crofocus X-ray source (Cu Kα radiation), an Incoatec Montel multilayer focusing monochromator, four JJ X-Ray collimating slits and a Bruker Hi-Star two dimensional (2D) area detector. All the scattering data were recorded with a 1.59 m sample to detector distance and all the instrumentation apart from the detector were held under high vacuum in order to avoid scattering from air. In publication **VI**, SAXS was measured using Xenocs Xeuss 3.0 instrument. Cu Kα radiation source was used, the sample to detector distance was 600 mm and the entire instrument, including the detector, was kept under vacuum during the measurements.

For all the measurements, the scattering vector q was calibrated using a silver behenate standard and the 2D scattering data were converted into SAXS curves by azimuthal averaging. The samples were sealed within steel washers and covered from both sides with Kapton film that scatters no X-rays in the measured q region.

4. Results and Discussion

In this section the results of the publications are discussed in their numerical order. All obtained results are presented in the publications and only the results most relevant to the production and characterization of self-assembled protein cage structures are presented here in detail.

4.1 Self-Assembly with Organic Synthetic Materials

4.1.1 Thermo-Responsive Self-Assembly of Ferritin

In publication **I**, aFT was complexed with synthetic block copolymers carrying both cationic and thermo-responsive segments. The research was an attempt to controllably trigger supramolecular self-assembly of aFT without need for chemical or genetic modifications of the protein. The self-assembly process is controlled by two separate phenomena: the electrostatic interaction between cationic PDMAEMA block of the polymer and anionic aFT, and the thermo-responsive solubility of the PDEGMA block into the surrounding aqueous media. The electrostatic interactions bind the molecules together but increasing the surrounding electrolyte concentration enough will cause disassembly, as the interactions become screened. The thermo-responsive block undergoes LCST behaviour in water, enabling control over the self-assembly of the system by an external stimulus. This behaviour is reversible, and it is possible to go back and forth between the two states by increasing and decreasing the temperature. As the system undergoes changes in response to alterations in temperature and electrolyte concentration of the solution, it can be considered multi-responsive.

DLS measurements revealed the thermo-reponsive tendencies of the system, which were studied as a function of both temperature and electrolyte concentration of the solution (Table 1, Figure 14). The polymer solutions were titrated into sample solutions with initial aFT concentration of 100 mg/L and varying concentration of NaCl. The salt concentration alters the strength of the electrostatic attraction between the PDMAEMA and aFT but does not affect the hydrogen bonding between PDEGMA and the solvent as significantly. Hypothetically, an electrolyte concentration region should exist where cationic blocks keep the polymers attached to aFT surfaces, but electrostatic interactions are screened enough that polycations do not cause adjacent proteins to bind with each other, which would cause aggregation regardless of the state of the thermo-responsive block. Such conditions enable supramolecular self-assembly to be triggered by

turning the thermo-responsive block hydrophobic, as they collapse to the surface of the aFT and render the protein hydrophobic as well, causing them to aggregate. At low salt concentrations (150 mM and below), the electrostatic interactions between aFT and PDMAEMA remained so strong that aggregates were formed regardless of the temperature, as κ^{-1} was likely so large that individual polymers could affect two or even more proteins at once, pulling them together. At higher NaCl concentrations (200 and 250 mM), the electrostatic interactions were screened enough that PDMAEMA alone could no longer cause aggregation. However, it was still holding the polymer chains attached to aFT, and as the temperature was increased above LCST, aggregation was observed. Increasing polymer concentration had the tendency to slightly decrease the size of the formed aggregates, likely because diminishing the number of aFT charges enabled more dense packing. At even higher NaCl concentration (300 and 350 mM), the effect of the polymer concentration changed and the aggregates form at the higher temperature only at low polymer concentration. Addition of polymer into the sample disassembled the system back to free particles.

Table 1. Thermo-responsive behaviour of PDMAEMA-PDEGMA block copolymers observed in DLS measurements.

NaCl	25 °C, 20 mg/L polymer	25 °C, 80 mg/L polymer	50 °C, 20 mg/L polymer	50 °C, 80 mg/L polymer
100 mM	aggregation	aggregation	aggregation	aggregation
200 mM	free particles	free particles	aggregation	aggregation
300 mM	free particles	free particles	aggregation	free particles

The study was conducted using both diblock and triblock copolymers. Diblock had one cationic and one thermo-responsive block, and in triblock the thermo-responsive block was located between two cationic blocks. To enhance the effect of the thermo-responsive block, its mass ratio to the cationic block was roughly double. Hence, in triblock copolymer PDMAEMA blocks were half the mass of the PDEGMA block each. Complexes of triblock copolymer and aFT followed the same general behaviour as diblock complexes, but the effects were more enhanced. The trend of decreasing aggregate size with increasing polymer concentration was more profound than with diblock complexes, assumedly because a single triblock chain could link two aFT molecules together more effectively even at high NaCl concentrations. Additionally, more triblock polymers brought the proteins closer together and diminished the size of the aggregates. At 300 and 350 mM NaCl solutions, triblock complexes displayed thermo-responsive behaviour through a broader polymer concentration range than diblock complexes before disassembling back to free particles.

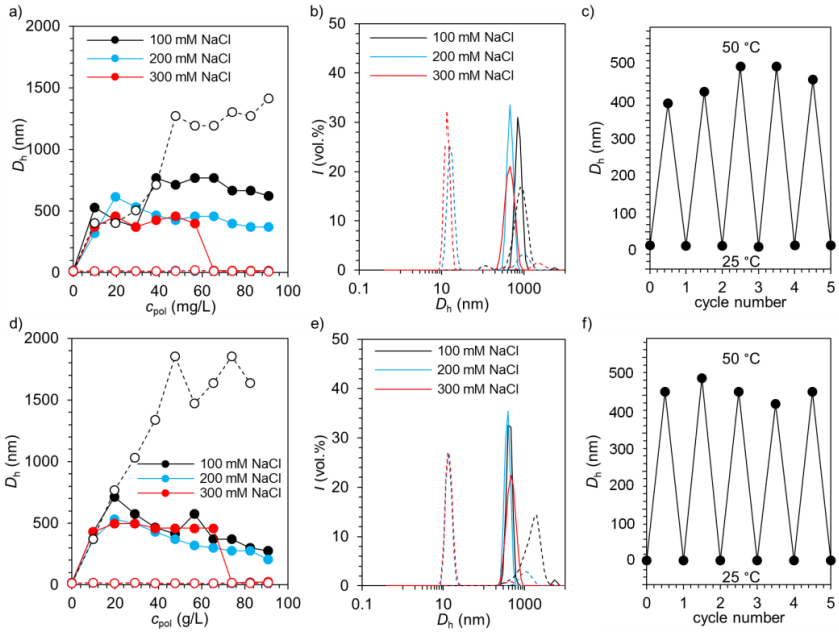

Figure 14. DLS data of aFT self-assembly with the thermo-responsive di- and triblock copolymers. In graphs a), b), d) and e) dashed lines and empty symbols represent measurements at 25 °C and full lines and filled symbols at 50 °C. a) Hydrodynamic diameter of titration of diblock copolymer into aFT solution in three different NaCl concentrations. b) Volume distributions of assemblies from graph a) at polymer concentration 50 mg/L at both temperatures. c) Hydrodynamic diameter of aFT assemblies at 50 mg/L polymer and 200 mM NaCl solution when repeatedly cycled between 25 and 50 °C. Graphs d–f) are identical to a–c), respectively, except that triblock copolymer is used instead of diblock.

The results of DLS measurements were confirmed using TEM imaging. The temperature of the samples could not be controlled in real time during the imaging, so the sample preparation and drying was done at both room temperature (Figure 15.a-c) and at 50 °C (Figure 15.d–e) to induce the effect of thermo-responsiveness. The images showed that presence of polymers led to association between neighbouring aFT even in samples prepared at room temperature. This was expected as the samples did not contain NaCl as its concentration would have increased in the samples during the drying and disassembled the structures. Heavy aggregation was observed in the samples prepared at 50 °C even though they were smaller than DLS results would have led to expect. This was likely an artefact caused by drying of the samples, as the role of solvent molecules in the sytems was lost. No significant differences were observed between the samples containing diblock and the ones containing triblock copolymers.

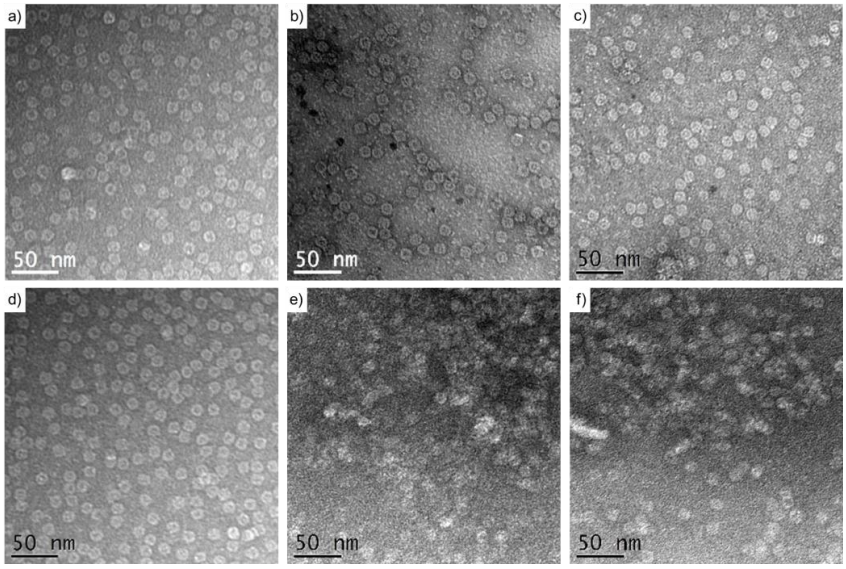

Figure 15. Negatively stained TEM images of the aFT assemblies with thermo-responsive di- and triblock copolymers. a) Free aFT without polymer. b) aFT complexed with diblock copolymer. c) aFT complexed with triblock copolymer. Images d–f) had identical sample compositions as a–c), respectively, but sample preparation was done at 50 °C while a–c) were prepared at 25 °C. All the polymer containing samples had a polymer to protein mass ratio of 1:2.

4.1.2 Aggregation of CCMV with Cationic Lignin

In publication **II**, the effectiveness of colloidal lignin particles with cationic surface charge (c-CLPs) to form aggregates with CCMV was studied in aqueous solutions. This method could find practical applications in wastewater treatment or purification of drinking water in areas where safe potable water is hard to find. Lignin is available in high amounts and the purification method has low energy requirements, making it viable for both uses. Anionic colloidal lignin particles (CLPs) and dissolved cationic lignin were used for comparison in the aggregation experiments to confirm the effects of cationic charges and colloidal morphology. These species were used for comparison because c-CLPs were produced by adsorbing cationic lignin onto CLPs.

DLS measurements revealed CLPs to have a diameter of roughly 109 nm and c-CLPs 122 nm, making them approximately four times larger than the CCMV capsid. At a weight ratio of c-CLPs to CCMV of 4:1 in water, particles with an average diameter of 207 nm were detected, suggesting aggregation as the diameter was larger than if c-CLPs would have a monolayer of CCMV adsorbed onto their surface (Figure 16.a). Additionally, in this mixing ratio no free CCMV was detected with DLS, suggesting either complete uptake or at least reduction of CCMV concentration below the detection limit of the used instrument setup.

Gel EMSA experiments were carried out to compare binding efficiencies of c-CLPs, CLPs and cationic lignin with CCMV. With a constant CCMV concentration and steadily increasing amount of lignin species, it was shown that all the tested lignin materials hindered the migration of the virus (Figure 16.b). This suggests that the electrostatic interactions were not the only forces driving the

assembly, as even the anionic CLPs caused aggregation. However, c-CLPs were found to be the most effective co-assembly agents, as they resulted in the greaest reduction in the amount of migrating CCMV under the tested conditions. The gel EMSA results were quantified by relating band intensity to CCMV concentration to highlight the differences between the samples (Figure 16.c). The mechanism of binding appears to be different for CLPs and c-CLPs, as the anionic particles began to hinder the migration of the virus at lower lignin concentrations than the cationic ones, but did not ultimately reach the same efficiency. Previous literature suggest that hydrophobic interactions may significantly contribute to the binding.[276,277] In case of c-CLPs, it is likely that the same interactions that were present in CLP systems were enhanced by the electrostatic interactions, even if the overall strength of the hydrophobic interactions may have decreased due to improved solubility caused by the highly charged surface. The combined effects resulted in higher affinity for CCMV at high concentration of the cationic species than CLPs have.

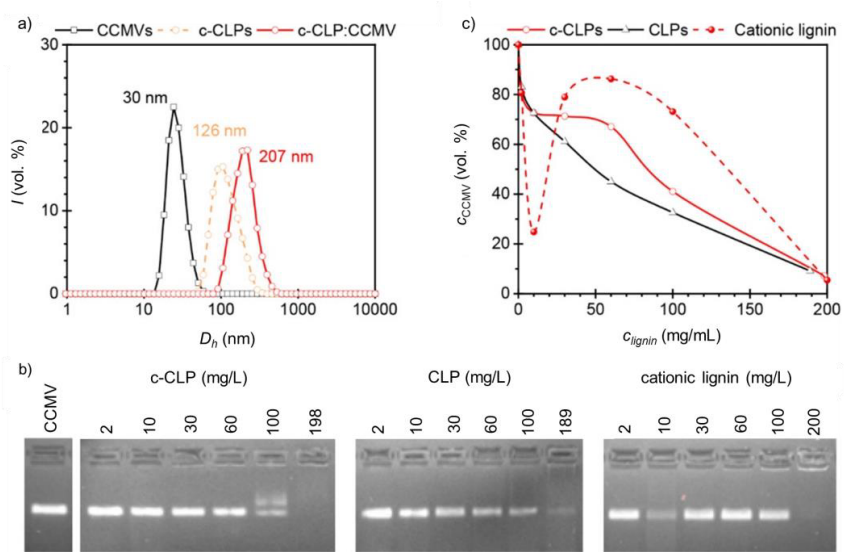

Figure 16. Complexation of CCMV with lignin. a) DLS measurements of free CCMV, lone c-CLPs and CCMV complexed with c-CLP. b) Agarose gel EMSA images of free CCMV and CCMV complexed with c-CLPs, CLPs and cationic lignin. The CCMV concentration was constant in each sample (50 mg/L) and lignin concentration increased in each well from left to right. c) Quantification of results from b) by relating band intensity to virus concentration. Data point of CCMV complexed with cationic lignin at 10 mg/L lignin concentration may be an outlier, as the observation deviates from otherwise fairly consistent pattern and in b) the band is clearly different to previous and next well.

As stated above, the practical applications of virus aggregation include removal of viruses from water supplies. The small size of viruses makes them difficult to be removed from solutions and their neutralization typically requires large energy input or usage of potentially hazardous compounds. Lignin is a tempting alternative as it is environmentally friendly and available in large quantities at a relatively low price. Even though EMSA results suggest that c-CLPs were not

as effective as virus removal or inactivation methods based on halogen compounds[278] and heavy metals,[279] they could be used as a pretreatment step to lower the energy and materials requirements of subsequent steps. In the publication, c-CLPs were shown effective for removal of CCMV as aggregates by both centrifugation-assisted sedimentation and filtration (Figure 17). At a weight ratio of c-CLP to CCMV of 2:1, the centrifugation method reduced the CCMV concentration of the sample by approximately 75 % and filtration by 79 %. The filtration experiments were done through a porous filtering membrane by syringe filtration using a pore size of 0.45 μm, which was larger than the observed aggregates. Therefore, the efficiency of CCMV removal might have been further enhanced by using a denser membrane. This membrane was also shown to be ineffective in filtering out CCMV that had not been complexed with lignin. Repeated aggregation and removal cycles may improve the efficiency of the process, but this was not tested. To better simulate wastewater treatment, the centrifugation method was also tested in solutions containing NaCl, $CaCl_2$ and Na_2SO_4, as in real conditions other impurities besides viruses are also present, and low molecular weight electrolytes can affect the aggregation by screening. All the solutions had a salt concentration of 1 mM, which is comparable to typical wastewater samples from real systems.[280–282] Two-way analysis of variance of the obtained results showed that the presence of salts could not be said to affect the efficiency of CCMV removal (p-value 0.17) but the difference between binding with c-CLPs and CLPs was significant (p-value 0.01). Thus, the charge of c-CLPs contributed to the aggregation even in the presence of additional electrolytes.

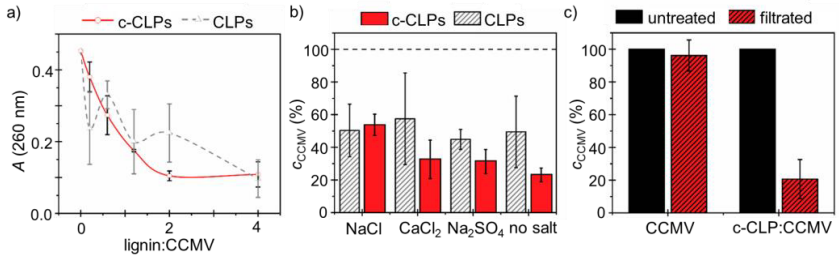

Figure 17. CCMV removal from water by centrifugation and filtration. a) Absorbance of supernatant after centrifugation as a a function of ligning to CCMV ratio. b) Remaining CCMV concentration in supernatant after centrifugation in 1 mM NaCl, $CaCl_2$ and Na_2SO_4 solutions and water with lignin to CCMV ratio of 2:1. c) Remaining CCMV concentration in solution after filtration though 0.45 μm porous membrane in solutions with and without c-CLPs (c-CLP to CCMV ratio 2:1).

4.2 Crystalline Hybrid Self-Assembly

Publication **III** describes self-assembly of both CCMV and aFT with a recombinant fusion protein. The protein was GFP appended with supercharged cationic polypeptide K72, which was composed of 72 repeating polypeptide blocks with a sequence GVGKP (where G is glysine, V valine, K lysine and P proline). The polypeptide was a linear chain extending out from GFP where it was covalently linked and each K residue carried a positive charge. Due to the additional amino

acid residues in K72 besides lysine, the chain was relatively flexible despite the high amount of charges. This provided the recombinant protein with more freedom in the self-assembly compared to if the charges were fixed on the surface of GFP. The study describes a proof-of-concept system and demonstrates that neutral proteins can be incorporated into electrostatically self-assembling protein cage systems by providing them with charged tags. The system enabled reversible assembly of multiple complex functional particles and used only the exterior of the protein cages as binding sites, leaving the cavity potentially available for additional particles.

Formation of the assemblies was studied using DLS by titrating cationic species into an initial sample solution containing either CCMV or aFT. For comparison, the studies were conducted using both the recombinant protein GFP-K72 and only the cationic peptide chain K72 without GFP (Figure 18.a-b). CCMV complexes formed at a very low concentration of both GFP-K72 and K72 and the samples retained constant derived count rate with further increase of the cationic species. Assemblies containing GFP were larger than those that did not, which was expected as GFP is itself a folded protein structure and each of them occupied a space of some nanometers in diameter. Self-assembly of aFT complexes proceeded in a different manner, as the size of the assemblies kept increasing with concentration of the cationic species. Initially, the count rate also increased during the titration, but it reached a peak at aFT to cationic species weight ratio of approximately 5:2 and dropped steeply with further addition of cationic species. Count rate in DLS indicates the number of scattered photons that reach the detector and it increases with both size and number of particles in the solution and is dependant on properties of the particles, for example their refractive index and adsorption.[283] As hydrodynamic radius of the complexes increased steadily throughout addition of the cationic species, the initial increase and following decrease in count rate suggest that a large amount of aggregates was formed first and they later combined with each other into larger complexes, possibly causing sedimentation. Both K72 and GFP-K72 complexes had similar trend in count rate, but GFP-K72 complexes went through it at lower concentration than K72 complexes.

All CCMV and aFT aggregates with both K72 and GFP-K72 could be disassembled by increasing the overall electrolyte concentration in the sample solution by adding NaCl (Figure 18.c-d). CCMV complexes and aFT – K72 complex underwent rapid decrease in count rate with increasing NaCl concentration after a high enough concentration had been reached, but aFT – GFP-K72 complex behaves differently. The count ratio increased sharply at low NaCl concentration, but then plummeted with additional increase. This suggests that the assemblies first broke into numerous small particles which then disassembled. The data imply that the CCMV and aFT assemblies were different from each other, and aFT – K72 and aFT – GFP-K72 complexes still different with each other.

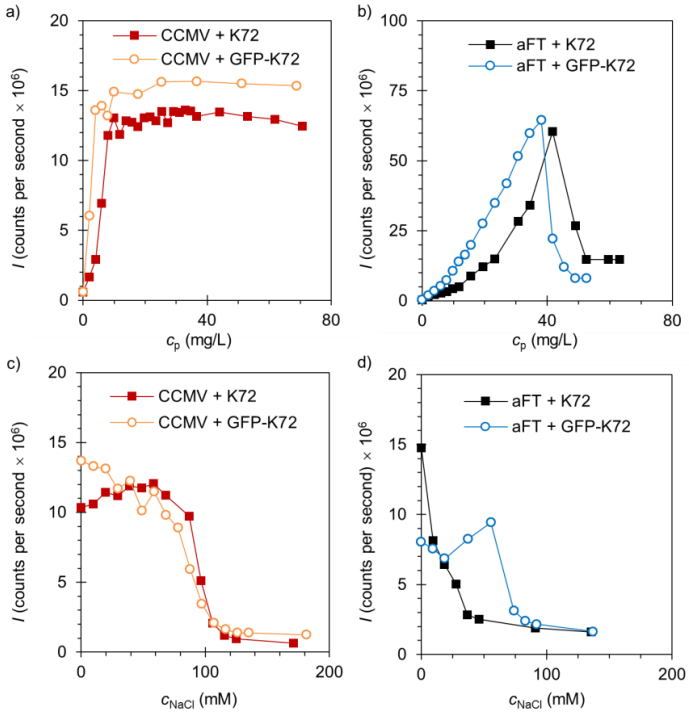

Figure 18. DLS measurements of CCMV complexed with K72 and GFP-K72. a) CCMV and b) aFT self-assembled in different ways, resulting in different scattering curves. The assemblies formed by c) CCMV and d) aFT disassembled when NaCl is titrated into the solution, but aFT – K72-GFP complexes followed a unique disassembly path.

SAXS analysis was used for further characterization of the assemblies. CCMV complexes with both K72 and GFP-K72 were arranged into crystalline lattices with a face centered cubic (fcc) structure (Figure 19.a). The packing was dense, as the smallest distance between the CCMV was calculated to be 28.5 nm, only 1.02 times the diameter of the cage. This suggests there was only a small amount of K72 between the viruses and GFP was confined within the voids of the assembled structure, as it would not have fitted into the interfaces between CCMV cages. aFT also assembled into fcc lattices when complexed with K72. These structures were not as compact as CCMV complexes, as the separation between neighbouring aFT cages was 14.0 nm, 1.17 times their diameter. The difference in the packing density could be explained by the smaller size of the aFT compared to CCMV, causing absolute distances between these two cages to be relatively larger for aFT. Additionally, aFT – GFP-K72 complexes did not form crystal lattices under the studied conditions. The pores between aFT units in a crystal lattice would likely be too small to house GFP and GFP-K72 is not rigid enough to act as a co-assembly agent (Figure 19.b). This likely led to formation of amorphous structures.

The presence of crystalline lattices was confirmed by cryo-TEM imaging to eliminate any artefacts caused by drying of the samples. Both CCMV complexes were crystalline throughout the samples and the spatial orientation could be clearly seen in the bevelled pattering of the particles (Figure 19.d–e). aFT – K72

had crystalline and amorphous regions (Figure 19.f) but no clear crystalline regions were observed in aFT – GFP-K72 complexes (Figure 19.g).

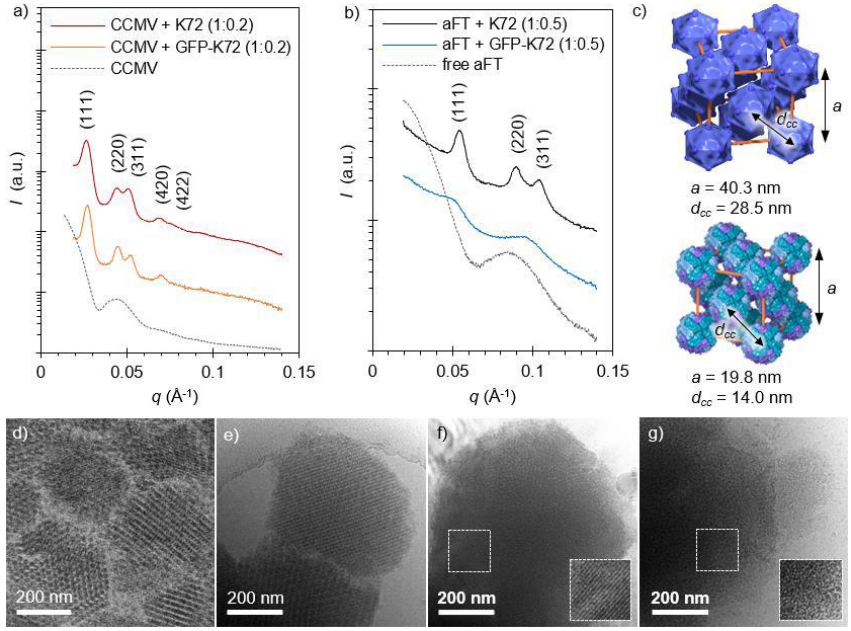

Figure 19. SAXS and cryo-TEM analysis of the protein cages complexed with the fusion proteins. SAXS scattering patterns from a) CCMV complexes with K72 and GFP-K72 and b) aFT complex with K72 were used to calculate c) the crystal dimensions of the assembled structures. aFT – GFP-K72 was not crystalline. The datasets in a) and b) have been separated vertically to avoid overlapping of the curves. Cryo TEM images of d) CCMV – K72 and e) CCMV GFP-K72 showed clear crystalline structures throughout the samples, but f) aFT – K72 was only partially crystalline and g) aFT – GFP-K72 not at all. The square areas separated by dashed lines in f) and g) are magnified in the insets of the images.

In publication **IV**, multifunctional self-assembling host materials were developed by complexing aFT with synthetic cyclophanes using electrostatic interactions. Two cyclophanes were used, cup shaped resorcin[4]arene and cylindrical pillar[5]arene. A library of these molecules carrying different amounts of cationic charges and neutral spacers were prepared, as well as a control resorcin[4]arene carrying only neutral and negatively charged groups. The used cyclophane molecules are presented in Figure 20.a and are from here on referred to by their number of charged groups, resorcin[4]arenes being R(16+), R(8+), R(4+) and R(4-) and pillar[5]arenes P(10+) and P(5+). The self-assembly of these molecules with aFT was studied in aqueous solutions of varying NaCl concentration and pH to tune the strength of the electrostatic interactions.

The self-assembly process was initially followed by DLS to determine the optimal ratio of cyclophanes to aFT (Figure 20.b). Due to their high charge density, R(16+), R(8+) and P(10+) had a strong tendency to assemble and cyclophane to protein mass ratio of less than 1:5 was sufficient to reach stable structures. The lower amount of cationic charges on R(4+) and P(5+) did not achieve similar binding and mass ratio of 1:2 was required for assembly and even then the derived count rate was much lower than in the complexes formed with the more

densely charged cyclophanes, suggesting fewer or smaller assemblies or both. As expected, R(4-) did not undergo any assembly with aFT under the studied conditions. The results suggest that electrostatic interactions were the driving force for the self-assembly, which was further confirmed by titration of the formed assemblies with NaCl solution. All the formed assemblies could be disassembled in this manner, but P(10+) underwent more dramatic decrease in derived count rate (Figure 20.c). This is likely because the resorcinarenes possessed some amphiphilic nature due to their asymmetrical shape and different functional groups on different sides of the ring, decreasing the effect of the electrostatic interactions. P(5+) did not achieve high degree of assembly to begin with, which is why the disassembly also had less dramatic effect.

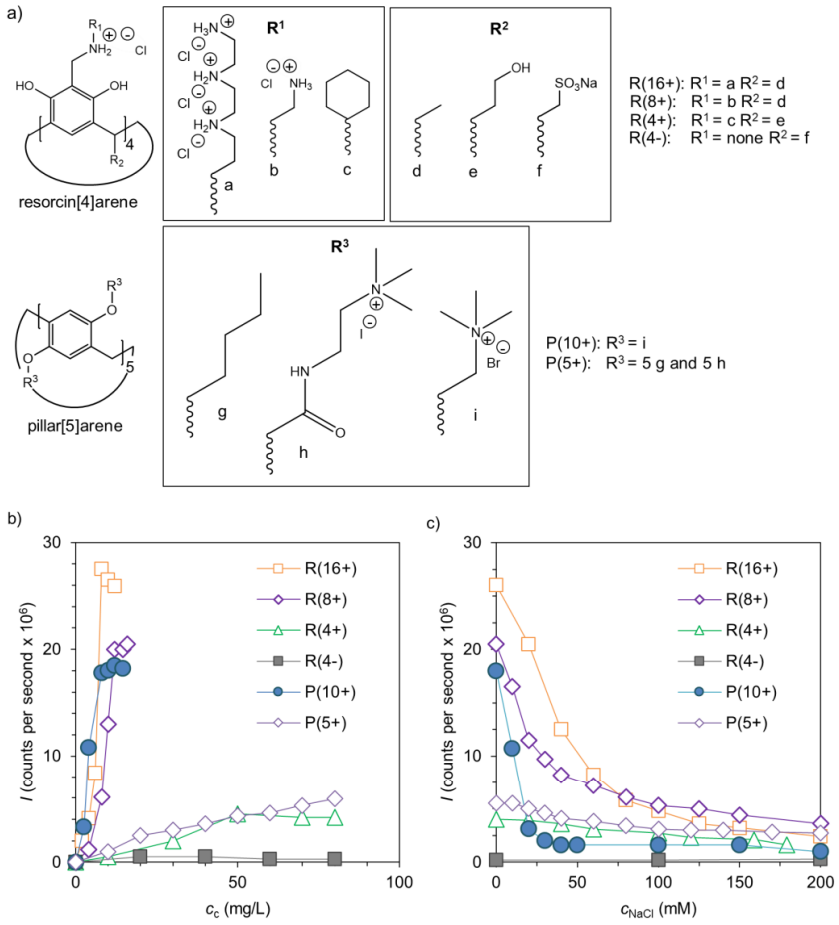

Figure 20. Cyclophane structures and DLS analysis of complexation with aFT. a) Structures of resorcin[4]arenes and pillar[5]arenes modified to carry specific amount of charges. DLS figures of b) aFT self-assembly when solution was titrated with the cyclophanes and c) disassembly of the formed complexes when titrated with NaCl. The titration of R(16+), R(8+) and P(10+) was stopped when the derived count rate ceiced to increase.

The assembly was further optimised by complexing all the cyclophanes with aFT at solutions with NaCl concentration varying between 0 and 40 mM and studying the assemblies with SAXS (Figure 21.a). A low concentration of low molecular weight electrolytes was assumed to enable the assemblies to form by dynamic mechanism striving for equilibrium, favouring highly ordered structures due to the symmetry of both aFT and the cyclophanes. However, the only sample which produced assemblies with a high degree of order was P(10+) in 20 mM NaCl solution. For resorcinarenes, the inability to form ordered structures was likely due to the amphiphilic nature of the molecules. For P(5+) the number of charged groups was supposedly not high enough to direct the self-assembling of aFT. In P(10+) the symmetry and amount of charges were both optimal, enabling formation of crystals that SAXS confirmed to have fcc structure (Figure 21.b). Distance between the neighbouring aFT centres was 14.5 nm, which equals 1.21 times the diameter of aFT. This implicates that P(10+) was not housed only in the voids in the structure, but also between neighbouring aFT cages preventing them from getting into close proximity of each other. The suggested structure was further confirmed by cryo-TEM imaging, which showed clear spatial orientation where all the fcc projections could be detected and an integration of the profile along the [110] projection axis also yielded distance of 14.5 nm between neighbouring aFT (Figure 21.c–e). Individual P(10+) molecules could not be distinguished in the images, but the aFT structure could be observed to be highly porous and capable of housing the cyclophane in the voids.

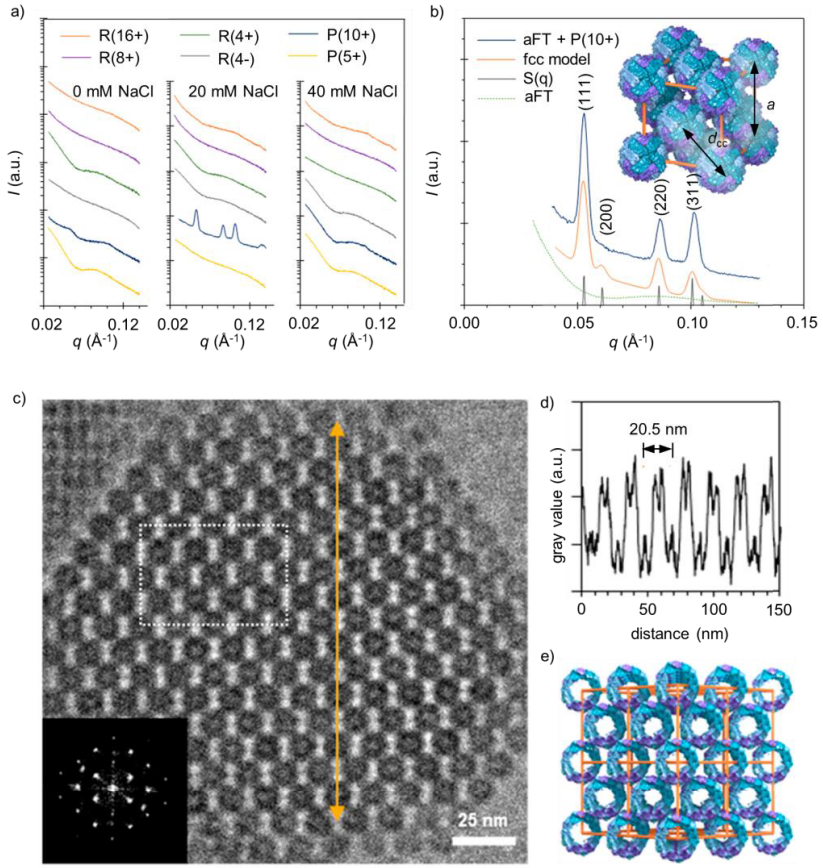

Figure 21. Analysis of the aFT-cyclophane complexes. a) SAXS analysis of aFT complexed with all the studied cyclophanes in varying NaCl solutions, where b) P(10+) complexes at 20 mM showed fcc structure with a = 20.5 nm and d_{cc} = 14.5 nm. The datasets in a) and b) have been separated vertically to avoid overlapping of the curves. c) Cryo-TEM image of the crystal viewed along the [110] projection axis and the fast Fourier transform along the same axis (inset) showed the high order of the structure. d) Integrated profile along the yellow arrow in c) supports SAXS result a = 20.5 nm. e) Schematic representation of the area marked by dashed white line in c) demonstrates the porous structure of the crystals.

4.3 Self-Assembly of Enzyme Loaded Ferritin

In publication **V**, self-assembly properties of TmFtn were studied, both the ability of individual protein cages to disassemble and reassemble to encapsulate cargo molecules, as well as co-crystal self-assembly of the cages with AuNPs. Self-assembly of TmFtn was compared with that of AfFtn, which was described in section 2.1.1 to undergo facile cargo encapsulation. AfFtn possesses tetrahedral symmetry which leaves the cargo exposed to environmental factors, unlike TmFtn which has more closed octahedral symmetry. TmFtn also has the advantage of undergoing electrolyte induced self-assembly and it is shown to be thermostable, making it the superior choice for encapsulation processes, as it can protect the cargo in more demanding conditions. The robust cage is ideal for directed assembly of cargo molecules. Self-assembly of TmFtn was studied using cages loaded with lysozyme enzyme to ensure that loading does not hinder

the process and the cage can be used to incorporate additional biomolecules into the structures. Lysozyme is positively charged, increasing its affinity towards the oppositely charged cavity within TmFtn.

Supramolecular self-assembly of both proteins was induced using cationic AuNPs consisting of a solid gold core that has a diameter of 2.5 nm and cationic ligand surface, and the entire particles had a hydrodynamic diameter of 8.5 nm.[136] SAXS analysis of the lysozyme carrying TmFtn and AuNP complexes was conducted in aqueous solutions with NaCl concentration ranging from 0 to 90 mM to enhance formation of ordered assemblies (Figure 22.a). The data show that up to 60 mM NaCl TmFtn and AuNP were both arranged into interpenetrating fcc structures of equal spacing, making the ratio of the particles in the lattices 1:1 (Figure 22.b). Too low or too high electrolyte concentration reduced crystallinity of the samples, with optimum found at 20 mM NaCl. The spacing of neighbouring particles was determined to be 14.5 nm, which is 1.21 times the diameter of TmFtn. These dimensions match perfectly with an fcc model of spheres with dimensions of 12.0 and 8.5. The structures were further confirmed by cryo-TEM, in which highly ordered regions stretching over several hundred nanometers could be observed, as AuNPs give excellent contrast to the images (Figure 22.c). The separation between neighbouring particles could be determined to be 14.4 nm, corresponding well to the SAXS data (Figure 22.d). Furthermore, lysozyme activity assay showed that the lysozyme encapsulated in the assembly to remained enzymatically active (Figure 22.e). However, the activity was reduced to roughly half of that of free and aFT encapsulated lysozyme that were not assembled into crystals. This is most likely due to decreased access of substrates to the enzymes at the centre of the assemblies.

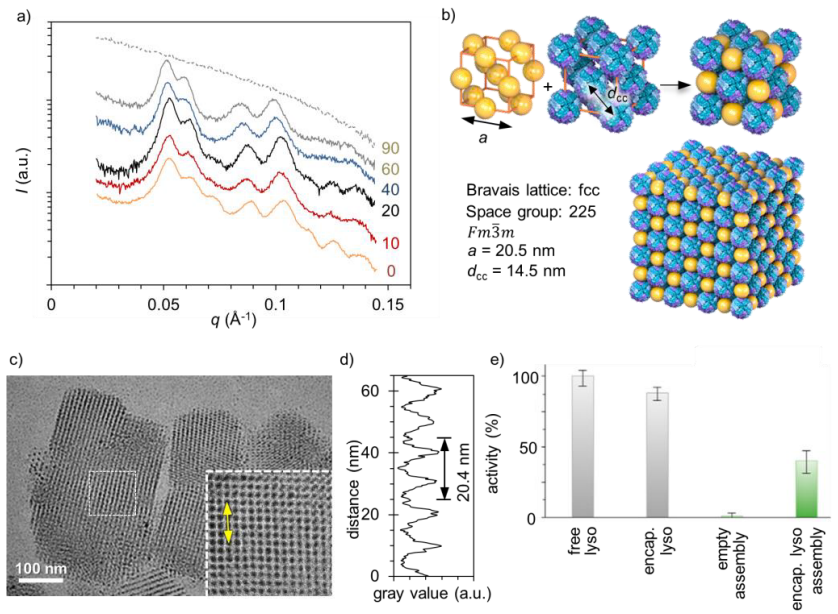

Figure 22. Self-assembly of TmFtn loaded with lysozyme and AuNPs. a) SAXS data of the complexes in varying NaCl concentration. Samples at 20 mM NaCl showed the most distinct scattering pattern. The datasets have been separated vertically to avoid overlapping of the curves. b) Schematic presentation of the interpenetrating fcc structures of TmFtn and AuNP with calculated spatial distances a = 20.5 nm and d_{cc} = 14.5 nm. c) Cryo-TEM image of the crystal structures. The inset is a magnified view along the [100] projection axis from another similar area of the same sample, where d) an integrated profile along the yellow arrow yielded average period between the particles a = 20.4 nm. e) Lysozyme activity assay from free and TmFtn encapsulated lysozyme, assembly with empty TmFtn and assembly with lysozyme encapsulated TmFtn.

Self-assembly of AfFtn with AuNPs was also studied to compare the difference between the octahedral and tetrahedral symmetry. The channels along the 3-fold axes house specific charged sites and are likely relevant for the electrostatic self-assembly of the cages, likely leading to differences in the formed assemblies of the two ferritin.[284] Under the same conditions used for screening with TmFtn, no crystalline lattices were detected in SAXS measurements (Figure 23.b). The data have distinguishable pattern that was suppressed with sufficiently high NaCl concentration in the solution, but this could not be fitted with any closely packed crystal model. The scattering may well have arisen from several separate factors in the samples which are difficult to separate from each other and the structure of the assemblies was likely amorphous. Therefore, TmFtn was found more effective for guiding encapsulated molecules into crystalline lattices.

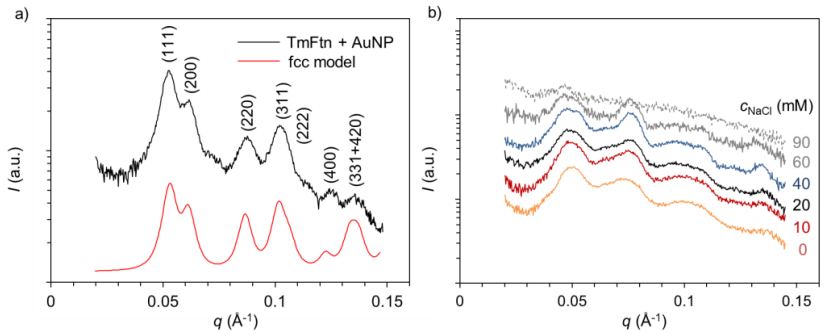

Figure 23. Comparison of TmFtn and AfFtn self-assembly with AuNPs. a) At 20 mM NaCl solution, TmFtn complexes can be fitted with $Fm\bar{3}m$ model and scattering maxima in the data can be identified, but b) AfFtn does not form assemblies with similar crystal structures in the measured solution conditions. Thee datasets have been separated vertically to avoid overlapping of the curves.

4.4 Mesoporous Silica from Ferritin Scaffolds

Publication **VI** describes synthesis of mesoporous silica by using aFT crystals as templates. Crystals were encased in silica using a sol-gel reaction and the proteins were removed by calcination. Such method transfers the well-oriented structure of the crystals into the silica, resulting in material with uniform size and specific spatial orientation of the pores.

aFT was crystallized using Cd^{2+} ions from $CdSO_4$ as co-assembly agents. The small size of the ions led to densely packed aFT crystals, as the cations only comprised a small portion of the assemblies. The crystallization was carried out using HDVD and $CdSO_4$ was encased in agarose gel to promote growth of large crystals. Optical microscopy (OM) and SEM showed octahedral crystals which reached dimensions of over 100 µm in diameter (Figure 24.a–b). SAXS analysis revealed the crystals to have a dense fcc structure with 13.0 nm between centres of two neighbouring aFT cages, only 1.08 times the diameter of the proteins (Figure 24.c–d).

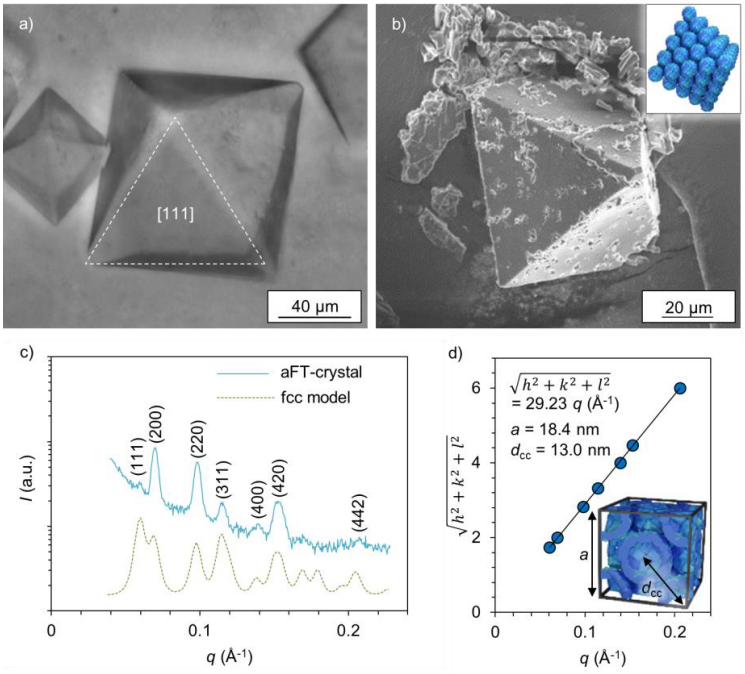

Figure 24. aFT crystallization with $CdSO_4$. a) OM and b) SEM showed large octahedral crystals formed by eight [111] planes. c) Fcc structure was identified in SAXS analysis and d) linear fit of the quadric Miller indices of assigned reflections for $Fm\bar{3}m$ as a function of measured *q*-vector positions yielded lattice dimensions ***a*** = 18.4 nm and d_{cc} = 13.0 nm.

The crystals were encased in silica by a sol-gel reaction with TEOS and TMAPS, which were pre-hydrolyzed into small cationic clusters that condensed slowly into silica network. The precursor clusters were attracted to the crystals by electrostatic interactions, concentrating the silica formation inside and around them, resulting in individual crystals encased in silica. They retained their 3D structure, as the octaherdral structure of the objects could be clearly seen after the sol-gel reaction in both OM and SEM images (Figure 25.a-b). SAXS suggests that the material still had fcc structure with the same dimensions as the unmodified aFT crystals (Figure 25.e), although the scattering peaks are not as as distinct as for the free crystals. The signals could be improved by further optimization of the sol-gel process, as in the current setup the precise concentration of aFT and silica in the solution cannot be known and the amounts of material may have been insufficient.

To remove aFT, the material was calcinated at 500 °C, which did not affect silica. Octahedral shapes could still be observed after calcination (Figure 25.c-d). SAXS analysis revealed that silica mostly retained the crystal structure of the aFT crystals, as fcc structure could be identified in the scattering pattern with 12.7 nm between centers of the pores (Figure 25.e-f). However, the detected scattering was again weak and obscured more by the intensity from the direct beam than the samples in solution. This may suggest that only sections of the materials were mesoporous, reducing the significance of the structure in the system. Removal of aFT from the samples was confirmed using elemental analysis,

which showed that amount of organic material was reduced to less than 3 weight % of the sample in calcination (Figure 25.g). The method should also be applicable for other protein cages, making it a versatile way of producing mesoporous silica, although up-scaling of the process needs to be improved for real-life applications.

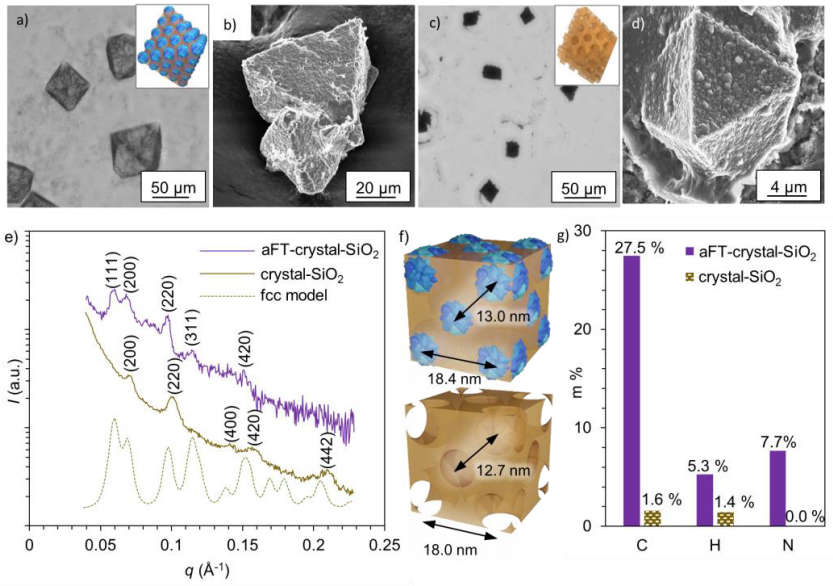

Figure 25. Characterization of silica materials. a) OM and b) SEM images of silica encased aFT crystals show that the octahedral habit of the crystals was retained during sol-gel reaction. c) OM and d) SEM of calcinated materials show that the habit persisted also after calcination. e) SAXS analysis confirmed that the inner crystal structure was also retained during silica encasing and was transferred to the calcinated material. The datasets have been separated vertically to avoid overlapping of the curves. f) Schematic representation with defined dimensions demonstrates that the silica remained relatively unchanged during calcination. g) Removal of aFT during calcination was confirmed by elemental analysis, which showed that mass proportion of organic material was reduced from roughly 40 % to 3 %.

5. Conclusions and Outlook

The conducted research demonstrates the effectiveness of electrostatic interactions in supramolecular self-assembly of two protein cages, ferritin and CCMV. Both were assembled into disordered aggregates as well as ordered co-crystals with various functional synthetic particles. All the assembly processes were carried out without modification of the cages, emphasizing the simplicity of the assembly even though the cages themselves are highly complex molecules. Publications **I** and **II** present disordered aggregation of ferritin and CCMV, respectively, and are focusing on the self-assembly process itself. Publications **III-VI** demonstrate formation of crystalline protein cage lattices and the obtained structures are analysed in detail to emphasize the significance of protein cage assembly in formation of nanostructures.

In publication **I**, thermo-responsive self-assembling ferritin complexes were prepared by combining ferritin with synthetic block-copolymers in aqueous solutions. The polymers contained thermo-responsive PDEGMA block, which underwent LCST behaviour at 33 °C, and cationic PDEGMA block, which attached to the surface of ferritin by electrostatic interactions. Due to the electrostatic bonding, the complexes were sensitive to the overall electrolyte concentration of the solutions in addition to temperature. Below the transition temperature of PDEGMA, the components remained hydrophilic, but at low electrolyte concentrations some aggregation was still observed due to the electrostatic crosslinking between multiple ferritin cages. When the solution was heated beyond 33 °C, thermo-responsive blocks collapsed to the surfaces of ferritin and formed a hydrophobic shell, leading to formation of large aggregates at medium and high electrolyte concentrations. The transition between the two states of the thermo-responsive block was reversible and the assemblies could be disassembled and reassembled repeatedly by ramping the temperature up and down. Additionally, disassembly could be triggered by increasing the electrolyte concentration, as it screens the electrostatic interactions between ferritin and the cationic blocks. Ferritin was complexed with both diblock copolymer composed of a single thermo-responsive and cationic block, as well as triblock copolymer where the thermo-responsive block was located between two cationic blocks. However, no significant differences were observed between the ferritin complexes prepared using these polymers.

Publication **II** introduces the concept of using c-CLPs for removal of viruses from water by electrostatic self-assembly. Lignin is produced in large quantities, making it an affordable raw material, but lacks high value practical applications.

Cationic lignin could be used as a co-assembly agent with negatively charged virus particles, as large aggregates can be removed more efficiently than individual viruses. Effectiveness of anionic CLPs, cationic lignin and c-CLPs in removal of low concentrations of CCMV were compared in aqueous solutions. All were capable of binding viruses, suggesting that additional interactions besides electrostatic caused the aggregation, but c-CLPs were found to be the most efficient. This was assumedly because CLPs interact with CCMV by hydrophobic interactions and cationic lignin by electrostatic interactions, but c-CLPs by both and therefore had the highest binding affinity. As the binding is a self-assembly process, no additional energy input was required besides mixing of the solutions to bring the lignin materials and viruses into contact. The removal of viruses from solution after complexation with c-CLPs was studied by sedimentation and filtration. The CCMV concentration of the samples could be cut down by 75 % using sedimentation and 79 % using filtration. This is less than can be achieved by using halogen compounds or heavy metals, but these materials are highly toxic and would need to be removed from the water afterwards. As a biobased material, c-CLPs could be effective in wastewater treatment. The self-assembly was also studied in dilute electrolyte solutions, as they better simulate wastewater, and the assembly was not significantly affected.

In publication **III**, ferritin and CCMV were complexed with fusion protein composing of GFP and a cationic K72 tail to demonstrate incorporation of additional functionalities into protein cage assemblies without occupying the cavity of the cage. GFP acted as a model compound proving that even complex molecules like proteins can be added to the structures using electrostatic interactions. For comparison, complexes were also formed using plain K72 without GFP. Both ferritin and CCMV formed assemblies with both cationic species, but the assembly process proceeded differently for the two protein cages. As the assembly was electrostatic, the structures could also be disassembled by increasing the electrolyte concentration. SAXS and cryo-TEM analysis revealed that the CCMV complexes with both K72 and GFP-K72 were crystalline, but with aFT only the K72 complexes were crystalline and GFP-K72 amorphous. This difference could be explained by the smaller spaces between the closely packed crystal structures of ferritin, which cannot house the GFP molecules, and GFP-K72 not being rigid enough to form crystal lattices. Dense packing of CCMV complexes and inability of aFT to form crystals suggests that GFP was housed inside the complexes, not only on the outside. Therefore, it was concluded that protein cages and cationic functional particles can be used to produce crystalline systems with spatially oriented functional sites, provided that the molecules are sterically compatible.

Publication **IV** demonstrates a similar concept, but with higher degree of orientation in the assemblies. Ferritin was complexed with synthetic cyclophanes carrying varying amounts of cationic charges. Variants of cup-like resorcin[4]arene and tubular pillar[5]arene were used, but only ones with high enough amount of charges were capable of assembling into large aggregates. The structures could be disassembled by drastically increasing electrolyte concentration of the solution, but at low concentrations highly ordered structures

could be produced. Ferritin complexes with pillar[5]arene that had a high amount of charges symmetrically on both sides of the ring assembled into crystal lattices with fcc structure. Due to their small size cyclophanes fit not only in the cavities between the assembled cages, but also between the interfaces of neighbouring cages, enabling all the molecules in the systems to have specific spatial orientation.

In publication **V**, self-assembly and lysozyme cargo encapsulation of TmFtn cage were studied as well as supramolecular self-assembly of the loaded cage with AuNPs. These properties were compared with AfFtn, which has open tetrahedral symmetry, while TmFtn has closed octahedral. Therefore, TmFtn cage is more stable and offers better protection for any encapsulated molecules, but the encapsulation was also shown to be possible by controlling electrolyte concentration of the solution. It was also shown that cargo carrying TmFtn assembled into crystalline lattices with AuNPs under conditions where AfFtn did not, and that the lysozyme in these crystals retained its enzymatic activity, although the activity was reduced.

In publication **VI**, mesoporous silica was produced by encasing aFT crystals in silica using sol-gel reaction. Large crystals were produced by optimised crystallization conditions and the protein crystal structures persisted during silica encapsulation. Formation of silica was focused to the crystals by using cationic silica precursor clusters that are attracted to aFT by electrostatic interactions. aFT was afterwards removed by calcination and silica retained the orientation and order of the crystals as voids, enabling production of materials with uniform size distribution and spatial orientation of pores.

The publications show that electrostatic interactions can be effectively used to induce supramolecular self-assembly of spherical protein cages. Protein cages are viable materials for the production of advanced nanomaterials as they can encapsulate smaller molecules inside them and assemble into larger structures. The properties of both the cages and the oppositely charged co-assembly agents define the structure of the assemblies, and both disoriented aggregates and crystalline structures can be obtained depending on the selection of molecules. The latter systems require specific control over the solution conditions, while random aggregation is more robust. The systems are extremely versatile, as protein cages with charged exterior are available in various sizes and shapes and can be modified to carry additional functionalities. Also, a vast pool of co-assembly agents is available as they basically only need to be within a certain size range and have a high enough charge density of opposing charge than the protein cage. The publications present the use of both synthetic organic and inorganic cationic molecules in self-assembly with anionic protein cages, and analysis of the formed structures. The greatest advantage of the electrostatic self-assembly is the simplicity, and no protein cage modification is required for the assembly to occur. However, additional functions can be added to the co-assembly agents, for example to enable environmental responsiveness. Also, specific control over the solution conditions can be used to produce highly ordered crystal lattices, with the locations of both the protein cages and the co-assembly agents known.

Currently, protein cages are in their own right a topic of interest in research as their selectivity and robustness can be matched by few other molecules. Therefore, studying their higher-order structures can give rise to even more advanced applications. The most promising field for supramolecular protein cage assemblies appears to be biomedicine, as the biocompatibility of the molecules enables their use in such applications. Other promising applications include catalysis systems and optically active and conductive materials. The required amounts of materials need remain relatively low, as protein cages are still not the most affordable material. The co-assembly agents can vary from simple and readily available particles to advanced synthetic molecules, depending on what kind of properties are required from the systems. However, electrostatic interactions may fail to perform well in conditions where electrolyte concentrations are higher than in the presented research, for example in vivo. Therefore, future studies should focus on preparing materials with greater tolerance to variations in solution conditions or ones that can be stabilized in their assembled state. Living bodies show diversity in factors like pH and temperature in different locations, so the systems used in them should be robust in order to remain functional. The systems presented in the publications are model systems proving that such concepts are viable and worth further study.

References

(1) Whitesides, G. M.; Grzybowski, B. Self-Assembly at All Scales. *Science* **2002**, *295*, 2418–2421.

(2) Arango-Restrepo, A.; Barragán, D.; Rubi, J. M. Self-Assembling Outside Equilibrium: Emergence of Structures Mediated by Dissipation. *Phys. Chem. Chem. Phys.* **2019**, *21*, 17475–17493.

(3) Fendler, J. H. Chemical Self-Assembly for Electronic Applications. *Chem. Mater.* **2001**, *13*, 3196–3210.

(4) Yan, X.; Zhu, P.; Li, J. Self-Assembly and Application of Diphenylalanine-Based Nanostructures. *Chem. Soc. Rev.* **2010**, *39*, 1877–1890.

(5) Vigderman, L.; Khanal, B. P.; Zubarev, E. R. Functional Gold Nanorods: Synthesis, Self-Assembly, and Sensing Applications. *Adv. Mater.* **2012**, *24*, 4811–4841.

(6) Fichman, G.; Gazit, E. Self-Assembly of Short Peptides to Form Hydrogels: Design of Building Blocks, Physical Properties and Technological Applications. *Acta Biomater.* **2014**, *10*, 1671–1682.

(7) Riess, G. Micellization of Block Copolymers. *Prog. Polym. Sci.* **2003**, *28*, 1107–1170.

(8) Stephanopoulos, N.; Ortony, J. H.; Stupp, S. I. Self-Assembly for the Synthesis of Functional Biomaterials. *Acta Mater.* **2013**, *61*, 912–930.

(9) Zhang, S. Fabrication of Novel Biomaterials through Molecular Self-Assembly. *Nat. Biotechnol.* **2003**, *21*, 1171–1178.

(10) Amendola, V.; Meneghetti, M. Self-Healing at the Nanoscale. *Nanoscale* **2009**, *1*, 74–88.

(11) Yeh, Y.-C.; Tang, R.; Mout, R.; Jeong, Y.; Rotello, V. M. Fabrication of Multiresponsive Bioactive Nanocapsules through Orthogonal Self-Assembly. *Angew. Chem. Int. Ed.* **2014**, *53*, 5137–5141.

(12) Grzelczak, M.; Vermant, J.; Furst, E. M.; Liz-Marzán, L. M. Directed Self-Assembly of Nanoparticles. *ACS Nano* **2010**, *4* 3591–3605.

(13) Contreras-García, J.; Johnson, E. R.; Keinan, S.; Chaudret, R.; Piquemal, J.-P.; Beratan, D. N.; Yang, W. NCIPLOT: A Program for Plotting Noncovalent Interaction Regions. *J. Chem. Theory Comput.* **2011**, *7*, 625–632.

(14) Vieira, V. M. P.; Liljeström, V.; Posocco, P.; Laurini, E.; Pricl, S.; Kostiainen, M. A.; Smith, D. K. Emergence of Highly-Ordered Hierarchical Nanoscale Aggregates on Electrostatic Binding of Self-Assembled Multivalent (SAMul) Cationic Micelles with Polyanionic Heparin. *J. Mater. Chem. B* **2017**, *5*, 341–347.

(15) Grzybowski, B. A.; Winkleman, A.; Wiles, J. A.; Brumer, Y.; Whitesides, G. M. Electrostatic Self-Assembly of Macroscopic Crystals Using Contact Electrification. *Nat. Mater.* **2003**, *2*, 241–245.

(16) Bai, Y.; Luo, Q.; Liu, J. Protein Self-Assembly via Supramolecular Strategies. *Chem. Soc. Rev.* **2016**, *45*, 2756–2767.

(17) Volatron, J.; Carn, F.; Kolosnjaj-Tabi, J.; Javed, Y.; Vuong, Q. L.; Gossuin, Y.; Ménager, C.; Luciani, N.; Charron, G.; Hémadi, M.; Alloyeau, D.; Gazeau, F. Ferritin Protein Regulates the Degradation of Iron Oxide Nanoparticles. *Small* **2017**, *13*, 1602030.

(18) Rabe, B.; Vlachou, A.; Pante, N.; Helenius, A.; Kann, M. Nuclear Import of Hepatitis B Virus Capsids and Release of the Viral Genome. *Proc. Natl. Acad. Sci. U.S.A* **2003**, *100*, 9849–9854.

(19) Roos, W. H.; Ivanovska, I. L.; Evilevitch, A.; Wuite, G. J. L. Viral Capsids: Mechanical Characteristics, Genome Packaging and Delivery Mechanisms. *Cell. Mol. Life Sci.* **2007**, *64*, 1484–1497.

(20) Flenniken, M. L.; Liepold, L. O.; Crowley, B. E.; Willits, D. A.; Young, M. J.; Douglas, T. Selective Attachment and Release of a Chemotherapeutic Agent from the Interior of a Protein Cage Architecture. *Chem. Commun.* **2005**, 4, 447–449.

(21) Hooker, J. M.; Datta, A.; Botta, M.; Raymond, K. N.; Francis, M. B. Magnetic Resonance Contrast Agents from Viral Capsid Shells: A Comparison of Exterior and Interior Cargo Strategies. *Nano Lett.* **2007**, *7*, 2207–2210.

(22) Aumiller, W. M.; Uchida, M.; Douglas, T. Protein Cage Assembly across Multiple Length Scales. *Chem. Soc. Rev.* **2018**, *47*, 3433–3469.

(23) Maassen, S. J.; van der Ham, A. M.; Cornelissen, J. J. L. M. Combining Protein Cages and Polymers: From Understanding Self-Assembly to Functional Materials. *ACS Macro Lett.* **2016**, *5*, 987–994.

(24) Zhang, Y.; Orner, B. P. Self-Assembly in the Ferritin Nano-Cage Protein Superfamily. *Int. J. Mol. Sci.* **2011**, *12*, 5406–5421.

(25) Hagan, M. F.; Chandler, D. Dynamic Pathways for Viral Capsid Assembly. *Biophys. J.* **2006**, *91*, 42–54.

(26) Yamashita, I.; Iwahori, K.; Kumagai, S. Ferritin in the Field of Nanodevices. *Biochim. Biophys. Acta Gen. Subj.* **2010**, *1800*, 846–857.

(27) Sasaki, E.; Hilvert, D. Self-Assembly of Proteinaceous Multishell Structures Mediated by a Supercharged Protein. *J. Phys. Chem. B* **2016**, *120*, 6089–6095.

(28) Smith, A. M.; Lee, A. A.; Perkin, S. The Electrostatic Screening Length in Concentrated Electrolytes Increases with Concentration. *J. Phys. Chem. Lett.* **2016**, *7*, 2157–2163.

(29) Zhu, J.; He, K.; Dai, Z.; Gong, L.; Zhou, T.; Liang, H.; Liu, J. Self-Assembly of Luminescent Gold Nanoparticles with Sensitive PH-Stimulated Structure Transformation and Emission Response toward Lysosome Escape and Intracellular Imaging. *Anal. Chem.* **2019**, *91*, 8237–8243.

(30) Kwak, D.; Han, J. T.; Lee, J. H.; Lim, H. S.; Lee, D. H.; Cho, K. Facile Control of Thermo-Responsive Wettability through an All-Electrostatic Self-Assembling Process. *Surf. Sci.* **2008**, *602*, 3100–3105.

(31) Liljeström, V.; Seitsonen, J.; Kostiainen, M. A. Electrostatic Self-Assembly of Soft Matter Nanoparticle Cocrystals with Tunable Lattice Parameters. *ACS Nano* **2015**, *9*, 11278–11285.

(32) Kent, S. B. H. Total Chemical Synthesis of Proteins. *Chem. Soc. Rev.* **2009**, *38*, 338–351.

(33) Lai, Y.-T.; Reading, E.; Hura, G. L.; Tsai, K.-L.; Laganowsky, A.; Asturias, F. J.; Tainer, J. A.; Robinson, C. V.; Yeates, T. O. Structure of a Designed Protein Cage That Self-Assembles into a Highly Porous Cube. *Nat. Chem.* **2014**, *6*, 1065–1071.

(34) Diaz, D.; Care, A.; Sunna, A. Bioengineering Strategies for Protein-Based Nanoparticles. *Genes* **2018**, *9*, 370.

(35) Recalcati, S.; Invernizzi, P.; Arosio, P.; Cairo, G. New Functions for an Iron Storage Protein: The Role of Ferritin in Immunity and Autoimmunity. *J. Autoimmun.* **2008**, *30*, 84–89.

(36) Noad, R.; Roy, P. Virus-like Particles as Immunogens. *Trends Microbiol.* **2003**, *11*, 438–444.

(37) Garcea, R. L.; Gissmann, L. Virus-like Particles as Vaccines and Vessels for the Delivery of Small Molecules. *Curr. Opin. Biotechnol.* **2004**, *15*, 513–517.

(38) Makino, A.; Harada, H.; Okada, T.; Kimura, H.; Amano, H.; Saji, H.; Hiraoka, M.; Kimura, S. Effective Encapsulation of a New Cationic Gadolinium Chelate into Apoferritin and Its Evaluation as an MRI Contrast Agent. *Nanomedicine NBM* **2011**, *7*, 638–646.

(39) Azuma, Y.; Zschoche, R.; Tinzl, M.; Hilvert, D. Quantitative Packaging of Active Enzymes into a Protein Cage. *Angew. Chem. Int. Ed.* **2016**, *55*, 1531–1534.

(40) Yi, H.; Yan, M.; Huang, D.; Zeng, G.; Lai, C.; Li, M.; Huo, X.; Qin, L.; Liu, S.; Liu, X.; Li, B.; Wang, H.; Shen, M.; Fu, Y.; Guo, X. Synergistic Effect of Artificial Enzyme and 2D Nano-Structured Bi_2WO_6 for Eco-Friendly and Efficient Biomimetic Photocatalysis. *Appl. Catal. B* **2019**, *250*, 52–62.

(41) Marcotte, E. M.; Pellegrini, M.; Ng, H.-L.; Rice, D. W.; Yeates, T. O.; Eisenberg, D. Detecting Protein Function and Protein-Protein Interactions from Genome Sequences. *Science* **1999**, *285*, 751–753.

(42) Uchida, M.; Klem, M. T.; Allen, M.; Suci, P.; Flenniken, M.; Gillitzer, E.; Varpness, Z.; Liepold, L. O.; Young, M.; Douglas, T. Biological Containers: Protein Cages as Multifunctional Nanoplatforms. *Adv. Mater.* **2007**, *19*, 1025–1042.

(43) Yildiz, I.; Shukla, S.; Steinmetz, N. F. Applications of Viral Nanoparticles in Medicine. *Curr. Opin. Biotechnol.* **2011**, *22*, 901–908.

(44) Jordan, P. C.; Patterson, D. P.; Saboda, K. N.; Edwards, E. J.; Miettinen, H. M.; Basu, G.; Thielges, M. C.; Douglas, T. Self-Assembling Biomolecular Catalysts for Hydrogen Production. *Nat. Chem.* **2016**, *8*, 179–185.

(45) Flenniken, M. L.; Willits, D. A.; Brumfield, S.; Young, M. J.; Douglas, T. The Small Heat Shock Protein Cage from *Methanococcus Jannaschii* Is a Versatile Nanoscale Platform for Genetic and Chemical Modification. *Nano Lett.* **2003**, *3*, 1573–1576.

(46) Liljeström, V.; Ora, A.; Hassinen, J.; Rekola, H. T.; Nonappa; Heilala, M.; Hynninen, V.; Joensuu, J. J.; Ras, R. H. A.; Törmä, P.; Ikkala, O.; Kostiainen, M. A. Cooperative Colloidal Self-Assembly of Metal-Protein Superlattice Wires. *Nat. Commun.* **2017**, *8*, 671.

(47) Lončar, N.; Rozeboom, H. J.; Franken, L. E.; Stuart, M. C. A.; Fraaije, M. W. Structure of a Robust Bacterial Protein Cage and Its Application as a Versatile Biocatalytic Platform through Enzyme Encapsulation. *Biochem. Biophys. Res. Commun.* **2020**, *529*, 548–553.

(48) Beck, T.; Tetter, S.; Künzle, M.; Hilvert, D. Construction of Matryoshka-Type Structures from Supercharged Protein Nanocages. *Angew. Chem. Int. Ed.* **2015**, *127*, 951–954.

(49) Ma-Ham, A.; Wu, H.; Wang, J.; Kang, X.; Zhang, Y.; Lin, Y. Apoferritin-Based Nanomedicine Platform for Drug Delivery: Equilibrium Binding Study of Daunomycin with DNA. *J. Mater. Chem.* **2011**, *21*, 8700–8708.

(50) Molino, N. M.; Wang, S.-W. Caged Protein Nanoparticles for Drug Delivery. *Curr. Opin. Biotechnol.* **2014**, *28*, 75–82.

(51) Czapar, A. E.; Steinmetz, N. F. Plant Viruses and Bacteriophages for Drug Delivery in Medicine and Biotechnology. *Curr. Opin. Biotechnol.* **2017**, *38*, 108–116.

(52) Bode, S. A.; Minten, I. J.; Nolte, R. J. M.; Cornelissen, J. J. L. M. Reactions inside Nanoscale Protein Cages. *Nanoscale* **2011**, *3*, 2376–2389.

(53) Huard, D. J. E.; Kane, K. M.; Tezcan, F. A. Re-Engineering Protein Interfaces Yields Copper-Inducible Ferritin Cage Assembly. *Nat. Chem. Biol.* **2013**, *9*, 169–176.

(54) Uchida, M.; McCoy, K.; Fukuto, M.; Yang, L.; Yoshimura, H.; Miettinen, H. M.; LaFrance, B.; Patterson, D. P.; Schwarz, B.; Karty, J. A.; Prevelige, P. E.; Lee, B.; Douglas, T. Modular Self-Assembly of Protein Cage Lattices for Multistep Catalysis. *ACS Nano* **2018**, *12*, 942–953.

(55) Wang, Z.; Huang, P.; Jacobson, O.; Wang, Z.; Liu, Y.; Lin, L.; Lin, J.; Lu, N.; Zhang, H.; Tian, R.; Niu, G.; Liu, G.; Chen, X. Biomineralization-Inspired Synthesis of Copper Sulfide–Ferritin Nanocages as Cancer Theranostics. *ACS Nano* **2016**, *10*, 3453–3460.

(56) Liu, X.; Jin, W.; Theil, E. C. Opening Protein Pores with Chaotropes Enhances Fe Reduction and Chelation of Fe from the Ferritin Biomineral. *Proc. Natl. Acad. Sci. U.S.A* **2003**, *100*, 3653–3658.

(57) Chen, L.; Bai, G.; Yang, R.; Zang, J.; Zhou, T.; Zhao, G. Encapsulation of β-Carotene within Ferritin Nanocages Greatly Increases Its Water-Solubility and Thermal Stability. *Food Chem.* **2014**, *149*, 307–312.

(58) Douglas, T.; Young, M. Host–Guest Encapsulation of Materials by Assembled Virus Protein Cages. *Nature* **1998**, *393*, 152–155.

(59) Kasyutich, O.; Ilari, A.; Fiorillo, A.; Tatchev, D.; Hoell, A.; Ceci, P. Silver Ion Incorporation and Nanoparticle Formation inside the Cavity of Pyrococcus Furiosus Ferritin: Structural and Size-Distribution Analyses. *J. Am. Chem. Soc.* **2010**, *132*, 3621–3627.

(60) Uchida, M.; Flenniken, M. L.; Allen, M.; Willits, D. A.; Crowley, B. E.; Brumfield, S.; Willis, A. F.; Jackiw, L.; Jutila, M.; Young, M. J.; Douglas, T. Targeting of Cancer Cells with Ferrimagnetic Ferritin Cage Nanoparticles. *J. Am. Chem. Soc.* **2006**, *128*, 16626–16633.

(61) Arosio, P.; Ingrassia, R.; Cavadini, P. Ferritins: A Family of Molecules for Iron Storage, Antioxidation and More. *Biochim. Biophys. Acta Gen. Subj.* **2009**, *1790*, 589–599.

(62) Jutz, G.; van Rijn, P.; Santos Miranda, B.; Böker, A. Ferritin: A Versatile Building Block for Bionanotechnology. *Chem. Rev.* **2015**, *115*, 1653–1701.

(63) Zang, J.; Chen, H.; Zhao, G.; Wang, F.; Ren, F. Ferritin Cage for Encapsulation and Delivery of Bioactive Nutrients: From Structure, Property to Applications. *Crit. Rev. Food Sci. Nutr.* **2017**, *57*, 3673–3683.

(64) Liu, X.; Theil, E. C. Ferritins: Dynamic Management of Biological Iron and Oxygen Chemistry. *Acc. Chem. Res.* **2005**, *38*, 167–175.

(65) Bai, L.; Xie, T.; Hu, Q.; Deng, C.; Zheng, R.; Chen, W. Genome-Wide Comparison of Ferritin Family from Archaea, Bacteria, Eukarya, and Viruses: Its Distribution, Characteristic Motif, and Phylogenetic Relationship. *Sci. Nat.* **2015**, *102*, 64.

(66) Dörner, M. H.; Salfeld, J.; Will, H.; Leibold, E. A.; Vass, J. K.; Munro, H. N. Structure of Human Ferritin Light Subunit Messenger RNA: Comparison with Heavy Subunit Message and Functional Implications. *Proc. Natl. Acad. Sci. U.S.A* **1985**, *82*, 3139–3143.

(67) Rouault, T. A. The Role of Iron Regulatory Proteins in Mammalian Iron Homeostasis and Disease. *Nat. Chem. Biol.* **2006**, *2*, 406–414.

(68) Fan, R.; Chew, S. W.; Cheong, V. V.; Orner, B. P. Fabrication of Gold Nanoparticles Inside Unmodified Horse Spleen Apoferritin. *Small* **2010**, *6*, 1483–1487.

(69) Fan, K.; Cao, C.; Pan, Y.; Lu, D.; Yang, D.; Feng, J.; Song, L.; Liang, M.; Yan, X. Magnetoferritin Nanoparticles for Targeting and Visualizing Tumour Tissues. *Nat. Nanotech.* **2012**, *7*, 459–464.

(70) Wang, J.; Pantopoulos, K. Regulation of Cellular Iron Metabolism. *Biochem. J.* **2011**, *434*, 365–381.

(71) Maity, B.; Hishikawa, Y.; Lu, D.; Ueno, T. Recent Progresses in the Accumulation of Metal Ions into the Apo-Ferritin Cage: Experimental and Theoretical Perspectives. *Polyhedron* **2019**, *172*, 104–111.

(72) Truffi, M.; Fiandra, L.; Sorrentino, L.; Monieri, M.; Corsi, F.; Mazzucchelli, S. Ferritin Nanocages: A Biological Platform for Drug Delivery, Imaging and Theranostics in Cancer. *Pharmacol. Res.* **2016**, *107*, 57–65.

(73) Crichton, R. R.; Declercq, J.-P. X-Ray Structures of Ferritins and Related Proteins. *Biochim. Biophys. Acta Gen. Subj.* **2010**, *1800*, 706–718.

(74) Nakajima, H.; Kondo, M.; Nakane, T.; Abe, S.; Nakao, T.; Watanabe, Y.; Ueno, T. Construction of an Enterobactin Analogue with Symmetrically Arranged Monomer Subunits of Ferritin. *Chem. Commun.* **2015**, *51*, 16609–16612.

(75) Zhou, K.; Zang, J.; Chen, H.; Wang, W.; Wang, H.; Zhao, G. On-Axis Alignment of Protein Nanocage Assemblies from 2D to 3D through the Aromatic Stacking Interactions of Amino Acid Residues. *ACS Nano* **2018**, *12*, 11323–11332.

(76) Hamburger, A. E.; West, A. P.; Hamburger, Z. A.; Hamburger, P.; Bjorkman, P. J. Crystal Structure of a Secreted Insect Ferritin Reveals a Symmetrical Arrangement of Heavy and Light Chains. *J. Mol. Biol.* **2005**, *349*, 558–569.

(77) Chou, M. L.; Burnouf, T. Current Methods to Manufacture Human Platelet Lysates for Cell Therapy and Tissue Engineering: Possible Trends in Product Safety and Standardization. *ISBT Sci. Ser.* **2017**, *12*, 168–175.

(78) de Turris, V.; Cardoso Trabuco, M.; Peruzzi, G.; Boffi, A.; Testi, C.; Vallone, B.; Celeste Montemiglio, L.; Georges, A. D.; Calisti, L.; Benni, I.; Bonamore, A.; Baiocco, P. Humanized Archaeal Ferritin as a Tool for Cell Targeted Delivery. *Nanoscale* **2017**, *9*, 647–655.

(79) Johnson, E.; Cascio, D.; Sawaya, M. R.; Gingery, M.; Schröder, I. Crystal Structures of a Tetrahedral Open Pore Ferritin from the Hyperthermophilic Archaeon Archaeoglobus Fulgidus. *Structure* **2005**, *13,* 637–648.

(80) Tatur, J.; Hagen, W. R.; Matias, P. M. Crystal Structure of the Ferritin from the Hyperthermophilic Archaeal Anaerobe Pyrococcus Furiosus. *J. Biol. Inorg. Chem.* **2007**, *12*, 615–630.

(81) Ceci, P.; Forte, E.; Di Cecca, G.; Fornara, M.; Chiancone, E. The Characterization of Thermotoga Maritima Ferritin Reveals an Unusual Subunit Dissociation Behavior and Efficient DNA Protection from Iron-Mediated Oxidative Stress. *Extremophiles* **2011**, *15*, 431–439.

(82) Klem, M. T.; Young, M.; Douglas, T. Biomimetic Synthesis of Photoactive α-Fe_2O_3 Templated by the Hyperthermophilic Ferritin from Pyrococus Furiosus. *J. Mater. Chem.* **2010**, *20*, 65–67.

(83) Kang, Y. J.; Uchida, M.; Shin, H.-H.; Douglas, T.; Kang, S. Biomimetic FePt Nanoparticle Synthesis within Pyrococcus Furiosus Ferritins and Their Layer-by-Layer Formation. *Soft Matter* **2011**, *7*, 11078.

(84) Monti, D. M.; Ferraro, G.; Merlino, A. Ferritin-Based Anticancer Metallodrug Delivery: Crystallographic, Analytical and Cytotoxicity Studies. *Nanomedicine NBM* **2019**, *20*, 101997.

(85) Tetter, S.; Hilvert, D. Enzyme Encapsulation by a Ferritin Cage. *Angew. Chem. Int. Ed.* **2017**, *56*, 14933–14936.

(86) Sana, B.; Johnson, E.; Le Magueres, P.; Criswell, A.; Cascio, D.; Lim, S. The Role of Nonconserved Residues of Archaeoglobus Fulgidus Ferritin on Its Unique Structure and Biophysical Properties. *J. Biol. Chem.* **2013**, *288*, 32663–32672.

(87) Swift, J.; Butts, C. A.; Cheung-Lau, J.; Yerubandi, V.; Dmochowski, I. J. Efficient Self-Assembly of Archaeoglobus Fulgidus Ferritin around Metallic Cores. *Langmuir* **2009**, *25*, 5219–5225.

(88) Liepold, L. O.; Revis, J.; Allen, M.; Oltrogge, L.; Young, M.; Douglas, T. Structural Transitions in Cowpea Chlorotic Mottle Virus (CCMV). *Phys. Biol.* **2005**, *2*, S166–S172.

(89) Douglas, T.; Strable, E.; Willits, D.; Aitouchen, A.; Libera, M.; Young, M. Protein Engineering of a Viral Cage for Constrained Nanomatrials Synthesis. *Adv. Mater.* **2002**, *14*, 415–418.

(90) Yang, L.; Liu, A.; Cao, S.; Putri, R. M.; Jonkheijm, P.; Cornelissen, J. J. L. M. Self-Assembly of Proteins: Towards Supramolecular Materials. *Chem. Eur. J.* **2016**, *22*, 15570–15582.

(91) Konecny, R.; Trylska, J.; Tama, F.; Zhang, D.; Baker, N. A.; Brooks, C. L.; McCammon, J. A. Electrostatic Properties of Cowpea Chlorotic Mottle Virus and Cucumber Mosaic Virus Capsids. *Biopolymers* **2006**, *82*, 106–120.

(92) Kovács, F.; Tarnai, T.; Guest, S. D.; Fowler, P. W. Double–Link Expandohedra: A Mechanical Model for Expansion of a Virus. *Proc. R. Soc. Lond. A* **2004**, *460*, 3191–3202.

(93) Speir, J. A.; Munshi, S.; Wang, G.; Baker, T. S.; Johnson, J. E. Structures of the Native and Swollen Forms of Cowpea Chlorotic Mottle Virus Determined by X-Ray Crystallography and Cryo-Electron Microscopy. *Structure* **1995**, *3*, 63–78.

(94) Brasch, M.; de la Escosura, A.; Ma, Y.; Uetrecht, C.; Heck, A. J. R.; Torres, T.; Cornelissen, J. J. L. M. Encapsulation of Phthalocyanine Supramolecular Stacks into Virus-like Particles. *J. Am. Chem. Soc.* **2011**, *133*, 6878–6881.

(95) Tagit, O.; de Ruiter, M. V.; Brasch, M.; Ma, Y.; Cornelissen, J. J. L. M. Quantum Dot Encapsulation in Virus-like Particles with Tuneable Structural Properties and Low Toxicity. *RSC Adv.* **2017**, *7*, 38110–38118.

(96) Miao, Y.; Johnson, J. E.; Ortoleva, P. J. All-Atom Multiscale Simulation of Cowpea Chlorotic Mottle Virus Capsid Swelling. *J. Phys. Chem. B* **2010**, *114*, 11181–11195.

(97) Albert, F. G.; Fox, J. M.; Young, M. J. Virion Swelling Is Not Required for Cotranslational Disassembly of Cowpea Chlorotic Mottle Virus in Vitro. *J. Virol.* **1997**, *71*, 4296–4299.

(98) Basu, G.; Allen, M.; Willits, D.; Young, M.; Douglas, T. Metal Binding to Cowpea Chlorotic Mottle Virus Using Terbium(III) Fluorescence. *J. Biol. Inorg. Chem.* **2003**, *8*, 721–725.

(99) Tama, F.; Brooks, C. L. The Mechanism and Pathway of PH Induced Swelling in Cowpea Chlorotic Mottle Virus. *J. Mol. Biol.* **2002**, *318*, 733–747.

(100) Sauer, M.; Streich, D.; Meier, W. PH-Sensitive Nanocontainers. *Adv. Mater.* **2001**, *13*, 1649–1651.

(101) Smith, T. J.; Chase, E.; Schmidt, T.; Perry, K. L. The Structure of Cucumber Mosaic Virus and Comparison to Cowpea Chlorotic Mottle Virus. *J. Virol.* **2000**, *74*, 7578–7586.

(102) Schoonen, L.; Pille, J.; Borrmann, A.; Nolte, R. J. M.; van Hest, J. C. M. Sortase A-Mediated N-Terminal Modification of Cowpea Chlorotic Mottle Virus for Highly Efficient Cargo Loading. *Bioconjug. Chem.* **2015**, *26*, 2429–2434.

(103) Minten, I. J.; Hendriks, L. J. A.; Nolte, R. J. M.; Cornelissen, J. J. L. M. Controlled Encapsulation of Multiple Proteins in Virus Capsids. *J. Am. Chem. Soc.* **2009**, *131*, 17771–17773.

(104) Tour, J. M. Top-Down versus Bottom-Up Fabrication of Graphene-Based Electronics. *Chem. Mater.* **2014**, *26*, 163–171.

(105) Biswas, A.; Bayer, I. S.; Biris, A. S.; Wang, T.; Dervishi, E.; Faupel, F. Advances in Top–down and Bottom–up Surface Nanofabrication: Techniques, Applications & Future Prospects. *Adv. Colloid Interface Sci.* **2012**, *170*, 2–27.

(106) Björk, J.; Hanke, F.; Stafström, S. Mechanisms of Halogen-Based Covalent Self-Assembly on Metal Surfaces. *J. Am. Chem. Soc.* **2013**, *135*, 5768–5775.
(107) Fu, S.; An, G.; Sun, H.; Luo, Q.; Hou, C.; Xu, J.; Dong, Z.; Liu, J. Laterally Functionalized Pillar[5]Arene: A New Building Block for Covalent Self-Assembly. *Chem. Commun.* **2017**, *53*, 9024–9027.
(108) Kulkarni, C. V. Lipid Crystallization: From Self-Assembly to Hierarchical and Biological Ordering. *Nanoscale* **2012**, *4*, 5779–5791.
(109) Grzelczak, M.; Liz-Marzán, L. M.; Klajn, R. Stimuli-Responsive Self-Assembly of Nanoparticles. *Chem. Soc. Rev.* **2019**, *48*, 1342–1361.
(110) Wang, J.; Liu, K.; Xing, R.; Yan, X. Peptide Self-Assembly: Thermodynamics and Kinetics. *Chem. Soc. Rev.* **2016**, *45*, 5589–5604.
(111) Liu, Q.; Wang, H.; Shi, X.; Wang, Z.-G.; Ding, B. Self-Assembled DNA/Peptide-Based Nanoparticle Exhibiting Synergistic Enzymatic Activity. *ACS Nano* **2017**, *11*, 7251–7258.
(112) Feng, D.; Gao, T.-N.; Fan, M.; Li, A.; Li, K.; Wang, T.; Huo, Q.; Qiao, Z.-A. A General Ligand-Assisted Self-Assembly Approach to Crystalline Mesoporous Metal Oxides. *NPG Asia Mater.* **2018**, *10*, 800–809.
(113) Grzybowski, B. A.; Wilmer, C. E.; Kim, J.; Browne, K. P.; Bishop, K. J. M. Self-Assembly: From Crystals to Cells. *Soft Matter* **2009**, *5*, 1110.
(114) Zhou, K.; Chen, H.; Zhang, S.; Wang, Y.; Zhao, G. Disulfide-Mediated Reversible Two-Dimensional Self-Assembly of Protein Nanocages. *Chem. Commun.* **2019**, *55*, 7510–7513.
(115) Whitesides, G. M.; Boncheva, M. Beyond Molecules: Self-Assembly of Mesoscopic and Macroscopic Components. *Proc. Natl. Acad. Sci. U.S.A* **2002**, *99*, 4769–4774.
(116) Guo, S.; Song, Y.; He, Y.; Hu, X.-Y.; Wang, L. Highly Efficient Artificial Light-Harvesting Systems Constructed in Aqueous Solution Based on Supramolecular Self-Assembly. *Angew. Chem. Int. Ed.* **2018**, *57*, 3163–3167.
(117) Liu, Y.; Zhang, C.; Hao, D.; Zhang, Z.; Wu, L.; Li, M.; Feng, S.; Xu, X.; Liu, F.; Chen, X.; Bo, Z. Enhancing the Performance of Organic Solar Cells by Hierarchically Supramolecular Self-Assembly of Fused-Ring Electron Acceptors. *Chem. Mater.* **2018**, *30*, 4307–4312.
(118) Imholt, L.; Dong, D.; Bedrov, D.; Cekic-Laskovic, I.; Winter, M.; Brunklaus, G. Supramolecular Self-Assembly of Methylated Rotaxanes for Solid Polymer Electrolyte Application. *ACS Macro Lett.* **2018**, *7*, 881–885.
(119) Moughton, A. O.; O'Reilly, R. K. Noncovalently Connected Micelles, Nanoparticles, and Metal-Functionalized Nanocages Using Supramolecular Self-Assembly. *J. Am. Chem. Soc.* **2008**, *130*, 8714–8725.
(120) Miao, L.; Fan, Q.; Zhao, L.; Qiao, Q.; Zhang, X.; Hou, C.; Xu, J.; Luo, Q.; Liu, J. The Construction of Functional Protein Nanotubes by Small Molecule-Induced Self-Assembly of Cricoid Proteins. *Chem. Commun.* **2016**, *52*, 4092–4095.
(121) Jang, Y.; Choi, W. T.; Heller, W. T.; Ke, Z.; Wright, E. R.; Champion, J. A. Engineering Globular Protein Vesicles through Tunable Self-Assembly of Recombinant Fusion Proteins. *Small* **2017**, *13*, 1700399.
(122) Willerich, I.; Gröhn, F. Molecular Structure Encodes Nanoscale Assemblies: Understanding Driving Forces in Electrostatic Self-Assembly. *J. Am. Chem. Soc.* **2011**, *133*, 20341–20356.
(123) Cademartiri, R.; Stan, C. A.; Tran, V. M.; Wu, E.; Friar, L.; Vulis, D.; Clark, L. W.; Tricard, S.; Whitesides, G. M. A Simple Two-Dimensional Model System to Study Electrostatic-Self-Assembly. *Soft Matter* **2012**, *8*, 9771.

(124) Lindgren, E. B.; Derbenev, I. N.; Khachatourian, A.; Chan, H.-K.; Stace, A. J.; Besley, E. Electrostatic Self-Assembly: Understanding the Significance of the Solvent. *J. Chem. Theory Comput.* **2018**, *14*, 905–915.
(125) Gröhn, F. Electrostatic Self-Assembly as Route to Supramolecular Structures. *Macromol. Chem. Phys.* **2008**, *209*, 2295–2301.
(126) Artyukhin, A. B.; Bakajin, O.; Stroeve, P.; Noy, A. Layer-by-Layer Electrostatic Self-Assembly of Polyelectrolyte Nanoshells on Individual Carbon Nanotube Templates. *Langmuir* **2004**, *20*, 1442–1448.
(127) Kalsin, A. M.; Fialkowski, M.; Paszewski, M.; Smoukov, S. K.; Bishop, K. J. M.; Grzybowski, B. A. Electrostatic Self-Assembly of Binary Nanoparticle Crystals with a Diamond-Like Lattice. *Science* **2006**, *312*, 420–424.
(128) Künzle, M.; Eckert, T.; Beck, T. Binary Protein Crystals for the Assembly of Inorganic Nanoparticle Superlattices. *J. Am. Chem. Soc.* **2016**, *138*, 12731–12734.
(129) Kotov, N. A.; Dekany, I.; Fendler, J. H. Layer-by-Layer Self-Assembly of Polyelectrolyte-Semiconductor Nanoparticle Composite Films. *J. Phys. Chem.* **1995**, *99*, 13065–13069.
(130) Debye, P.; Hückel, E. Zur Theorie Der Elektrolyte. *Phys. Z.* **1923**, *24*, 185–206.
(131) Kontogeorgis, G. M.; Maribo-Mogensen, B.; Thomsen, K. The Debye-Hückel Theory and Its Importance in Modeling Electrolyte Solutions. *Fluid Phase Equilib.* **2018**, *462*, 130–152.
(132) Fredrickson, G. H.; Liu, A. J.; Bates, F. S. Entropic Corrections to the Flory-Huggins Theory of Polymer Blends: Architectural and Conformational Effects. *Macromolecules* **1994**, *27*, 2503–2511.
(133) Michaeli, I.; Overbeek, J. Th. G.; Voorn, M. J. Phase Separation of Polyelectrolyte Solutions. *J. Polym. Sci.* **1957**, *23*, 443–450.
(134) Spruijt, E.; Westphal, A. H.; Borst, J. W.; Cohen Stuart, M. A.; van der Gucht, J. Binodal Compositions of Polyelectrolyte Complexes. *Macromolecules* **2010**, *43*, 6476–6484.
(135) Sing, C. E. Development of the Modern Theory of Polymeric Complex Coacervation. *Adv. Colloid Interface Sci.* **2017**, *239*, 2–16.
(136) Kostiainen, M. A.; Hiekkataipale, P.; Laiho, A.; Lemieux, V.; Seitsonen, J.; Ruokolainen, J.; Ceci, P. Electrostatic Assembly of Binary Nanoparticle Superlattices Using Protein Cages. *Nat. Nanotech.* **2012**, *8*, 52–56.
(137) Faul, C. F. J.; Antonietti, M. Ionic Self-Assembly: Facile Synthesis of Supramolecular Materials. *Adv. Mater.* **2003**, *15*, 673–683.
(138) Gaddam, P.; Ducker, W. Electrostatic Screening Length in Concentrated Salt Solutions. *Langmuir* **2019**, *35*, 5719–5727.
(139) Velev, O. D. Self-Assembly of Unusual Nanoparticle Crystals. *Science* **2006**, *312*, 376–377.
(140) Liljeström, V.; Mikkilä, J.; Kostiainen, M. A. Self-Assembly and Modular Functionalization of Three-Dimensional Crystals from Oppositely Charged Proteins. *Nat. Commun.* **2014**, *5*, 4445.
(141) Palchoudhury, S.; Zhou, Z.; Ramasamy, K.; Okirie, F.; Prevelige, P. E.; Gupta, A. Self-Assembly of P22 Protein Cages with Polyamidoamine Dendrimer and Inorganic Nanoparticles. *J. Mater. Res.* **2017**, *32*, 465–472.
(142) Zhao, S.; Zhang, M.; Wang, Z.; Xian, X. Enhanced High-Rate Performance of $Li_4Ti_5O_{12}$ Microspheres/Multiwalled Carbon Nanotubes Composites Prepared by Electrostatic Self-Assembly. *Electrochim. Acta* **2018**, *276*, 73–80.
(143) Pu, C.; Wan, J.; Liu, E.; Yin, Y.; Li, J.; Ma, Y.; Fan, J.; Hu, X. Two-Dimensional Porous Architecture of Protonated GCN and Reduced Graphene Oxide via Electrostatic Self-Assembly Strategy for High Photocatalytic Hydrogen Evolution under Visible Light. *Appl. Surf. Sci.* **2017**, *399*, 139–150.

(144) Jian, X.; Li, J.; Yang, H.; Cao, L.; Zhang, E.; Liang, Z. Carbon Quantum Dots Reinforced Polypyrrole Nanowire via Electrostatic Self-Assembly Strategy for High-Performance Supercapacitors. *Carbon* **2017**, *114*, 533–543.

(145) Gao, N.; Yang, W.; Nie, H.; Gong, Y.; Jing, J.; Gao, L.; Zhang, X. Turn-on Theranostic Fluorescent Nanoprobe by Electrostatic Self-Assembly of Carbon Dots with Doxorubicin for Targeted Cancer Cell Imaging, in Vivo Hyaluronidase Analysis, and Targeted Drug Delivery. *Bios. Bioelectron.* **2017**, *96*, 300–307.

(146) Hu, J.; Meng, H.; Li, G.; Ibekwe, S. I. A Review of Stimuli-Responsive Polymers for Smart Textile Applications. *Smart Mater. Struct.* **2012**, *21*, 053001.

(147) Gil, E.; Hudson, S. Stimuli-Reponsive Polymers and Their Bioconjugates. *Prog. Polym. Sci.* **2004**, *29*, 1173–1222.

(148) Roy, D.; Brooks, W. L. A.; Sumerlin, B. S. New Directions in Thermoresponsive Polymers. *Chem. Soc. Rev.* **2013**, *42*, 7214.

(149) Wang, A.; Shi, W.; Huang, J.; Yan, Y. Adaptive Soft Molecular Self-Assemblies. *Soft Matter* **2016**, *12*, 337–357.

(150) Alarcón, C. de las H.; Pennadam, S.; Alexander, C. Stimuli Responsive Polymers for Biomedical Applications. *Chem. Soc. Rev.* **2005**, *34*, 276–285.

(151) Vasantha, V. A.; Jana, S.; Lee, S. S.-C.; Lim, C.-S.; Teo, S. L.-M.; Parthiban, A.; Vancso, J. G. Dual Hydrophilic and Salt Responsive Schizophrenic Block Copolymers – Synthesis and Study of Self-Assembly Behavior. *Polym. Chem.* **2015**, *6*, 599–606.

(152) Peterson, G. I.; Larsen, M. B.; Boydston, A. J. Controlled Depolymerization: Stimuli-Responsive Self-Immolative Polymers. *Macromolecules* **2012**, *45*, 7317–7328.

(153) Stoffelen, C.; Voskuhl, J.; Jonkheijm, P.; Huskens, J. Dual Stimuli-Responsive Self-Assembled Supramolecular Nanoparticles. *Angew. Chem. Int. Ed.* **2014**, *53*, 3400–3404.

(154) Jiang, F.; Chen, S.; Cao, Z.; Wang, G. A Photo, Temperature, and PH Responsive Spiropyran-Functionalized Polymer: Synthesis, Self-Assembly and Controlled Release. *Polymer* **2016**, *83*, 85–91.

(155) Jochum, F. D.; Theato, P. Temperature- and Light-Responsive Smart Polymer Materials. *Chem. Soc. Rev.* **2013**, *42*, 7468–7483.

(156) Guragain, S.; Bastakoti, B. P.; Malgras, V.; Nakashima, K.; Yamauchi, Y. Multi-Stimuli-Responsive Polymeric Materials. *Chem. Eur. J.* **2015**, *21*, 13164–13174.

(157) Zhao, Q.; Li, X.; Lu, J.; Liu, Y.; Sha, L.; Di, D.; Wang, S. TPGS and Cypate Gated Mesoporous Carbon for Enhanced Thermochemotherapy of Tumor. *Colloids Surf. A: Physiochem. Eng. Asp.* **2020**, *591*, 124544.

(158) Warren, N. J.; Armes, S. P. Polymerization-Induced Self-Assembly of Block Copolymer Nano-Objects via RAFT Aqueous Dispersion Polymerization. *J. Am. Chem. Soc.* **2014**, *136*, 10174–10185.

(159) Cai, M.; Ding, Y.; Wang, L.; Huang, L.; Lu, X.; Cai, Y. Synthesis of One-Component Nanostructured Polyion Complexes via Polymerization-Induced Electrostatic Self-Assembly. *ACS Macro Lett.* **2018**, *7*, 208–212.

(160) Tóth-Szeles, E.; Horváth, J.; Holló, G.; Szűcs, R.; Nakanishi, H.; Lagzi, I. Chemically Coded Time-Programmed Self-Assembly. *Mol. Syst. Des. Eng.* **2017**, *2*, 274–282.

(161) Fuchise, K.; Kakuchi, R.; Lin, S.-T.; Sakai, R.; Sato, S.-I.; Satoh, T.; Chen, W.-C.; Kakuchi, T. Control of Thermoresponsive Property of Urea End-Functionalized Poly(*N* -Isopropylacrylamide) Based on the Hydrogen Bond-Assisted Self-Assembly in Water. *J. Polym. Sci. A Polym. Chem.* **2009**, *47*, 6259–6268.

(162) Karjalainen, E.; Aseyev, V.; Tenhu, H. Upper or Lower Critical Solution Temperature, or Both? Studies on Cationic Copolymers of N-Isopropylacrylamide. *Polym. Chem.* **2015**, *6*, 3074–3082.
(163) Noh, M.; Mok, Y.; Lee, S.; Kim, H.; Lee, S. H.; Jin, G.; Seo, J.-H.; Koo, H.; Park, T. H.; Lee, Y. Novel Lower Critical Solution Temperature Phase Transition Materials Effectively Control Osmosis by Mild Temperature Changes. *Chem. Commun.* **2012**, *48*, 3845–3847.
(164) Lambert, F. L. Entropy Is Simple, Qualitatively. *J. Chem. Educ.* **2002**, *79*, 1241–1246.
(165) Zhang, Q.; Weber, C.; Schubert, U. S.; Hoogenboom, R. Thermoresponsive Polymers with Lower Critical Solution Temperature: From Fundamental Aspects and Measuring Techniques to Recommended Turbidimetry Conditions. *Mater. Horiz.* **2017**, *4*, 109–116.
(166) Seuring, J.; Agarwal, S. Polymers with Upper Critical Solution Temperature in Aqueous Solution. *Macromol. Rapid Commun.* **2012**, *33*, 1898–1920.
(167) Wang, J.; Yu, H.; Zhou, X.; Liu, X.; Zhang, R.; Lu, Z.; Zheng, J.; Gu, L.; Liu, K.; Wang, D.; Jiao, L. Probing the Crystallographic Orientation of Two-Dimensional Atomic Crystals with Supramolecular Self-Assembly. *Nat. Commun.* **2017**, *8*, 377.
(168) Zabelin, V.; Dunbar, L. A.; Le Thomas, N.; Houdré, R.; Kotlyar, M. V.; O'Faolain, L.; Krauss, T. F. Self-Collimating Photonic Crystal Polarization Beam Splitter. *Opt. Lett.* **2007**, *32*, 530–532.
(169) Schulz, S. A.; O'Faolain, L.; Beggs, D. M.; White, T. P.; Melloni, A.; Krauss, T. F. Dispersion Engineered Slow Light in Photonic Crystals: A Comparison. *J. Opt.* **2010**, *12*, 104004.
(170) Takahashi, Y.; Gotoh, Y.; Akimoto, J.; Mizuta, S.; Tokiwa, K.; Watanabe, T. Anisotropic Electrical Conductivity in $LiCoO_2$ Single Crystal. *J. Solid State Chem.* **2002**, *164*, 1–4.
(171) Amin, R.; Balaya, P.; Maier, J. Anisotropy of Electronic and Ionic Transport in $LiFePO_4$ Single Crystals. *Electrochem. Solid-State Lett.* **2007**, *10*, A13–A16.
(172) Cheng, H.; Yang, N.; Lu, Q.; Zhang, Z.; Zhang, H. Syntheses and Properties of Metal Nanomaterials with Novel Crystal Phases. *Adv. Mater.* **2018**, *30*, 1707189.
(173) Fan, Z.; Zhang, H. Crystal Phase-Controlled Synthesis, Properties and Applications of Noble Metal Nanomaterials. *Chem. Soc. Rev.* **2016**, *45*, 63–82.
(174) Xu, Q.; Xu, S.-M.; Tian, R.; Lu, C. Significantly Enhanced Thermoelectric Properties of Organic–Inorganic Hybrids with a Periodically Ordered Structure. *ACS Appl. Mater. Interfaces* **2020**, *12*, 13371–13377.
(175) Behrens, S.; Rahn, K.; Habicht, W.; Böhm, K.-J.; Rösner, H.; Dinjus, E.; Unger, E. Nanoscale Particle Arrays Induced by Highly Ordered Protein Assemblies. *Adv. Mater.* **2002**, *14*, 1621–1625.
(176) McMillan, R. A.; Paavola, C. D.; Howard, J.; Chan, S. L.; Zaluzec, N. J.; Trent, J. D. Ordered Nanoparticle Arrays Formed on Engineered Chaperonin Protein Templates. *Nat. Mater.* **2002**, *1*, 247–252.
(177) Aliprandi, A.; Mauro, M.; De Cola, L. Controlling and Imaging Biomimetic Self-Assembly. *Nat. Chem.* **2016**, *8*, 10–15.
(178) Stein, A.; Wilson, B. E.; Rudisill, S. G. Design and Functionality of Colloidal-Crystal-Templated Materials—Chemical Applications of Inverse Opals. *Chem. Soc. Rev.* **2013**, *42*, 2763–2803.
(179) Zhang, H.; Xin, X.; Sun, J.; Zhao, L.; Shen, J.; Song, Z.; Yuan, S. Self-Assembled Chiral Helical Nanofibers by Amphiphilic Dipeptide Derived from D- or L-Threonine and Application as a Template for the Synthesis of Au and Ag Nanoparticles. *J. Colloid Interface Sci.* **2016**, *484*, 97–106.

(180) Blake, A. J.; Champness, N. R.; Hubberstey, P.; Li, W.-S.; Withersby, M. A.; Schröder, M. Inorganic Crystal Engineering Using Self-Assembly of Tailored Building-Blocks. *Coord. Chem. Rev.* **1999**, *183*, 117–138.

(181) Ueno, T. Porous Protein Crystals as Reaction Vessels. *Chem. Eur. J.* **2013**, *19*, 9096–9102.

(182) Sontz, P. A.; Bailey, J. B.; Ahn, S.; Tezcan, F. A. A Metal Organic Framework with Spherical Protein Nodes: Rational Chemical Design of 3D Protein Crystals. *J. Am. Chem. Soc.* **2015**, *137*, 11598–11601.

(183) Wang, Z.; Wei, J.; Morse, P.; Dash, J. G.; Vilches, O. E.; Cobden, D. H. Phase Transitions of Adsorbed Atoms on the Surface of a Carbon Nanotube. *Science* **2010**, *327*, 552–555.

(184) Welch, P.; Muthukumar, M. Molecular Mechanisms of Polymer Crystallization from Solution. *Phys. Rev. Lett.* **2001**, *87*, 218302.

(185) Abe, H.; Ohtani, K.; Suzuki, D.; Chida, Y.; Shimada, Y.; Matsumoto, S.; Inouye, M. Alternating 2,6-/3,5-Substituted Pyridine-Acetylene Macrocycles: π-Stacking Self-Assemblies Enhanced by Intermolecular Dipole–Dipole Interaction. *Org. Lett.* **2014**, *16*, 828–831.

(186) Schlittler, R. R.; Seo, J. K.; Gimzewski, J. K.; Durkan, C.; Saifullah, M. S. M.; Welland, M. E. Single Crystals of Single-Walled Carbon Nanotubes Formed by Self-Assembly. *Science* **2001**, *292*, 1136–1139.

(187) Lu, Y.; Yin, Y.; Li, Z.-Y.; Xia, Y. Colloidal Crystals Made of Polystyrene Spheroids: Fabrication and Structural/Optical Characterization. *Langmuir* **2002**, *18*, 7722–7727.

(188) Lai, Y.-T.; King, N. P.; Yeates, T. O. Principles for Designing Ordered Protein Assemblies. *Trends Cell Biol.* **2012**, *22*, 653–661.

(189) Verwegen, M.; Cornelissen, J. J. L. M. Clustered Nanocarriers: The Effect of Size on the Clustering of CCMV Virus-Like Particles With Soft Macromolecules. *Macromol. Biosci.* **2015**, *15*, 98–110.

(190) Moradi, M.; Kim, J. C.; Qi, J.; Xu, K.; Li, X.; Ceder, G.; Belcher, A. M. A Bio-Facilitated Synthetic Route for Nano-Structured Complex Electrode Materials. *Green Chem.* **2016**, *18*, 2619–2624.

(191) Bishop, K. J. M.; Wilmer, C. E.; Soh, S.; Grzybowski, B. A. Nanoscale Forces and Their Uses in Self-Assembly. *Small* **2009**, *5*, 1600–1630.

(192) Mikkilä, J.; Anaya-Plaza, E.; Liljeström, V.; Caston, J. R.; Torres, T.; de la Escosura, A.; Kostiainen, M. A. Hierarchical Organization of Organic Dyes and Protein Cages into Photoactive Crystals. *ACS Nano* **2016**, *10*, 1565–1571.

(193) Hocini, A.; Moukhtari, R.; Khedrouche, D.; Kahlouche, A.; Zamani, M. Magneto-Photonic Crystal Microcavities Based on Magnetic Nanoparticles Embedded in Silica Matrix. *Opt. Commun.* **2017**, *384*, 111–117.

(194) Abe, S.; Ueno, T. Design of Protein Crystals in the Development of Solid Biomaterials. *RSC Adv.* **2015**, *5*, 21366–21375.

(195) Li, M.; Liu, H.; Lv, T.; Ding, M. Synergistic Effect of the Valence Bond Environment and Exposed Crystal Facets of the TiO_2/SnS_2 Heterojunction for Achieving Enhanced Electrocatalytic Oxygen Evolution. *J. Mater. Chem. A* **2018**, *6*, 3488–3499.

(196) Cohen-Hadar, N.; Wine, Y.; Nachliel, E.; Huppert, D.; Gutman, M.; Frolow, F.; Freeman, A. Monitoring the Stability of Crosslinked Protein Crystals Biotemplates: A Feasibility Study. *Biotechnol. Bioeng.* **2006**, *94*, 1005–1011.

(197) Zhang, L.; Bailey, J. B.; Subramanian, R. H.; Groisman, A.; Tezcan, F. A. Hyperexpandable, Self-Healing Macromolecular Crystals with Integrated Polymer Networks. *Nature* **2018**, *557*, 86–91.

(198) Mano, J. F. Stimuli-Responsive Polymeric Systems for Biomedical Applications. *Adv. Eng. Mater.* **2008**, *10*, 515–527.

(199) Tian, H.; Tang, Z.; Zhuang, X.; Chen, X.; Jing, X. Biodegradable Synthetic Polymers: Preparation, Functionalization and Biomedical Application. *Prog. Polym. Sci.* **2012**, *37*, 237–280.
(200) Goonoo, N.; Bhaw-Luximon, A.; Bowlin, G. L.; Jhurry, D. An Assessment of Biopolymer- and Synthetic Polymer-Based Scaffolds for Bone and Vascular Tissue Engineering: Polymer-Based Scaffolds for Bone and Vascular Tissue Engineering. *Polym. Int.* **2013**, *62*, 523–533.
(201) Blackman, L. D.; Gunatillake, P. A.; Cass, P.; Locock, K. E. S. An Introduction to Zwitterionic Polymer Behavior and Applications in Solution and at Surfaces. *Chem. Soc. Rev.* **2019**, *48*, 757–770.
(202) Meng, X.; Perry, S. L.; Schiffman, J. D. Complex Coacervation: Chemically Stable Fibers Electrospun from Aqueous Polyelectrolyte Solutions. *ACS Macro Lett.* **2017**, *6*, 505–511.
(203) Dobrynin, A.; Rubinstein, M. Theory of Polyelectrolytes in Solutions and at Surfaces. *Prog. Polym. Sci.* **2005**, *30*, 1049–1118.
(204) Millot, M.-C.; Debranche, T.; Pantazaki, A.; Gherghi, I.; Sébille, B.; Vidal-Madjar, C. Ion-Exchange Chromatographic Supports Obtained by Formation of Polyelectrolyte Multi-Layers for the Separation of Proteins. *Chromatographia* **2003**, *58*, 365–373.
(205) de Grooth, J.; Reurink, D. M.; Ploegmakers, J.; de Vos, W. M.; Nijmeijer, K. Charged Micropollutant Removal With Hollow Fiber Nanofiltration Membranes Based On Polycation/Polyzwitterion/Polyanion Multilayers. *ACS Appl. Mater. Interfaces* **2014**, *6*, 17009–17017.
(206) Chollakup, R.; Smitthipong, W.; Eisenbach, C. D.; Tirrell, M. Phase Behavior and Coacervation of Aqueous Poly(Acrylic Acid)−Poly(Allylamine) Solutions. *Macromolecules* **2010**, *43*, 2518–2528.
(207) Fu, J.; Schlenoff, J. B. Driving Forces for Oppositely Charged Polyion Association in Aqueous Solutions: Enthalpic, Entropic, but Not Electrostatic. *J. Am. Chem. Soc.* **2016**, *138*, 980–990.
(208) Shen, K.; Wang, Z.-G. Polyelectrolyte Chain Structure and Solution Phase Behavior. *Macromolecules* **2018**, *51*, 1706–1717.
(209) Jaeger, W.; Bohrisch, J.; Laschewsky, A. Synthetic Polymers with Quaternary Nitrogen Atoms—Synthesis and Structure of the Most Used Type of Cationic Polyelectrolytes. *Prog. Polym. Sci.* **2010**, *35*, 511–577.
(210) Mergel, O.; Kühn, P. T.; Schneider, S.; Simon, U.; Plamper, F. A. Influence of Polymer Architecture on the Electrochemical Deposition of Polyelectrolytes. *Electrochim. Acta* **2017**, *232*, 98–105.
(211) Pranantyo, D.; Xu, L. Q.; Neoh, K.-G.; Kang, E.-T.; Ng, Y. X.; Teo, S. L.-M. Tea Stains-Inspired Initiator Primer for Surface Grafting of Antifouling and Antimicrobial Polymer Brush Coatings. *Biomacromolecules* **2015**, *16*, 723–732.
(212) Chen, Y.; Liu, W.; Zeng, G.; Liu, Y. Microporous PDMAEMA-Based Stimuli-Responsive Hydrogel and Its Application in Drug Release. *J. Appl. Polym. Sci.* **2017**, *134*, 45326.
(213) Kim, K.; Chen, W. C. W.; Heo, Y.; Wang, Y. Polycations and Their Biomedical Applications. *Prog. Polym. Sci.* **2016**, *60*, 18–50.
(214) Liu, L.; Yi, H.; He, H.; Pan, H.; Cai, L.; Ma, Y. Tumor Associated Macrophage-Targeted MicroRNA Delivery with Dual-Responsive Polypeptide Nanovectors for Anti-Cancer Therapy. *Biomaterials* **2017**, *134*, 166–179.
(215) Licciardi, M.; Campisi, M.; Cavallaro, G.; Cervello, M.; Azzolina, A.; Giammona, G. Synthesis and Characterization of Polyaminoacidic Polycations for Gene Delivery. *Biomaterials* **2006**, *27*, 2066–2075.
(216) Deming, T. J. Synthesis of Side-Chain Modified Polypeptides. *Chem. Rev.* **2016**, *116*, 786–808.

(217) Rosilo, H.; McKee, J. R.; Kontturi, E.; Koho, T.; Hytönen, V. P.; Ikkala, O.; Kostiainen, M. A. Cationic Polymer Brush-Modified Cellulose Nanocrystals for High-Affinity Virus Binding. *Nanoscale* **2014**, *6*, 11871–11881.

(218) Shen, Y.; Fu, X.; Fu, W.; Li, Z. Biodegradable Stimuli-Responsive Polypeptide Materials Prepared by Ring Opening Polymerization. *Chem. Soc. Rev.* **2015**, *44*, 612–622.

(219) Bonduelle, C. Secondary Structures of Synthetic Polypeptide Polymers. *Polym. Chem.* **2018**, *9*, 1517–1529.

(220) Cohen-Erez, I.; Rapaport, H. Coassemblies of the Anionic Polypeptide γ-PGA and Cationic β-Sheet Peptides for Drug Delivery to Mitochondria. *Biomacromolecules* **2015**, *16*, 3827–3835.

(221) Ma, C.; Malessa, A.; Boersma, A. J.; Liu, K.; Herrmann, A. Supercharged Proteins and Polypeptides. *Adv. Mater.* **2020**, *32*, 1905309.

(222) Obermeyer, A. C.; Mills, C. E.; Dong, X.-H.; Flores, R. J.; Olsen, B. D. Complex Coacervation of Supercharged Proteins with Polyelectrolytes. *Soft Matter* **2016**, *12*, 3570–3581.

(223) Simon, A. J.; Zhou, Y.; Ramasubramani, V.; Glaser, J.; Pothukuchy, A.; Gollihar, J.; Gerberich, J. C.; Leggere, J. C.; Morrow, B. R.; Jung, C.; Glotzer, S. C.; Taylor, D. W.; Ellington, A. D. Supercharging Enables Organized Assembly of Synthetic Biomolecules. *Nat. Chem.* **2019**, *11*, 204–212.

(224) Lach, M.; Künzle, M.; Beck, T. Free-Standing Metal Oxide Nanoparticle Superlattices Constructed with Engineered Protein Containers Show in Crystallo Catalytic Activity. *Chem. Eur. J.* **2017**, *23*, 17482–17486.

(225) cram, D. J.; Cram, J. M. Cyclophane Chemistry: Bent and Battered Benzene Rings. *Acc. Chem. Res.* **1971**, *4*, 204–213.

(226) Guyard, L.; Audebert, P. Synthesis and Electrochemical Polymerization of Bis-Dithienyl Cyclophane. *Electrochem. Commun.* **2001**, *3*, 164–167.

(227) Morisaki, Y.; Chujo, Y. Cyclophane-Containing Polymers. *Prog. Polym. Sci.* **2008**, *33*, 346–364.

(228) Jeppesen, J. O.; Nielsen, M. B.; Becher, J. Tetrathiafulvalene Cyclophanes and Cage Molecules. *Chem. Rev.* **2004**, *104*, 5115–5132.

(229) Camacho, D. H.; Salo, E. V.; Ziller, J. W.; Guan, Z. Cyclophane-Based Highly Active Late-Transition-Metal Catalysts for Ethylene Polymerization. *Angew. Chem. Int. Ed.* **2004**, *43*, 1821–1825.

(230) Liu, Z.; Nalluri, S. K. M.; Stoddart, J. F. Surveying Macrocyclic Chemistry: From Flexible Crown Ethers to Rigid Cyclophanes. *Chem. Soc. Rev.* **2017**, *46*, 2459–2478.

(231) Neelakandan, P. P.; Ramaiah, D. DNA-Assisted Long-Lived Excimer Formation in a Cyclophane. *Angew. Chem. Int. Ed.* **2008**, *47*, 8407–8411.

(232) Li, C.; Ma, J.; Zhao, L.; Zhang, Y.; Yu, Y.; Shu, X.; Li, J.; Jia, X. Molecular Selective Binding of Basic Amino Acids by a Water-Soluble Pillar[5]Arene. *Chem. Commun.* **2013**, *49*, 1924–1926.

(233) Arvízu-Santamaría, A. G.; Navarro, R. E.; Soberanes, Y.; Velázquez, E. F.; Santacruz, H.; Inoue, M. Complexation of Neurotransmitters – Dopamine, Serotonin and Melatonin – with a DTPA-Based Cyclophane of High Rigidity: ^{1}H NMR Shift and Line-Broadening. *Supramol. Chem.* **2017**, *29*, 658–667.

(234) Roy, I.; Bobbala, S.; Zhou, J.; Nguyen, M. T.; Nalluri, S. K. M.; Wu, Y.; Ferris, D. P.; Scott, E. A.; Wasielewski, M. R.; Stoddart, J. F. ExTzBox: A Glowing Cyclophane for Live-Cell Imaging. *J. Am. Chem. Soc.* **2018**, *140*, 7206–7212.

(235) Ludwig, R.; Dzung, N. Calixarene-Based Molecules for Cation Recognition. *Sensors* **2002**, *2*, 397–416.

(236) Gutsche, C. D. Calixarenes. *Acc. Chem. Res.* **1983**, *16*, 161–170.

(237) Schneider, H.-J.; Schneider, U. The Host-Guest Chemistry of Resorcinarenes. *J. Incl. Phenom. Macrocycl. Chem.* **1994**, *19*, 67–83.
(238) Ogoshi, T.; Aoki, T.; Kitajima, K.; Fujinami, S.; Yamagishi, T.; Nakamoto, Y. Facile, Rapid, and High-Yield Synthesis of Pillar[5]Arene from Commercially Available Reagents and Its X-Ray Crystal Structure. *J. Org. Chem.* **2011**, *76*, 328–331.
(239) Hu, X.-Y.; Zhang, P.; Wu, X.; Xia, W.; Xiao, T.; Jiang, J.; Lin, C.; Wang, L. Pillar[5]Arene-Based Supramolecular Polypseudorotaxanes Constructed from Quadruple Hydrogen Bonding. *Polym. Chem.* **2012**, *3*, 3060–3063.
(240) Ramaiah, D.; Neelakandan, P. P.; Nair, Akhil. K.; Avirah, R. R. Functional Cyclophanes: Promising Hosts for Optical Biomolecular Recognition. *Chem. Soc. Rev.* **2010**, *39*, 4158–4168.
(241) Lahav, M.; Shipway, A. N.; Willner, I.; Nielsen, M. B.; Stoddart, J. F. An Enlarged Bis-Bipyridinium Cyclophane-Au Nanoparticle Superstructure for Selective Electrochemical Sensing Applications. *J. Electroanal. Chem.* **2000**, *482*, 217–221.
(242) González, P.; Serra, J.; Liste, S.; Chiussi, S.; León, B.; Pérez-Amor, M. Raman Spectroscopic Study of Bioactive Silica Based Glasses. *J. Non-Cryst. Solids* **2003**, *320*, 92–99.
(243) Chen, J.-F.; Ding, H.-M.; Wang, J.-X.; Shao, L. Preparation and Characterization of Porous Hollow Silica Nanoparticles for Drug Delivery Application. *Biomaterials* **2004**, *25*, 723–727.
(244) Yamamoto, E.; Kuroda, K. Colloidal Mesoporous Silica Nanoparticles. *BCSJ* **2016**, *89*, 501–539.
(245) Vojoudi, H.; Badiei, A.; Bahar, S.; Mohammadi Ziarani, G.; Faridbod, F.; Ganjali, M. R. A New Nano-Sorbent for Fast and Efficient Removal of Heavy Metals from Aqueous Solutions Based on Modification of Magnetic Mesoporous Silica Nanospheres. *J. Magn. Magn. Mater.* **2017**, *441*, 193–203.
(246) Cashin, V. B.; Eldridge, D. S.; Yu, A.; Zhao, D. Surface Functionalization and Manipulation of Mesoporous Silica Adsorbents for Improved Removal of Pollutants: A Review. *Environ. Sci. Water Res. Technol.* **2018**, *4*, 110–128.
(247) Delkash, M.; Ebrazi Bakhshayesh, B.; Kazemian, H. Using Zeolitic Adsorbents to Cleanup Special Wastewater Streams: A Review. *Micropor. Mesopor. Mater.* **2015**, *214*, 224–241.
(248) Wang, L.; Han, C.; Nadagouda, M. N.; Dionysiou, D. D. An Innovative Zinc Oxide-Coated Zeolite Adsorbent for Removal of Humic Acid. *J. Hazard. Mater.* **2016**, *313*, 283–290.
(249) Kuang, D.; Brezesinski, T.; Smarsly, B. Hierarchical Porous Silica Materials with a Trimodal Pore System Using Surfactant Templates. *J. Am. Chem. Soc.* **2004**, *126*, 10534–10535.
(250) Guliants, V. V.; Carreon, M. A.; Lin, Y. S. Ordered Mesoporous and Macroporous Inorganic Films and Membranes. *J. Membr. Sci.* **2004**, *235*, 53–72.
(251) Da'na, E. Adsorption of Heavy Metals on Functionalized-Mesoporous Silica: A Review. *Micropor. Mesopor. Mater.* **2017**, *247*, 145–157.
(252) Lin, Y.-S.; Haynes, C. L. Synthesis and Characterization of Biocompatible and Size-Tunable Multifunctional Porous Silica Nanoparticles. *Chem. Mater.* **2009**, *21*, 3979–3986.
(253) Yang, P.; Gai, S.; Lin, J. Functionalized Mesoporous Silica Materials for Controlled Drug Delivery. *Chem. Soc. Rev.* **2012**, *41*, 3679–3698.
(254) Zhou, Y.; Quan, G.; Wu, Q.; Zhang, X.; Niu, B.; Wu, B.; Huang, Y.; Pan, X.; Wu, C. Mesoporous Silica Nanoparticles for Drug and Gene Delivery. *Acta Pharm. Sin. B* **2018**, *8*, 165–177.

(255) Miyata, H.; Suzuki, T.; Fukuoka, A.; Sawada, T.; Watanabe, M.; Noma, T.; Takada, K.; Mukaide, T.; Kuroda, K. Silica Films with a Single-Crystalline Mesoporous Structure. *Nat. Mater.* **2004**, *3*, 651–656.

(256) Takahashi, R.; Sato, S.; Sodesawa, T.; Kawakita, M.; Ogura, K. High Surface-Area Silica with Controlled Pore Size Prepared from Nanocomposite of Silica and Citric Acid. *J. Phys. Chem. B* **2000**, *104*, 12184–12191.

(257) Zhao, L.; Yu, J.; Cheng, B.; Yu, C. A Novel Approach for the Synthesis of Monodispersed Porous Silica Microspheres with High Surface Area. *J. Non-Cryst. Solids* **2005**, *351*, 3593–3599.

(258) Zhao, D.; Feng, J.; Huo, Q.; Melosh, N.; Fredrickson, G. H.; Chmelka, B. F.; Stucky, G. D. Triblock Copolymer Syntheses of Mesoporous Silica with Periodic 50 to 300 Angstrom Pores. *Science* **1998**, *279*, 548–552.

(259) Yano, K.; Fukushima, Y. Particle Size Control of Mono-Dispersed Super-Microporous Silica Spheres. *J. Mater. Chem.* **2003**, *13*, 2577.

(260) Martens, J. A.; Jammaer, J.; Bajpe, S.; Aerts, A.; Lorgouilloux, Y.; Kirschhock, C. E. A. Simple Synthesis Recipes of Porous Materials. *Micropor. Mesopor. Mater.* **2011**, *140*, 2–8.

(261) Xu, C.; Lei, C.; Yu, C. Mesoporous Silica Nanoparticles for Protein Protection and Delivery. *Front. Chem.* **2019**, *7*, 290.

(262) Hudson, S.; Cooney, J.; Magner, E. Proteins in Mesoporous Silicates. *Angew. Chem. Int. Ed.* **2008**, *47*, 8582–8594.

(263) Velev, O. D.; Lenhoff, A. M. Colloidal Crystals as Templates for Porous Materials. *Curr. Opin. Colloid Interface Sci.* **2000**, *5*, 56–63.

(264) Jackson, E.; Ferrari, M.; Cuestas-Ayllon, C.; Fernández-Pacheco, R.; Perez-Carvajal, J.; de la Fuente, J. M.; Grazú, V.; Betancor, L. Protein-Templated Biomimetic Silica Nanoparticles. *Langmuir* **2015**, *31*, 3687–3695.

(265) Niu, Z.; Kabisatpathy, S.; He, J.; Lee, L. A.; Rong, J.; Yang, L.; Sikha, G.; Popov, B. N.; Emrick, T. S.; Russell, T. P.; Wang, Q. Synthesis and Characterization of Bionanoparticle—Silica Composites and Mesoporous Silica with Large Pores. *Nano Res.* **2009**, *2*, 474–483.

(266) Hess, D. M.; Naik, R. R.; Rinaldi, C.; Tomczak, M. M.; Watkins, J. J. Fabrication of Ordered Mesoporous Silica Films with Encapsulated Iron Oxide Nanoparticles Using Ferritin-Doped Block Copolymer Templates. *Chem. Mater.* **2009**, *21*, 2125–2129.

(267) Maleki, A.; Kettiger, H.; Schoubben, A.; Rosenholm, J. M.; Ambrogi, V.; Hamidi, M. Mesoporous Silica Materials: From Physico-Chemical Properties to Enhanced Dissolution of Poorly Water-Soluble Drugs. *J. Control. Release* **2017**, *262*, 329–347.

(268) Yue, W.; Zhou, W. Crystalline Mesoporous Metal Oxide. *Prog. Nat. Sci.* **2008**, *18*, 1329–1338.

(269) Vera-Robles, L. I.; González-Gracida, J.; Hernández-Gordillo, A.; Campero, A. Using the M13 Phage as a Biotemplate to Create Mesoporous Structures Decorated with Gold and Platinum Nanoparticles. *Langmuir* **2015**, *31*, 9188–9197.

(270) Yu, E.; Lo, A.; Jiang, L.; Petkus, B.; Ileri Ercan, N.; Stroeve, P. Improved Controlled Release of Protein from Expanded-Pore Mesoporous Silica Nanoparticles Modified with Co-Functionalized Poly(n-Isopropylacrylamide) and Poly(Ethylene Glycol) (PNIPAM-PEG). *Colloids Surf. B* **2017**, *149*, 297–300.

(271) Tu, J.; Boyle, A. L.; Friedrich, H.; Bomans, P. H. H.; Bussmann, J.; Sommerdijk, N. A. J. M.; Jiskoot, W.; Kros, A. Mesoporous Silica Nanoparticles with Large Pores for the Encapsulation and Release of Proteins. *ACS Appl. Mater. Interfaces* **2016**, *8*, 32211–32219.

(272) Bancroft, J. B.; Rees, M. W.; Dawson, J. R. O.; McLean, G. D.; Short, M. N. Some Properties of a Temperature-Sensitive Mutant of Cowpea Chlorotic Mottle Virus. *J. Gen. Virol.* **1972**, *16*, 69–81.

(273) Utsel, S.; Bruce, C.; Pettersson, T.; Fogelström, L.; Carlmark, A.; Malmström, E.; Wågberg, L. Physical Tuning of Cellulose-Polymer Interactions Utilizing Cationic Block Copolymers Based on PCL and Quaternized PDMAEMA. *ACS Appl. Mater. Interfaces* **2012**, *4*, 6796–6807.

(274) Weaver, L. G.; Stockmann, R.; Postma, A.; Thang, S. H. Multi-Responsive (Diethylene Glycol)Methyl Ether Methacrylate (DEGMA)-Based Copolymer Systems. *RSC Adv.* **2016**, *6*, 90923–90933.

(275) Kostiainen, M. A.; Hiekkataipale, P.; de la Torre, J. Á.; Nolte, R. J. M.; Cornelissen, J. J. L. M. Electrostatic Self-Assembly of Virus–Polymer Complexes. *J. Mater. Chem.* **2011**, *21*, 2112–2117.

(276) Palomino-Vizcaino, G.; Valencia Reséndiz, D. G.; Benítez-Hess, M. L.; Martínez-Acuña, N.; Tapia-Vieyra, J. V.; Bahena, D.; Díaz-Sánchez, M.; García-González, O. P.; Alvarez-Sandoval, B. A.; Alvarez-Salas, L. M. Effect of HPV16 L1 Virus-like Particles on the Aggregation of Non-Functionalized Gold Nanoparticles. *Biosens. Bioelectron.* **2018**, *100*, 176–183.

(277) Sinclair, T. R.; Patil, A.; Raza, B. G.; Reurink, D.; van den Hengel, S. K.; Rutjes, S. A.; de Roda Husman, A. M.; Roesink, H. D. W.; de Vos, W. M. Cationically Modified Membranes Using Covalent Layer-by-Layer Assembly for Antiviral Applications in Drinking Water. *J. Membr. Sci.* **2019**, *570–571*, 494–503.

(278) Shin, G.-A.; Sobsey, M. D. Inactivation of Norovirus by Chlorine Disinfection of Water. *Water Res.* **2008**, *42*, 4562–4568.

(279) Shimabuku, Q. L.; Arakawa, F. S.; Fernandes Silva, M.; Ferri Coldebella, P.; Ueda-Nakamura, T.; Fagundes-Klen, M. R.; Bergamasco, R. Water Treatment with Exceptional Virus Inactivation Using Activated Carbon Modified with Silver (Ag) and Copper Oxide (CuO) Nanoparticles. *Environ. Technol.* **2017**, *38*, 2058–2069.

(280) Suzuki, K.; Tanaka, Y.; Osada, T.; Waki, M. Removal of Phosphate, Magnesium and Calcium from Swine Wastewater through Crystallization Enhanced by Aeration. *Water Res.* **2002**, *36*, 2991–2998.

(281) Blaney, L.; Cinar, S.; SenGupta, A. Hybrid Anion Exchanger for Trace Phosphate Removal from Water and Wastewater. *Water Research* **2007**, *41*, 1603–1613.

(282) Acelas, N. Y.; Martin, B. D.; López, D.; Jefferson, B. Selective Removal of Phosphate from Wastewater Using Hydrated Metal Oxides Dispersed within Anionic Exchange Media. *Chemosphere* **2015**, *119*, 1353–1360.

(283) Hassan, P. A.; Rana, S.; Verma, G. Making Sense of Brownian Motion: Colloid Characterization by Dynamic Light Scattering. *Langmuir* **2015**, *31*, 3–12.

(284) Khare, G.; Gupta, V.; Nangpal, P.; Gupta, R. K.; Sauter, N. K.; Tyagi, A. K. Ferritin Structure from Mycobacterium Tuberculosis: Comparative Study with Homologues Identifies Extended C-Terminus Involved in Ferroxidase Activity. *PLoS ONE* **2011**, *6*, e18570.

Protein cages are advanced functional molecules with precise shapes and dimensions, making them suited for formation of supramolecular structures by self-assembly. Electrostatic interactions are an efficient way to carry out this process. The objective of this thesis is to present protein cages as building blocks for novel functional materials together with synthetic co-assembly agents. The properties of the assemblies and assembly processes were studied to demonstrate the versatility and ease of production of these hybrid materials, while focusing on systems with real life applications.

Aalto-DD 2/2021

ISBN 978-952-64-0227-7 (printed)
ISBN 978-952-64-0228-4 (pdf)
ISSN 1799-4934 (printed)
ISSN 1799-4942 (pdf)

Aalto University
School of Chemical Engineering
Department of Bioproducts and Biosystems
www.aalto.fi

BUSINESS + ECONOMY

ART + DESIGN + ARCHITECTURE

SCIENCE + TECHNOLOGY

CROSSOVER

DOCTORAL DISSERTATIONS